EUROPEAN ORGANISATION FOR NUCLEAR RESEARCH (CERN)

Submitted to: Phys. Rev. C.

CERN-EP-2020-246
26th January 2021

Two-particle azimuthal correlations in photonuclear ultraperipheral Pb+Pb collisions at 5.02 TeV with ATLAS

The ATLAS Collaboration

Two-particle long-range azimuthal correlations are measured in photonuclear collisions using 1.7 nb^{-1} of 5.02 TeV Pb+Pb collision data collected by the ATLAS experiment at the LHC. Candidate events are selected using a dedicated high-multiplicity photonuclear event trigger, a combination of information from the zero-degree calorimeters and forward calorimeters, and from pseudorapidity gaps constructed using calorimeter energy clusters and charged-particle tracks. Distributions of event properties are compared between data and Monte Carlo simulations of photonuclear processes. Two-particle correlation functions are formed using charged-particle tracks in the selected events, and a template-fitting method is employed to subtract the non-flow contribution to the correlation. Significant nonzero values of the second- and third-order flow coefficients are observed and presented as a function of charged-particle multiplicity and transverse momentum. The results are compared with flow coefficients obtained in proton–proton and proton–lead collisions in similar multiplicity ranges, and with theoretical expectations. The unique initial conditions present in this measurement provide a new way to probe the origin of the collective signatures previously observed only in hadronic collisions.

Contents

1 Introduction **2**

2 ATLAS detector and data sample **4**

3 Monte Carlo simulation **5**

4 Photonuclear event selection **6**
4.1 Reconstruction and event selection 6
4.2 Event properties 7

5 Two-particle correlations **11**
5.1 Non-flow subtraction 14
5.2 Factorization test 15
5.3 Physics backgrounds 19

6 Systematic uncertainties **19**

7 Results and discussion **21**

8 Conclusion **25**

1 Introduction

In ultrarelativistic collisions of lead nuclei at the Large Hadron Collider (LHC), the typical processes studied are those for which the nuclei have an impact parameter less than twice their radius ($b \lesssim 2R_A$). Such lead–lead (Pb+Pb) collisions are understood to create a quark–gluon plasma and result in a large number of particles in the final state which participate in collective motion as a consequence of the plasma evolution [1–3]. In addition to the particles produced in Pb+Pb collisions, those produced in high-energy proton–proton (pp) and proton–lead (p+Pb) collisions also exhibit a collective behavior which manifests as an event-wide azimuthal variation persisting broadly in pseudorapidity, initially observed as a 'ridge' [4–7]. This behavior is characterized in terms of nonzero single-particle azimuthal anisotropies, given by n^{th}-order Fourier coefficients, and here referred to as flow coefficients v_n. Nonzero v_n values have also been observed in significantly lower-energy (19.6–200 GeV) d+Au collisions at the Relativistic Heavy Ion Collider [8]. A natural question is whether such signatures persist in even smaller collision systems [9] and, if so, how this may influence the interpretation of these signatures in pp or p+Pb collisions.

In the prevailing paradigm, these observed anisotropies arise from the creation of a miniature region of quark–gluon plasma [10, 11], in which a hydrodynamic-like expansion of the system converts spatial nonuniformities in the initial state of the system into momentum-space anisotropies of the final-state particles. However, momentum correlations already present in the initial state of the collision may also persist into the final state [12]. The relative importance of these two explanations can be tested in collision systems where one or both of the 'beams' has a significantly simpler initial state. Recently, studies were performed in archived e^+e^- collision data at $\sqrt{s} = 91$ GeV from the ALEPH detector [13] and in archived ep collision data at $\sqrt{s} = 316$ GeV from the ZEUS detector [14] with a deep-inelastic-scattering selection

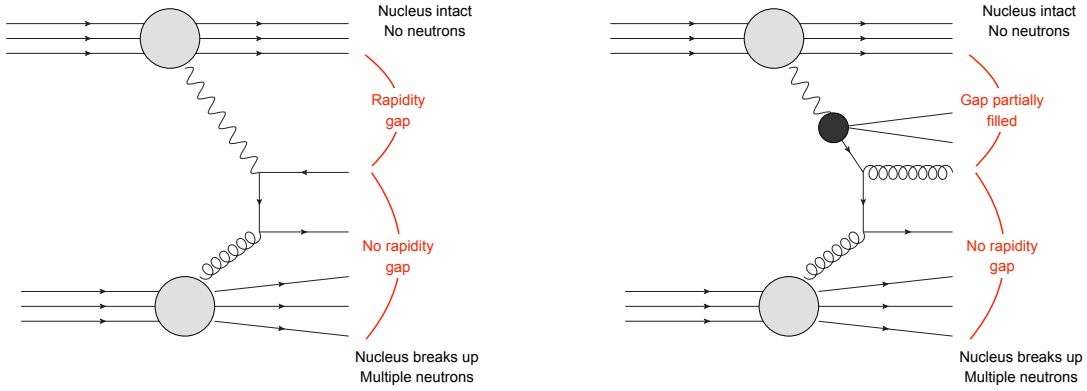

Figure 1: Diagrams representing different types of photonuclear collisions and the general features of their event topologies. *Left:* the direct process, in which the photon itself interacts with the nucleus. *Right:* the resolved process, in which the photon fluctuates into a hadronic state.

$Q^2 > 1$ GeV^2. A ridge signature was not observed, and experimental upper limits were set on the possible magnitude of v_n coefficients.

In addition to the hadronic Pb+Pb interactions described above, the strong electromagnetic (EM) fields of the fully ionized nuclei can induce interactions even when the nuclei have significantly larger impact parameters such that no hadronic interaction occurs ($b \gtrsim 2R_A$). In the equivalent photon approximation [15–17], these strong EM fields correspond to a flux of quasi-real, high-energy photons. These photons can be emitted coherently from the entire nucleus, producing a flux enhanced by a factor of Z^2 ($Z = 82$ for Pb) for photons up to 80 GeV at the LHC. These ultraperipheral collisions (UPC) [18, 19] have appreciable rates and include photon–photon ($\gamma\gamma$) and photonuclear (γ + A) interactions.

At the LHC, previous measurements of ultraperipheral processes in Pb+Pb collisions include light-by-light scattering ($\gamma\gamma \to \gamma\gamma$) [20–23], exclusive dilepton production ($\gamma\gamma \to e^+e^-$ and $\gamma\gamma \to \mu^+\mu^-$) [24–26], and the photonuclear production of various meson states ($\gamma + \mathrm{A} \to h + X$) [26–28]. In the photonuclear case, the photon may act as a point-like particle interacting with a parton in the nucleus (the 'direct' case). However, the vector-meson dominance picture [18, 29] suggests that the photon often fluctuates into a vector-meson state such as a ρ or ω (the 'resolved' case). In this case, the interaction proceeds as a meson–nucleus collision at an energy lower than that of the associated nucleon–nucleon collision. Figure 1 illustrates the direct and resolved photonuclear interactions. The photon–nucleon collision energy and the boost of the center-of-mass relative to the nucleus–nucleus rest frame depends on the photon energy and thus varies event to event. For photons with energies at the upper boundary of the coherence region, $E = 80$ GeV, the resulting photon–nucleon center-of-mass energy is approximately 900 GeV. Thus photonuclear collisions may be used to probe the dynamics of a system with a novel energy and geometry compared to pp or p+A collisions at the LHC, and to e^+e^- or ep collisions at LEP and HERA. Since photonuclear events are the photoproduction limit of deep inelastic scattering on nuclei, these measurements may also shed light on possible collective signatures at the future Electron Ion Collider [30, 31].

This paper presents a measurement of azimuthal anisotropies obtained via two-particle correlations in photonuclear collisions, where such analyses have not previously been undertaken. The data were recorded using a trigger designed to select minimum-bias and high-multiplicity photonuclear events in 1.7 nb^{-1} of Pb+Pb collisions at 5.02 TeV per nucleon pair delivered by the LHC in 2018. Photonuclear event candidates

are selected, and are distinguished from peripheral hadronic Pb+Pb events and other background events, using the topology of the distribution of particles in the event as measured in the zero-degree, forward, and barrel calorimeters, as well as the tracking systems through the reconstruction of pseudorapidity gaps [32, 33]. Properties of the selected events are compared with the expectations from Monte Carlo (MC) simulations of photonuclear processes.

Two-particle correlations as a function of relative separation in azimuth ($\Delta\phi$) and pseudorapidity[1] ($\Delta\eta$) are constructed for different selections of event charged-particle multiplicity and charged-particle kinematics. The non-flow contributions to the two-particle correlations (for example, jet correlations which give rise to a $\Delta\phi$ correlation structure) are suppressed by studying the correlations at large $\Delta\eta$, and the residual non-flow contribution is subtracted via the template-fitting method used extensively in prior ATLAS measurements [4, 5, 34]. In the template method, the correlation in high-multiplicity events is described as a combination of the correlation in lower-multiplicity events plus a component modulated by $\cos(2\Delta\phi)$ (and higher order) Fourier terms. The template method makes particular assumptions about how the non-flow component evolves with multiplicity. Although there are differences between the system explored in this measurement and those in previous two-particle correlation measurements, the sensitivity to the assumptions of the template method can be tested within the standard approach. The resulting magnitudes of the two-particle correlations are interpreted as arising from the product of global v_2 and v_3 values for individual particles, and are reported as a function of the reconstructed charged-particle multiplicity ($N_{\mathrm{ch}}^{\mathrm{rec}}$) and transverse momentum (p_{T}). The results are compared with other small collision systems at the LHC, and theoretical expectations from initial- and final-state physics mechanisms are discussed.

2 ATLAS detector and data sample

The ATLAS detector [35] covers nearly the entire solid angle around the collision point. The detector systems used for the measurements presented in this paper include the inner tracking detector, the electromagnetic (EM) and hadronic calorimeters, the zero-degree calorimeter (ZDC), and the trigger and data acquisition systems. The detector halves at positive and negative z-values are referred to as the A and C sides, respectively.

The inner-detector system is immersed in a 2 T axial magnetic field and provides charged-particle tracking in the range $|\eta| < 2.5$. The high-granularity silicon pixel detector covers the vertex region and typically provides four measurements per track. The innermost layer, the insertable B-layer [36–38], has been operating as a part of the silicon pixel detector since 2015.

The pixel detector is followed by the silicon microstrip tracker (SCT) which usually provides four measurement points per track. These silicon detectors are complemented by the transition radiation tracker, which enables radially extended track reconstruction up to $|\eta| = 2.0$.

The calorimeter system covers the pseudorapidity range $|\eta| < 4.9$. Within the region $|\eta| < 3.2$, electromagnetic calorimetry is provided by barrel and endcap high-granularity lead/liquid-argon (LAr) calorimeters, with an additional thin LAr presampler covering $|\eta| < 1.8$. Hadronic calorimetry is

[1] ATLAS uses a right-handed coordinate system with its origin at the nominal interaction point (IP) in the center of the detector and the z-axis along the beam pipe. The x-axis points from the IP to the center of the LHC ring, and the y-axis points upwards. Cylindrical coordinates (r, ϕ) are used in the transverse plane, ϕ being the azimuthal angle around the z-axis. The pseudorapidity is defined in terms of the polar angle θ as $\eta = -\ln\tan(\theta/2)$. Angular distance is measured in units of $\Delta R \equiv \sqrt{(\Delta\eta)^2 + (\Delta\phi)^2}$.

provided by a steel/scintillator-tile calorimeter, segmented into three barrel structures within $|\eta| < 1.7$, and two copper/LAr hadronic endcap calorimeters. The solid angle coverage is extended with the forward calorimeter (FCal), composed of copper/LAr and tungsten/LAr modules optimized for EM and hadronic measurements, respectively. The FCal detectors cover the regions $3.2 < |\eta| < 4.9$.

The minimum-bias trigger scintillator (MBTS) detects charged particles over $2.07 < |\eta| < 3.86$ using two hodoscopes of 12 counters positioned at $z = \pm 3.6$ m. The ZDC consists of EM and hadronic sections and plays a key role in identifying UPC events in heavy-ion collisions by primarily detecting neutrons resulting from the breakup of one or both nuclei. The ZDC modules are located at $z = \pm 140$ m from the IP. They measure neutral particles at pseudorapidities $|\eta| \geq 8.3$ and consist of layers of alternating quartz rods and tungsten plates.

A two-level trigger system [39] is used to select events. The first-level trigger (L1) is implemented in hardware and uses a subset of the detector information to restrict the accepted rate to at most 100 kHz. This is followed by a software-based high-level trigger (HLT) stage that reduces the accepted event rate to 1–4 kHz depending on the data-taking conditions during 2018 Pb+Pb operations.

The measurements presented in this paper were performed using the $\sqrt{s_{\mathrm{NN}}} = 5.02$ TeV Pb+Pb dataset collected with a variety of triggers in 2018, with a total integrated luminosity of 1.7 nb^{-1}. Photonuclear candidate events were first selected by the trigger by requiring one ZDC side (referred to as the Pb-going side) to have a minimum amount of energy at L1, $E > 1$ TeV, consistent with the presence of one or more neutrons. The other side (referred to as the photon-going side) was required to have an energy below a maximum-energy cutoff, $E < 1$ TeV, consistent with no neutrons. The cut value of $E = 1$ TeV is several multiples of the energy resolution away from the single-neutron peak at $E = 2.5$ TeV [24]. Thus, the selected topology is referred to as "0nXn" in the figures in this paper. Events were also required to satisfy an upper bound of 200 GeV on the total transverse energy deposited in the calorimeter at L1, for further rejection of hadronic Pb+Pb events.

After these requirements at L1, events had to pass either a minimum-bias (MB) trigger or one of several high-multiplicity triggers (HMT) with further requirements at the HLT stage. The MB trigger was defined by requiring at least one reconstructed online track with $p_{\mathrm{T}} > 0.4$ GeV. The HMTs were defined by requiring a larger number of tracks originating from the same vertex. The primary vertex, defined as the one with the largest scalar sum of p_{T}^2 values of associated tracks, was used. An HMT with a threshold of 15 tracks was defined by also requiring a hit in the MBTS at L1. Two HMTs with thresholds of 25 and 35 tracks were defined by requiring a minimum amount of energy in the calorimeter at L1. Finally, all HMTs had an additional HLT requirement of less than 5 GeV of transverse energy in the photon-going FCal, which rejected a large fraction of the 0nXn peripheral Pb+Pb background events. The 35-track HMT sampled the full luminosity of 1.7 nb^{-1} during data-taking. The 25-track HMT, 15-track HMT, and the MB trigger were configured with increasingly larger prescale factors, sampling 1.6 nb^{-1}, 0.13 nb^{-1}, and 1.0 μb^{-1} of data respectively.

3 Monte Carlo simulation

Monte Carlo (MC) simulations of the relevant physics processes were used to understand the performance of the detector, and provide distributions to be compared with the data. For all the generators and configurations listed below, the simulated events were passed through a GEANT4 simulation [40, 41] of the detector and reconstructed under the same conditions as the data.

A sample of one million peripheral Pb+Pb events was generated using HIJING v1.383 [42] with impact parameters in the range $10 < b < 20$ fm. These events were used to determine the charged-particle tracking efficiencies for the measurement, and to model the event properties of low-multiplicity, hadronic Pb+Pb events.

Several generators were used to simulate photonuclear interactions. For each of the cases below, events were generated with different minimum requirements on $N_{\mathrm{ch}}^{\mathrm{rec}}$ to provide good statistical coverage over the $N_{\mathrm{ch}}^{\mathrm{rec}}$ range accessed in data. First, the distribution of photon flux for ^{208}Pb beams at the LHC was calculated using STARLIGHT [43]. The flux distribution was passed to a multipurpose generator based on the Dual Parton Model (DPM) and referred to as DPMJET-III [44, 45], which simulated direct and resolved photon–lead (γ+Pb) interactions at the generator level, followed by a full GEANT4 simulation of the ATLAS detector. Thirteen million γ+Pb events were simulated in this way. Additionally, the flux from STARLIGHT was used to simulate two million γ+p events using DPMJET-III, where the energy of the proton was set equal to the energy per nucleon in the Pb beams. Finally, for an alternative description of these processes, PYTHIA 8.240 [46] configured with the NNPDF23LO parton distribution functions [47] and A14 set of tuned parameters [48] was used to generate twelve million γ+p events. The photon flux in PYTHIA was reweighted at the event level to match that calculated by STARLIGHT, and the simulation was configured to include both the direct and resolved photon interactions.

4 Photonuclear event selection

4.1 Reconstruction and event selection

Given the low particle multiplicities of UPC events, the charged-particle track and calorimeter energy-cluster reconstruction procedures follow those optimized for pp data-taking [49, 50]. Reconstructed charged-particle tracks are used in the analysis if they satisfy quality criteria as outlined in Ref. [51]. These include criteria for the minimum number of hits in the pixel and SCT detectors. Tracks are further required to have $p_{\mathrm{T}} > 0.4$ GeV, $|\eta| < 2.5$, and distances of closest approach to the primary reconstructed vertex in the longitudinal and transverse directions of less than 1.5 mm each. Clusters in the range $|\eta| < 4.9$ are constructed from topologically connected groups of calorimeter cells [52]. They are required to have $p_{\mathrm{T}} > 0.2$ GeV and to meet the significance criteria for the measured energy as outlined in Ref. [32] to suppress the contribution from electronic noise fluctuations.

Events are required to have a reconstructed primary vertex within $|z| < 90$ mm. Events compatible with multiple in-time interactions are tagged by the presence of multiple reconstructed vertices. These comprise less than 1% of the sample and are rejected. Events must pass a version of the ZDC-based energy selection described in Section 2 which uses the same threshold but an improved calibration for the ZDC energies determined after data-taking. Events are further characterized by their charged-particle multiplicity, $N_{\mathrm{ch}}^{\mathrm{rec}}$, which is defined as in previous ATLAS measurements of correlations in small systems [4, 5, 7] as the total number of reconstructed tracks, without efficiency correction, with $p_{\mathrm{T}} > 0.4$ GeV and $|\eta| < 2.5$. For the correlation analysis described in Section 5, events with a given $N_{\mathrm{ch}}^{\mathrm{rec}}$ were included in the analysis if they were selected by any of the HMTs which was more than 80% efficient for events with this $N_{\mathrm{ch}}^{\mathrm{rec}}$ value. For the study of event properties in Section 4.2, each $N_{\mathrm{ch}}^{\mathrm{rec}}$ range was only populated by the highest-sampled-luminosity HMT which was more than 99% efficient over the entire $N_{\mathrm{ch}}^{\mathrm{rec}}$ range. In either case, events with $N_{\mathrm{ch}}^{\mathrm{rec}} < 15$ were populated only by the MB trigger.

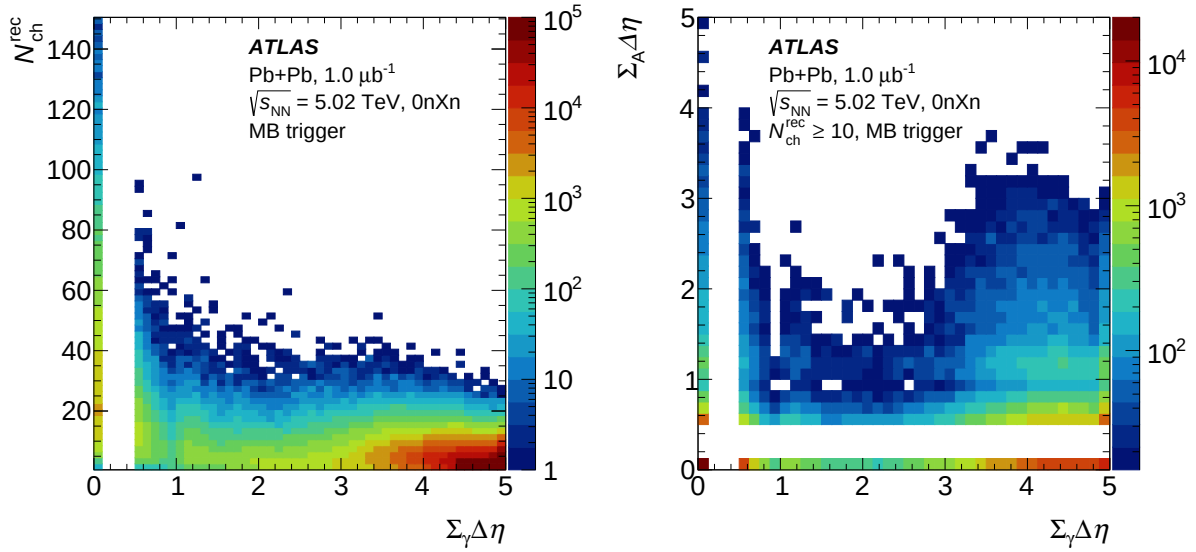

Figure 2: Left: Correlation of $N_{\mathrm{ch}}^{\mathrm{rec}}$ and $\Sigma_\gamma\Delta\eta$ for events selected by the MB trigger before application of gap-based event selection. Right: Correlation of $\Sigma_\gamma\Delta\eta$ and $\Sigma_A\Delta\eta$ for events selected by the MB trigger, with $N_{\mathrm{ch}}^{\mathrm{rec}} > 10$.

Reconstructed pseudorapidity gap quantities, constructed using the tracks and clusters in each event, are used to distinguish between different physics processes such as photonuclear collisions, low-activity (peripheral) hadronic Pb+Pb collisions, and $\gamma\gamma \to X$ processes. The requirement of a rapidity gap above a minimum value in the photon-going direction can efficiently remove peripheral Pb+Pb events. Rather than the traditional pseudorapidity gap quantity [32], which determines the pseudorapidity difference between the edge of the detector and closest particle, an alternative 'sum-of-gaps' definition is used, which adds together contiguous gaps separated by particle production concentrated in a narrow pseudorapidity regions. This alternative definition is used to retain a large selection efficiency for resolved photon events which may break up a large gap with a hadronic fragment localized in pseudorapidity (see Figure 1). The quantities $\Sigma_\gamma\Delta\eta$ and $\Sigma_A\Delta\eta$ correspond to the sum-of-gaps calculated in the photon-going and nucleus-going halves of the detector, respectively. They are calculated by first sorting the tracks and clusters in η. The differences in η between adjacent particles, $\Delta\eta$, are included in the sum if they are larger than 0.5. The value of 0.5 was observed in simulation to retain good efficiency for resolved photon events. The position at $\eta = 0$ is treated as if it were a particle which ends the sum-of-gaps calculation. Thus, $\Sigma_\gamma\Delta\eta$ and $\Sigma_A\Delta\eta$ range from 0 to 4.9.

In addition to the sum-of-gaps quantities defined above, the traditional edge gap quantity, constructed using clusters, $\Delta\eta_{\mathrm{edge}}^{\mathrm{cluster}}$, is defined as the pseudorapidity difference between the edge of the detector on the photon-going side, at $\eta = +4.9$, and the first reconstructed cluster. In the mixed-event construction discussed in Section 5, events are classified by their $\Delta\eta_{\mathrm{edge}}^{\mathrm{cluster}}$ as a way to characterize their overall topology without using charged-particle tracks.

4.2 Event properties

Figure 2 (left) shows the distribution of $\Sigma_\gamma\Delta\eta$ and $N_{\mathrm{ch}}^{\mathrm{rec}}$ values for events recorded with the MB trigger. The $\Sigma_\gamma\Delta\eta$ can have a value of zero or fall into the range $0.5 \leq \Sigma_\gamma\Delta\eta \leq 4.9$, with the lower value determined by

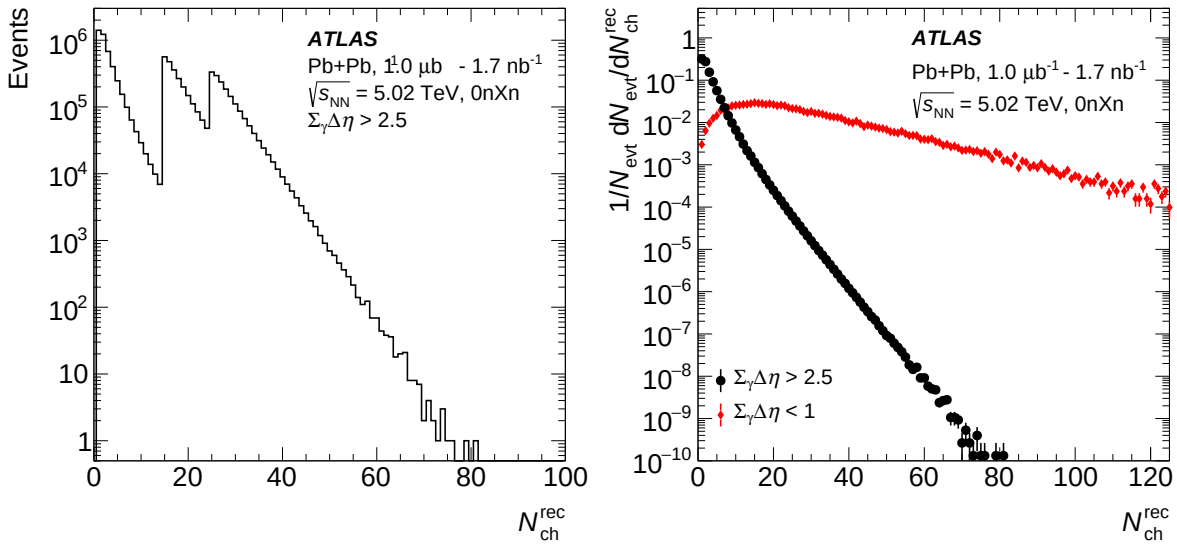

Figure 3: Left: Distribution of event charged-particle multiplicity, $N_{\mathrm{ch}}^{\mathrm{rec}}$, for the photonuclear event selection from multiple triggers, without prescale correction. Right: Distribution of event charged-particle multiplicity, $N_{\mathrm{ch}}^{\mathrm{rec}}$, for the photonuclear event selection (black) with corrections for trigger efficiency and prescale factors, and an alternative selection intended to select hadronic Pb+Pb events (red, see text).

the minimum gap size included in the sum. Events resulting from hadronic Pb+Pb collisions are at small $\Sigma_\gamma\Delta\eta$ and have a broad multiplicity distribution, whereas events from photon-induced processes are at large $\Sigma_\gamma\Delta\eta$ and have an $N_{\mathrm{ch}}^{\mathrm{rec}}$ distribution that falls steeply. Figure 2 (right) shows the distribution of $\Sigma_\gamma\Delta\eta$ and $\Sigma_A\Delta\eta$ values. Most hadronic Pb+Pb collisions have a broad pseudorapidity distribution of particles and hence have both small $\Sigma_\gamma\Delta\eta$ and small $\Sigma_A\Delta\eta$. In contrast, the photonuclear events have large $\Sigma_\gamma\Delta\eta$ but smaller values of $\Sigma_A\Delta\eta$. There is no significant yield of events with a large sum-of-gaps on both sides, which could signal the presence of photon–photon hadronic process backgrounds. The signal events for photonuclear collisions are defined by $\Sigma_\gamma\Delta\eta > 2.5$. No event selection is made on $\Sigma_A\Delta\eta$.

Figure 3 summarizes the multiplicity distribution observed in data after the event selection described above. The $N_{\mathrm{ch}}^{\mathrm{rec}}$ distribution for events passing the photonuclear event selection is shown in the left panel of Figure 3. The sawtooth pattern arises from the inclusion of the HMTs at different $N_{\mathrm{ch}}^{\mathrm{rec}}$ thresholds as described above. In each $N_{\mathrm{ch}}^{\mathrm{rec}}$ range, the selected photonuclear events have a steeply falling multiplicity distribution. The $N_{\mathrm{ch}}^{\mathrm{rec}}$ distribution for photonuclear events, fully corrected for the different luminosities sampled by the triggers and the $N_{\mathrm{ch}}^{\mathrm{rec}}$-dependent trigger efficiency, is shown using black circles in the right panel of Figure 3. It is compared with the distribution from events with $\Sigma_\gamma\Delta\eta < 1$, which mostly selects Pb+Pb hadronic events, which are backgrounds in this analysis. The selected photonuclear events have a significantly more steeply falling multiplicity distribution.

Figure 4 compares the multiplicity and sum-of-gap distributions in data and simulation. The left panel of Figure 4 shows the total $N_{\mathrm{ch}}^{\mathrm{rec}}$ distribution, corrected for the trigger efficiency and the different integrated luminosities sampled by the HMTs. This is compared with three distributions from MC generators, with the same gap-based selection requirements as the data. The data have the ZDC-based selection, while this is not applied to the MC samples as the generators do not model the nuclear-breakup processes relevant for forward neutron spectators. Including a ZDC requirement in MC events may thus impact the distributions if particle production in the detector is correlated with the nuclear fragmentation in the forward region.

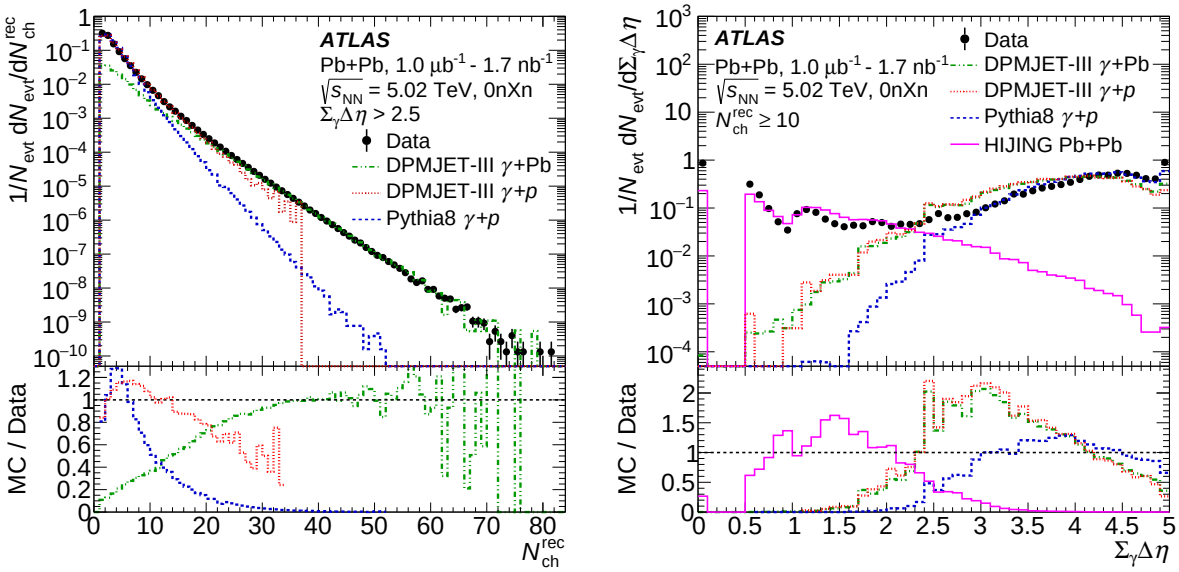

Figure 4: Left: $N_{\mathrm{ch}}^{\mathrm{rec}}$ distribution in data, corrected for trigger and reconstruction efficiency and normalized per event (black points), compared with that in DPMJET-III γ+Pb (dot-dashed green histogram), DPMJET-III γ+p (dotted red histogram), and Pythia γ+p (dashed blue histogram). The bottom panel shows the ratios of the MC distributions to the data distributions. Right: $\Sigma_\gamma\Delta\eta$ distribution in data for $N_{\mathrm{ch}}^{\mathrm{rec}} \geq 10$ (black points), normalized per event, and compared with that in DPMJET-III γ+Pb (dot-dashed green histogram), Pythia γ+p (dashed blue histogram), peripheral Hijing Pb+Pb (solid magenta histogram), and DPMJET-III γ+p (dotted red histogram).

Despite the limitations in the modeling of forward neutrons, a generator-level check requiring neutrons in the ZDC acceptance was performed and found not to impact the level of agreement between data and DPMJET-III. The distributions in Pythia and DPMJET-III γ+p are normalized to have the same integral as the data over the full $N_{\mathrm{ch}}^{\mathrm{rec}}$ range. The models show good agreement with the data at low $N_{\mathrm{ch}}^{\mathrm{rec}}$, but systematically predict too low a relative yield at higher $N_{\mathrm{ch}}^{\mathrm{rec}}$. DPMJET-III γ+Pb does not describe the full distribution, but has been normalized to have the same integral as the data in $N_{\mathrm{ch}}^{\mathrm{rec}} > 35$ to highlight its good agreement in this region over many orders of magnitude. With this normalization, DPMJET-III γ+Pb systematically predicts too low a relative yield for $N_{\mathrm{ch}}^{\mathrm{rec}} < 15$. This comparison either suggests the presence of other, non-photonuclear, processes in data at such low $N_{\mathrm{ch}}^{\mathrm{rec}} < 10$ values, or points to the need for improved modeling of this region in the simulation.

The right panel of Figure 4 shows the reconstructed $\Sigma_\gamma\Delta\eta$ distributions in data and simulation for selected events with $N_{\mathrm{ch}}^{\mathrm{rec}} > 10$, without the $\Sigma_\gamma\Delta\eta > 2.5$ requirement. Structures in the distributions correspond to transitions between detector subsystems and the change in the detector response as a function of η. At large $\Sigma_\gamma\Delta\eta$ values ≥ 2.5, the shape of the distribution in data is qualitatively similar to that in DPMJET-III γ+Pb and Pythia γ+p simulation. However, the distributions in the simulated photonuclear events decrease at smaller $\Sigma_\gamma\Delta\eta$ values, while the distribution in data rises. At low $\Sigma_\gamma\Delta\eta$, the shape in data is qualitatively similar to that in peripheral Hijing Pb+Pb events. This comparison suggests that the trigger-selected events contain a mixture of peripheral Pb+Pb events and genuine photonuclear events, with the latter dominant at $\Sigma_\gamma\Delta\eta > 2.5$. The possible impact of residual peripheral Pb+Pb events in the set of selected events is discussed in Section 6.

Figure 5 compares the charged-particle pseudorapidity distribution, $dN_{\mathrm{ch}}/d\eta$, in data and simulation. The left panel shows the $dN_{\mathrm{ch}}/d\eta$ in data, for charged particles with $0.4 < p_{\mathrm{T}} < 5$ GeV, for multiple

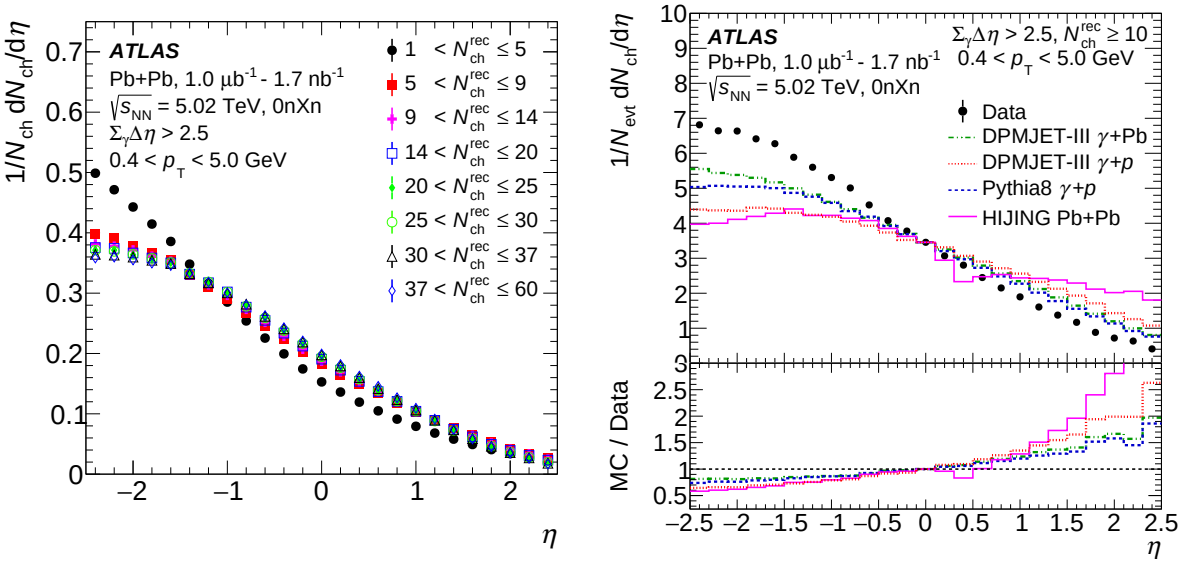

Figure 5: Left: Charged-particle pseudorapidity distribution, $dN_{\mathrm{ch}}/d\eta$, in selected $N_{\mathrm{ch}}^{\mathrm{rec}}$ ranges. The distributions are normalized to the same integral and are shown in arbitrary units. Here, positive and negative η denote the photon-going and nucleus-going directions, respectively. Right: $dN_{\mathrm{ch}}/d\eta$ distribution in data for $N_{\mathrm{ch}}^{\mathrm{rec}} > 10$ (black points), normalized per event, and compared with that in DPMJET-III γ+Pb (dot-dashed green histogram), Pythia γ+p (dashed blue histogram), peripheral Hijing Pb+Pb (solid magenta histogram), and DPMJET-III γ+p (dotted red histogram) with the same reconstruction-level selection as the data. All distributions have been normalized to have the same value as DPMJET-III γ+Pb at $\eta = 0$.

$N_{\mathrm{ch}}^{\mathrm{rec}}$ selections in photonuclear events. The distributions are corrected for tracking efficiency on a per-track basis, which ranges from 0.7–0.9 depending on track η and p_{T}. To compare the relative shapes between $N_{\mathrm{ch}}^{\mathrm{rec}}$ selections, the distributions are each normalized to have an integral of one. In all cases, the pseudorapidity distributions are strongly asymmetric, peaking at $\eta = -2.5$ (the nucleus-going direction) and then monotonically decreasing until $\eta = +2.5$ (the photon-going direction). This overall shape is even more asymmetric than that observed in, for example, p+Pb collisions at the LHC [53]. The $dN_{\mathrm{ch}}/d\eta$ shape remains similar over a wide range of multiplicities ($N_{\mathrm{ch}}^{\mathrm{rec}} > 10$). The selection with $N_{\mathrm{ch}}^{\mathrm{rec}} < 5$ results in an even more strongly asymmetric $dN_{\mathrm{ch}}/d\eta$ shape, suggesting that it may include photonuclear events at significantly lower energies or other processes. Additionally, as discussed above, the region $N_{\mathrm{ch}}^{\mathrm{rec}} < 10$ is not well described by simulation, and may contain a significant contribution from background events. On the basis of these observations, the two-particle correlation analysis is performed using events with $N_{\mathrm{ch}}^{\mathrm{rec}} \geq 10$. Additionally, an upper bound of $N_{\mathrm{ch}}^{\mathrm{rec}} = 60$ is used to remove the region with very few events.

The right panel in Figure 5 compares the pseudorapidity distribution of particles with $0.4 < p_{\mathrm{T}} < 5$ GeV in data for $N_{\mathrm{rec}}^{\mathrm{ch}} \geq 10$ with the four sets of simulated events, which have the same reconstruction-level selections as the data. While all three generators considered here systematically fail to predict a steep enough slope for the $dN_{\mathrm{ch}}/d\eta$ distribution, the distribution for DPMJET-III γ+Pb events is the most similar to that observed in data.

In general, no single generator is able to quantitatively describe in detail all of the features observed in data. The results here may be used to benchmark future developments in the modeling of photonuclear collisions. The two-particle correlation analysis described in Section 5, due its data-driven nature, does not rely on a detailed description of photonuclear events in simulation and therefore its results are not sensitive

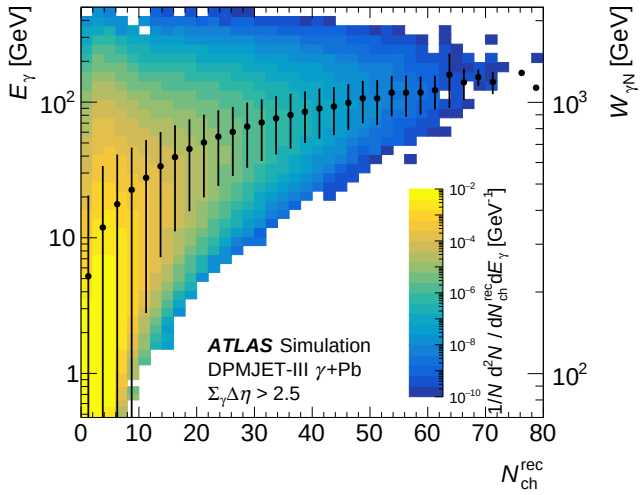

Figure 6: Correlation between photon energy E_γ and event multiplicity $N_{\text{ch}}^{\text{rec}}$ in simulated DPMJET-III γ+Pb events. The right-hand axis shows the center-of-mass energy W for the photon–nucleon collision system. The markers and vertical errors bars show the mean and standard deviation, respectively, of E_γ as a function of $N_{\text{ch}}^{\text{rec}}$.

to this mismodeling.

Since the DPMJET-III γ+Pb simulation and the data agree qualitatively in the $N_{\text{ch}}^{\text{rec}}$ and $\Sigma_\gamma\Delta\eta$ distributions, the simulated events provide an estimate of what ranges of photon energy in the laboratory frame, E_γ, and photon–nucleon center-of-mass energy, $W_{\gamma\text{N}}$, are selected for analysis by choosing various $N_{\text{ch}}^{\text{rec}}$ or $\Sigma_\gamma\Delta\eta$ values. These ranges are shown in Figure 6 as a function of $N_{\text{ch}}^{\text{rec}}$. In DPMJET-III, photonuclear events with a larger $N_{\text{ch}}^{\text{rec}}$ have a larger average E_γ and $W_{\gamma\text{N}}$. At $N_{\text{ch}}^{\text{rec}} = 10$, the mean values are $\langle E_\gamma \rangle = 26.8$ GeV and $\langle W_{\gamma\text{N}} \rangle = 519$ GeV, rising to $\langle E_\gamma \rangle = 123$ GeV and $\langle W_{\gamma\text{N}} \rangle = 1.11$ TeV at $N_{\text{ch}}^{\text{rec}} = 60$. However, even a narrow range of $N_{\text{ch}}^{\text{rec}}$ values selects events with a broad distribution of E_γ and $W_{\gamma\text{N}}$. At lower values of $N_{\text{ch}}^{\text{rec}} < 10$, the mean photon energy decreases rapidly and the range of photon energies increases, supporting the data-driven minimum value of $N_{\text{ch}}^{\text{rec}}$ determined above.

5 Two-particle correlations

This section describes the two-particle correlation and template fit procedures used to extract the azimuthal anisotropies, v_n. These procedures have been used in previous analyses of two-particle correlations in small systems [4, 5, 34, 54, 55], and are summarized here.

Correlations between pairs of charged particles are reported as a function of the pair's relative separation in pseudorapidity, $\Delta\eta = \eta^a - \eta^b$, and azimuth, $\Delta\phi = \phi^a - \phi^b$. The labels a and b denote kinematic selections on the first and second particle, which are generally different. If two particles each meet selections a and b, the pair is tabulated twice, once for each possible assignment. By convention, the distributions in $\Delta\eta$ and $\Delta\phi$, $Y(\Delta\phi, \Delta\eta)$, are averaged over events by normalizing them by the total yield of particles in selection a, N_a,

$$Y(\Delta\phi, \Delta\eta) = \frac{1}{N_a} \frac{d^2 N_{\text{pair}}}{d\Delta\phi \cdot d\Delta\eta}.$$

To correct for the charged-particle reconstruction efficiency, entries in the distribution are weighted by the product of the inverse efficiencies evaluated for the kinematics of the two particles. These efficiencies are derived from the HIJING simulation described in Section 3. In this analysis, all charged-particle tracks within $|\eta| < 2.5$ are considered, except the tracks which lie in the region $\eta > 4.9 - \Sigma_\gamma \Delta\eta$ (with positive η defined as the photon-going direction), if the sum-of-gaps extends into the tracker. There are two reasons to exclude these tracks. First, in simulations of photonuclear events, such particles are typically fragments of resolved photons, and not the bulk particles produced in the γ+Pb interaction which are being measured for possible collective signatures. Second, since these tracks are typically near the edge of the inner detector's acceptance, the $|\Delta\eta|$ restriction described below would result in a small number of tracks being paired many times, and thus making an disproportionately large contribution to the correlation function.

The one-dimensional $\Delta\phi$ normalized pair yields, $Y(\Delta\phi)$, are constructed by integrating over a restricted $|\Delta\eta|$ range, typically 2.0 to 5.0, designed to suppress the contributions to the correlation from non-flow effects (such as jets, particle decays, and resonances), as:

$$Y(\Delta\phi) = \int_{|\Delta\eta|=2.0}^{|\Delta\eta|=5.0} Y(\Delta\phi, |\Delta\eta|)\, d|\Delta\eta|.$$

In principle, due to finite coverage and detection efficiency introduced by a real detector, Y may contain acceptance effects that do not reflect physical particle pair correlations. To account for this, a mixed-event technique may be applied [56], in which particles a and b are taken from different events that have similar overall characteristics. The two events are required to have a ZDC signature on the same side (i.e. same directions of the photon and nucleus), and a similar charged-particle multiplicity, primary vertex position, and cluster edge gap $\Delta\eta_{\text{edge}}^{\text{cluster}}$. The mixed-event distribution $d^2N_{\text{mixed}}/(d\Delta\phi d\Delta\eta)$ contains the effects of the pair acceptance but not the physical correlations.

The acceptance effects can be corrected for by dividing the same-event pair distribution by the mixed-event ones. The two-dimensional (2-D) correlation function corrected for acceptance effects is

$$C(\Delta\phi, \Delta\eta) = \frac{1}{N_a} \frac{d^2N_{\text{pair}}}{d\Delta\phi d\Delta\eta} \Bigg/ \frac{1}{N_{\text{pair}}^{\text{mixed}}} \frac{d^2N_{\text{mixed}}}{d\Delta\phi d\Delta\eta},$$

where N_a is the total yield of particles with selection a, N_{mixed} is the yield in mixed events, and $N_{\text{pair}}^{\text{mixed}}$ is the total integral of the mixed-event distribution $d^2N_{\text{mixed}}/(d\Delta\phi d\Delta\eta)$. Without the mixing correction, the 2-D $Y(\Delta\phi, \Delta\eta)$ distributions have an artificial triangular shape in $\Delta\eta$, reflecting the convolution of the single-particle acceptances $|\eta^a, \eta^b| < 2.5$. This effect is removed by the mixing correction, and the $\Delta\eta$ dependence of structures in the 2-D $C(\Delta\phi, \Delta\eta)$ distributions become more evident.

Correlation functions are constructed for various selections on $N_{\text{ch}}^{\text{rec}}$ and p_{T}^a, with the p_{T} of particle b always in the range $0.4 < p_{\text{T}}^b < 2$ GeV. All events are given an equal statistical weight, and no corrections for the trigger efficiency or differences in sampled luminosity (for $N_{\text{ch}}^{\text{rec}}$ ranges that span contributions from multiple triggers) are performed. Although the mixed-event correction is necessary to properly construct the two-dimensional correlation functions presented below, it was found to ultimately have only a minor effect on the projected, one-dimensional $Y(\Delta\phi)$ distributions, producing compatible results but with increased statistical uncertainty. Thus the mixing correction is not applied for the nominal v_2 and v_3 results. Instead, it is used in the determination of systematic uncertainties associated with the pair acceptance of the detectors as described in Section 6.

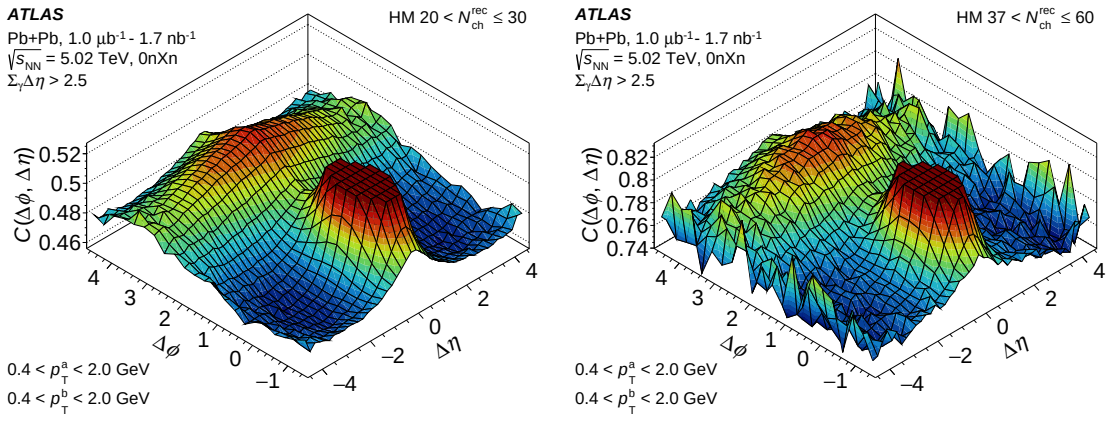

Figure 7: Two-dimensional normalized particle pair distributions in photonuclear events, corrected for acceptance effects with the mixed-event distribution, and presented as a function of $\Delta\eta$ and $\Delta\phi$. The peak at $(\Delta\phi, \Delta\eta) = (0, 0)$ is truncated to better show the structure of the correlation function. Each panel represents a different charged-particle multiplicity $N_{\mathrm{ch}}^{\mathrm{rec}}$ range for the selection $0.4 < (p_{\mathrm{T}}^{a}, p_{\mathrm{T}}^{b}) < 2.0$ GeV.

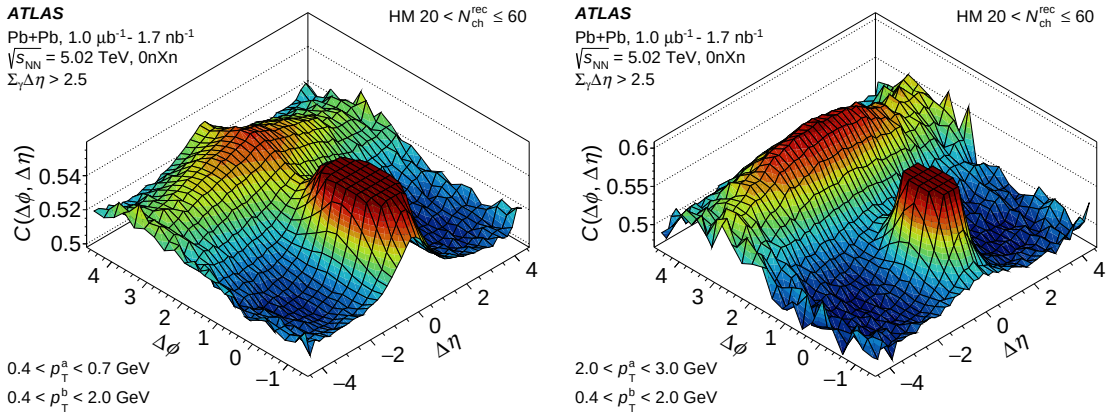

Figure 8: Two-dimensional normalized particle pair distributions in photonuclear events, corrected for acceptance effects with the mixed-event distribution, and presented as a function of $\Delta\eta$ and $\Delta\phi$. The peak at $(\Delta\phi, \Delta\eta) = (0, 0)$ is truncated to better show the structure of the correlation function. Each panel represents a different p_{T}^{a} range for the selection $20 < N_{\mathrm{ch}}^{\mathrm{rec}} < 60$ and $0.4 < p_{\mathrm{T}}^{b} < 2.0$ GeV.

Examples of two-dimensional $C(\Delta\phi, \Delta\eta)$ correlation functions are presented in Figure 7 and Figure 8. In Figure 7, particles a and b are required to have $0.4 < p_{\mathrm{T}}^{a} < 2$ GeV , and two example $N_{\mathrm{ch}}^{\mathrm{rec}}$ selections are shown. In Figure 8, correlation functions are presented for $20 < N_{\mathrm{ch}}^{\mathrm{rec}} < 60$, with two example p_{T} selections for particle a shown. The two-dimensional correlation functions have features which are broadly similar to those observed in pp collisions. There is a localized 'near-side' peak at $(\Delta\phi, \Delta\eta) \approx (0, 0)$ from correlations between jet fragments, and an extended 'away-side' ridge at $\Delta\phi \approx \pi$ which extends over a large $\Delta\eta$ range from correlations between fragments of azimuthally opposite jets. A quantitative analysis and non-flow subtraction are necessary to discern if there are additional ridge structures, as detailed below.

5.1 Non-flow subtraction

To remove the contribution to the correlation function from non-flow effects that persist as long-range contributions on the away side ($\Delta\phi \sim \pi$), a template fit procedure is employed. To perform the fit procedure, samples corresponding to events with low multiplicity (LM) and high multiplicity (HM) are selected. The shape of the non-flow contribution is assumed in the template procedure to be the same in the LM and HM samples. In this analysis, the LM events are chosen to have $15 \leq N_{\mathrm{ch}}^{\mathrm{rec}} \leq 20$.

The $Y(\Delta\phi)$ in HM events is parameterized as the sum of an azimuthally modulated pedestal (which expresses the azimuthal anisotropy) and a non-flow component, as follows:

$$\begin{aligned} Y^{\mathrm{HM}}(\Delta\phi) &= FY^{\mathrm{LM}}(\Delta\phi) + G\left\{1 + 2\sum_{n=2}^{4} v_{n,n}\cos(n\Delta\phi)\right\} \\ &= FY^{\mathrm{LM}}(\Delta\phi) + Y^{\mathrm{ridge}}(\Delta\phi). \end{aligned} \tag{1}$$

Above, $Y^{\mathrm{LM}}(\Delta\phi)$ is the correlation function in LM events, which is parameterized as a truncated Fourier series up to the fourth order (with coefficients c_n for $n = 0, \ldots, 4$). The values of F and G, the three $v_{n,n}$ values, and the five parameters c_n, describing the LM reference, are free parameters in the fit, but F and G are constrained such that the integrals of both sides of Eq. (1) are the same. Modulation terms up to fourth order ($v_{2,2}$, $v_{3,3}$, and $v_{4,4}$) are considered in the fit, in order to best describe the HM data. By fitting $Y^{\mathrm{LM}}(\Delta\phi)$ and $Y^{\mathrm{HM}}(\Delta\phi)$ simultaneously, the extracted uncertainty in F, G, and $v_{n,n}$ correctly accounts for the statistical uncertainty of both the LM and HM samples. An example of the simultaneous fit of the HM selection and LM reference is shown in Figure 9. Examples of the template fit in additional HM and p_{T}^{a} selections are shown in Figure 10. In the bottom panels of Figs. 9 and 10, the p-values are defined following the procedure described below.

The template fit is performed by minimizing the standard χ^2 between the data points and the functional form. However, the data points within the correlation functions contain nontrivial point-to-point correlations, since a single particle b may be used in combination with multiple particles of type a. The minimum of the χ^2 statistic, when calculated in the traditional way, is found at the appropriate values of the fit parameters. However, the p-value and the uncertainty in the parameter values, if also determined in the standard way, would be inaccurate. In order to properly account for these correlations and determine the parameter value uncertainties, a bootstrapping procedure was applied. Pseudo-experiments were generated by giving a random Poisson weight (with a mean of one) to individual events. These pseudo-experiments are independent sets of events drawn from the observed set of events with the same statistics and correlations as the real data. The parameters values extracted in the pseudo-experiments agreed with those in data and followed Gaussian distributions. The standard deviations of the parameters values extracted from the pseudo-experiments were used to set the statistical uncertainties in the final results, which are 10–30% larger than if they were estimated in the naïve way without taking the point-to-point correlations into account. The p-values from the bootstrapping experiment are presented in the template fit plots that follow.

The full set of $v_{2,2}$ and $v_{3,3}$ values are shown in Figure 11. The filled points show the non-flow subtracted results according to the template fit procedure in Eq. (1). The open points show the $v_{n,n}$ values that would be obtained if instead a direct Fourier decomposition of Y^{HM} were performed, without any attempt to account for the non-flow contribution. For most of the selections considered here, the non-flow subtraction

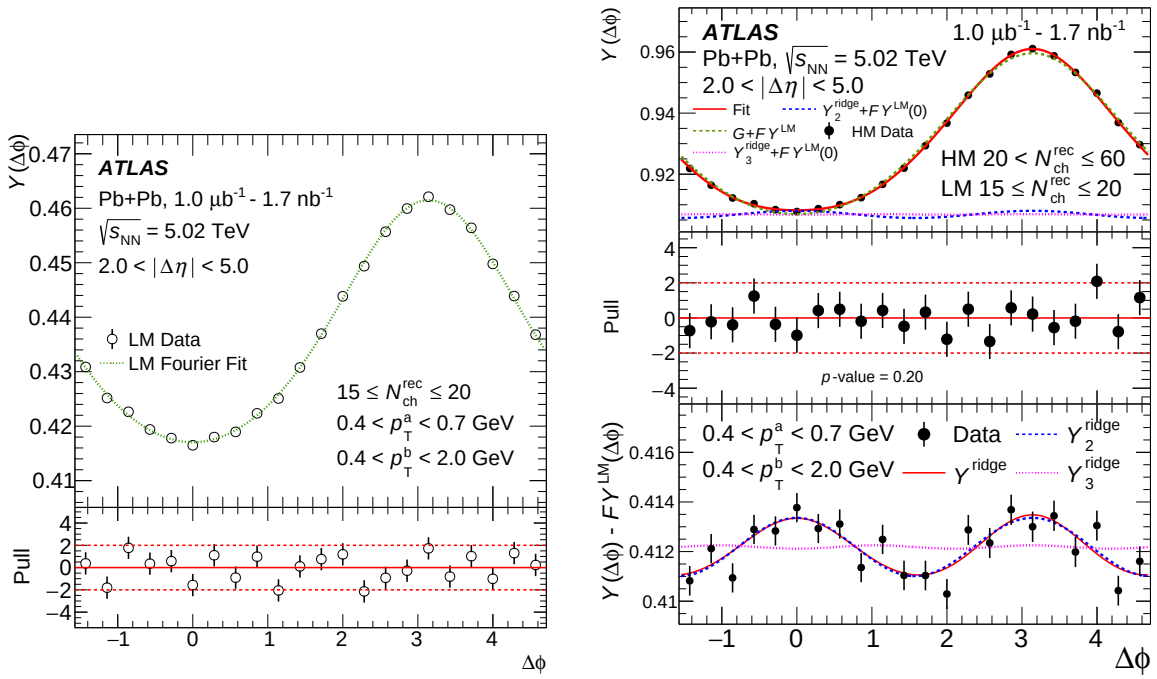

Figure 9: An example of the template-fitting procedure for a selected p_{T} range. The left plot displays the LM data with open markers and the simultaneous fit in the green dotted line. The lower panel displays the pull distribution. In the top panel of the right plot, the solid red line shows the total fit to the HM data in black markers. The dashed green line shows the scaled LM plus pedestal, while the dashed blue and dotted magenta lines indicate the two flow contributions to the fit, $Y_2^{\mathrm{ridge}} = G[1 + 2v_{2,2}\cos(2\Delta\phi)]$ and $Y_3^{\mathrm{ridge}} = G[1 + 2v_{3,3}\cos(3\Delta\phi)]$, shifted upwards by $FY^{\mathrm{LM}}(0)$ for visibility. The middle-right panel shows the pull distribution for the template fit in the top panel. The bottom-right panel shows the same set of data and fit components, where the scaled LM distribution has been subtracted to better isolate the modulation.

has a significant effect on the extracted $v_{2,2}$ and $v_{3,3}$ values. The resulting $v_{n,n}$ values are positive in all selections, with one exception: in the p_{T}^a-dependent results with a single HM selection, the $v_{2,2}$ value for $3 < p_{\mathrm{T}} < 5$ GeV is negative. Additionally, the $v_{2,2}$ value for $2 < p_{\mathrm{T}} < 3$ GeV is significantly lower than that for $1.2 < p_{\mathrm{T}} < 2$ GeV. In these selections, the $v_{3,3}$ values also rise significantly. The template fits to these selections are shown in Figure 12, and are discussed further below.

5.2 Factorization test

In the flow paradigm, a two-particle azimuthal modulation characterized by a $v_{n,n}$ value arises from the product of nonzero azimuthal anisotropies, v_n, for each particle. These are related via $v_{n,n}(p_{\mathrm{T}}^a, p_{\mathrm{T}}^b) = v_n(p_{\mathrm{T}}^a)v_n(p_{\mathrm{T}}^b)$, or $v_{n,n}(p_{\mathrm{T}}^a, p_{\mathrm{T}}^b) = v_n(p_{\mathrm{T}})^2$ if a and b are selected from the identical particle p_{T} range. Thus, a single-particle flow coefficient $v_n(p_{\mathrm{T}}^a)$ may be determined from two-particle $v_{n,n}$ values through $v_n(p_{\mathrm{T}}^a) = v_{n,n}(p_{\mathrm{T}}^a, p_{\mathrm{T}}^b)/v_n(p_{\mathrm{T}}^b) = v_{n,n}(p_{\mathrm{T}}^a, p_{\mathrm{T}}^b)/\sqrt{v_{n,n}(p_{\mathrm{T}}^b, p_{\mathrm{T}}^b)}$ for a given selection on reference particle b. To test whether the $v_{n,n}$ values in data are compatible with this picture, a factorization test can be performed in which v_n values for particle a are compared for different particle b selections. The results of this test for the v_2 values as a function of $N_{\mathrm{ch}}^{\mathrm{rec}}$ are shown in Figure 13. The test demonstrates that while the $v_{2,2}$ values for different p_{T}^b selections may be different, the v_2 values obtained for particle a as a function

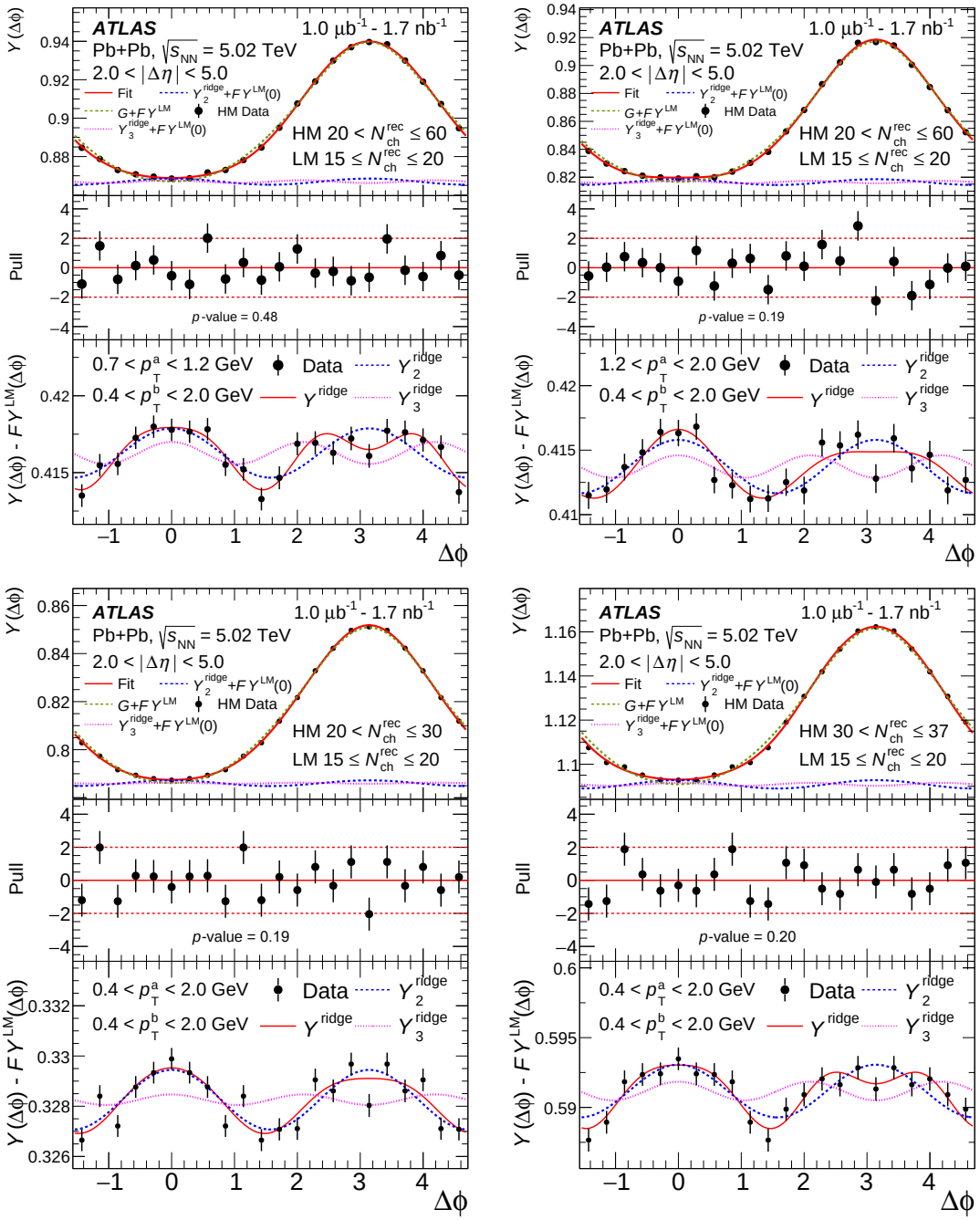

Figure 10: Selected template fit results for two p_{T}^{a} intervals (top row) and two $N_{\mathrm{ch}}^{\mathrm{rec}}$ intervals (bottom row). In the top panel of the right plot, the solid red line shows the total fit to the HM data in black markers. The dashed green line shows the scaled LM plus pedestal, while the dashed blue and dotted magenta lines indicate the two flow contributions to the fit, $Y_2^{\mathrm{ridge}} = G[1 + 2v_{2,2}\cos(2\Delta\phi)]$ and $Y_3^{\mathrm{ridge}} = G[1 + 2v_{3,3}\cos(3\Delta\phi)]$, shifted upwards by $FY^{\mathrm{LM}}(0)$ for visibility. The middle panels show the pull distribution for the template fits in the top panel. The p-values from the bootstrapping experiment are also shown in the middle panels. The bottom panels show the same set of data and fit components, where the scaled LM distribution has been subtracted from each to better isolate the modulation.

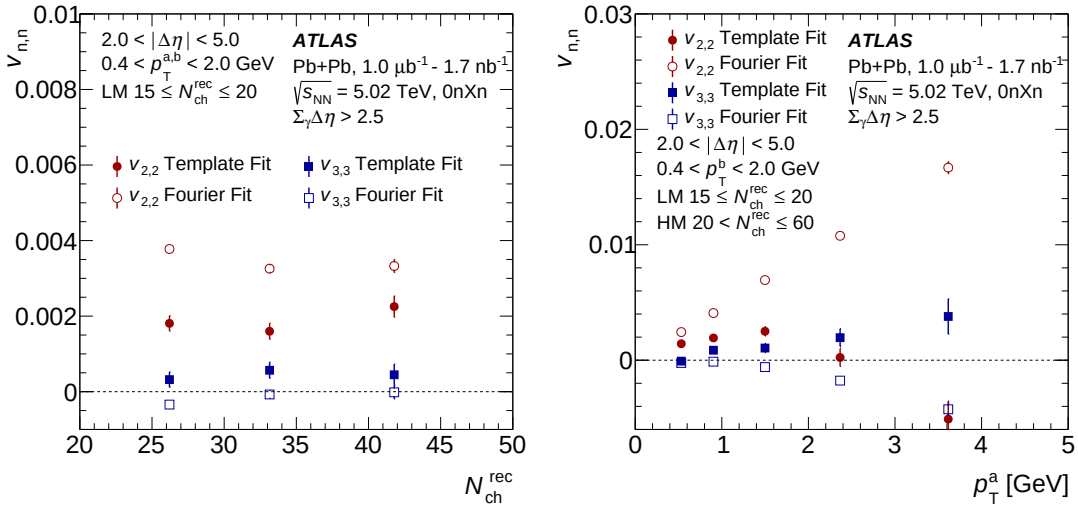

Figure 11: Summary of $v_{2,2}$ and $v_{3,3}$ results as obtained from a direct Fourier fit (open markers) and those obtained after the template-fitting subtraction (filled markers). Results are shown differential in $N_{\mathrm{ch}}^{\mathrm{rec}}$ for fixed p_{T}^{a} (left) and differential in p_{T}^{a} for fixed $N_{\mathrm{ch}}^{\mathrm{rec}}$ (right).

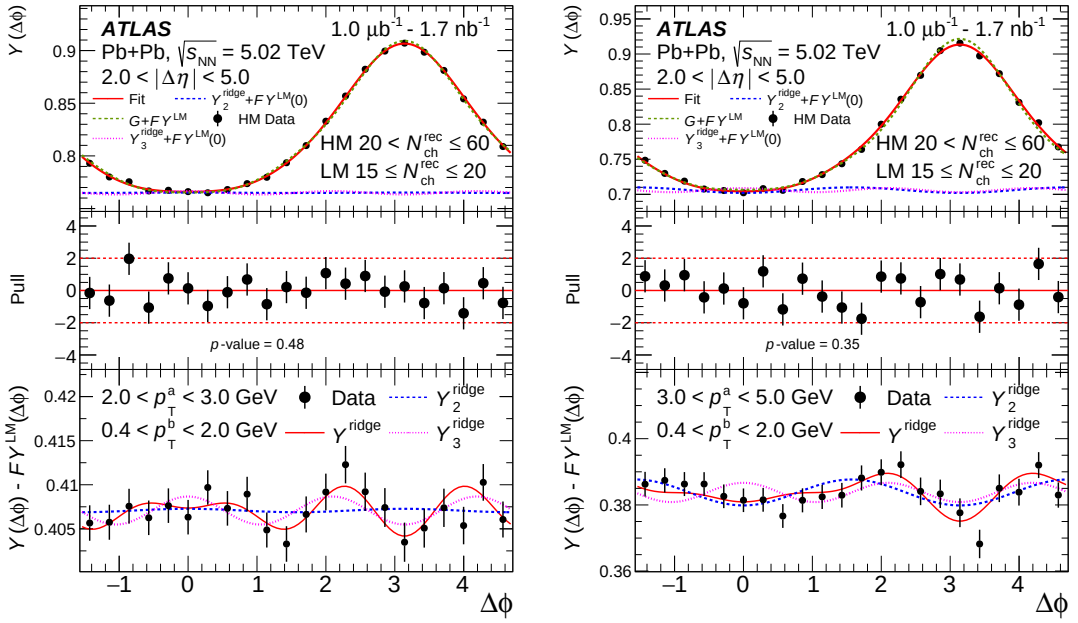

Figure 12: Selected template fit results for the highest p_{T}^{a} intervals. In the top panel of the right plot, the solid red line shows the total fit to the HM data in black markers. The dashed green line shows the scaled LM plus pedestal, while the dashed blue and dotted magenta lines indicate the two flow contributions to the fit, $Y_2^{\mathrm{ridge}} = G[1+2v_{2,2}\cos(2\Delta\phi)]$ and $Y_3^{\mathrm{ridge}} = G[1+2v_{3,3}\cos(3\Delta\phi)]$, shifted upwards by $FY^{\mathrm{LM}}(0)$ for visibility. The middle panels show the pull distribution for the template fits in the top panel. The p-values from the bootstrapping experiment are also shown in the middle panels. The bottom panels show the same set of data and fit components, where the scaled LM distribution has been subtracted from each to better isolate the modulation.

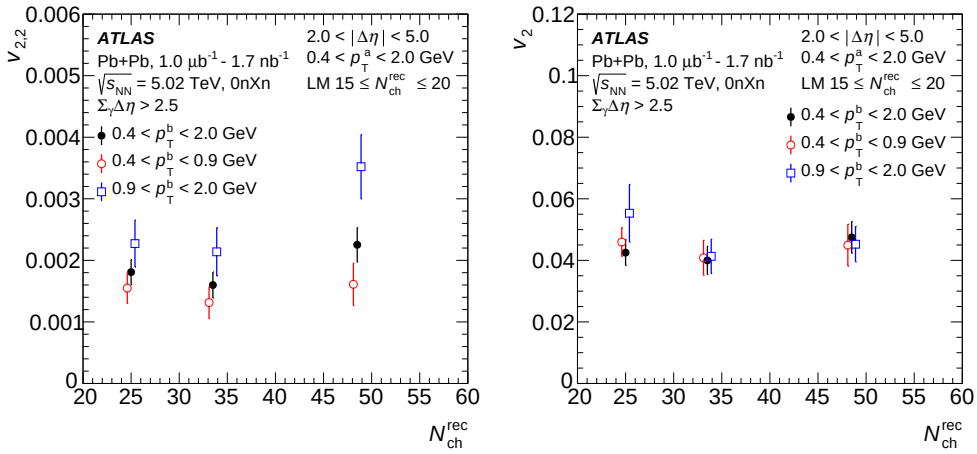

Figure 13: Summary of the factorization test for v_2 values as a function of N_{ch}^{rec}. Comparison of $v_{2,2}$ values (left) and derived v_2 values (right) using the same particle a selection, but different selections on particle b. Only statistical uncertainties are shown. The points are displaced horizontally for visibility.

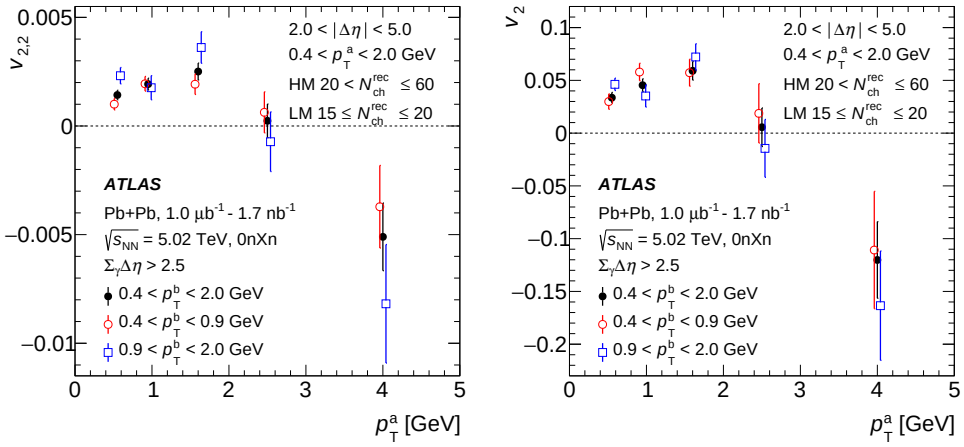

Figure 14: Summary of the factorization test for v_2 values as a function of p_T^a. Comparison of $v_{2,2}$ (left) and derived v_2 values (right) using the same particle a selection, but with different selections on particle b. Only statistical uncertainties are shown. The points are displaced horizontally for visibility.

of N_{ch}^{rec} are independent of the selection for particle b. This is a necessary condition of the paradigm that the observed $v_{2,2}$ values arise from the product of event-wide, single-particle v_2 azimuthal modulations.

Figure 14 shows the results of a factorization test as a function of particle a p_T. Although this test is more statistically limited than that for the N_{ch}^{rec}-dependent test above, the results for $p_T^a < 2$ GeV are compatible with the factorization assumption. Since non-flow effects are not necessarily expected to factorize, this validates an important assumption of the template procedure. For the selection with $p_T^a > 3$ GeV, the $v_{2,2}$ values obtained in Figure 14 are significantly negative, and are accompanied by large $v_{3,3}$ values. A negative $v_{2,2}$ value violates the expected factorization for particles with independent overall modulation, and thus cannot be interpreted as arising from hydrodynamic flow.

As can be seen from the growing Fourier $v_{2,2}$ values in Figure 11 and the large away-side peaks in Figure 12,

the non-flow contribution in these high-p_{T}^{a} selections is significantly larger than the magnitude of any possible modulation. Thus, the extraction of any genuine $\cos(n\Delta\phi)$ modulation is highly sensitive to assumptions in the template method about the scaling of the non-flow contribution between multiplicity classes. If violated, this could manifest as a reduced $v_{2,2}$ and increased $v_{3,3}$. This assumption is difficult to test given the limited data sample size for LM variations and factorization tests. Therefore, within the present uncertainties and techniques, the v_2 cannot be reliably extracted at high p_{T}. Finally, the statistical precision of the data does not allow similar tests of the v_3 values. In this case, their presented values assume that factorization holds.

In Section 7 the v_2 and v_3 values are presented for all p_{T} for completeness, although it should be noted that factorization has been demonstrated only for v_2 in the range $0.4 \leq p_{\mathrm{T}} \leq 2.0$ GeV.

5.3 Physics backgrounds

The measured v_n values are potentially biased by the presence of background events, primarily from peripheral hadronic Pb+Pb events, in the selected event sample. The purity of photonuclear events is estimated by fitting templates derived from simulated photonuclear and peripheral Pb+Pb events to distributions measured in data, and determining the fraction of selected events which are compatible with photonuclear interactions.

The purity was first estimated by fitting the $\Sigma_\gamma\Delta\eta$ distribution in data to the combination of distributions from DPMJET-III γ+Pb events and peripheral Hijing Pb+Pb events over the range $0.5 < \Sigma_\gamma\Delta\eta < 4.9$, with the relative contributions from each as free parameters. An example of these two contributions and the distribution in data is shown in the right panel of Figure 4. This fit was performed separately in each of the $N_{\mathrm{ch}}^{\mathrm{rec}}$ selections used in the measurement. The purity for the $\Sigma_\gamma\Delta\eta > 2.5$ selection is estimated to be greater than 98% in all $N_{\mathrm{ch}}^{\mathrm{rec}}$ selections used in the analysis. Thus, for the nominal results, no correction for a possible impurity in the selected events is performed.

6 Systematic uncertainties

The primary sources of systematic uncertainty are grouped by category and discussed below. The systematic uncertainties are evaluated by varying the procedure applied to the data, and are not directly derived from the simulation samples described in Section 4.2. Thus, the uncertainties do not depend on an accurate modeling of the photonuclear processes in simulation. The uncertainties from each source are ultimately combined in quadrature to obtain the total systematic uncertainty. For some individual sources below where only one variation of the analysis procedure was performed, the resulting uncertainty was symmetrized by adding an uncertainty of equal magnitude in the other direction. However, in general the final systematic uncertainties are not symmetric. The typical magnitudes of the systematic uncertainties are summarized in Table 1.

Pair-pseudorapidity difference. The two-particle correlation function is measured for pairs with $2.0 < |\Delta\eta| < 5.0$ as a way to strongly reduce the non-flow contribution, which varies much more strongly with $\Delta\eta$ than the genuine long-range azimuthal modulation. To test the sensitivity of the analysis to a potential residual contribution, the lower bound on $\Delta\eta$ is varied to 1.8 and to 2.2, and the impact of the resulting variations on the data is included as an uncertainty.

Table 1: Summary of sources of systematic uncertainty, and the typical values of their absolute magnitude. The last row shows the typical total uncertainties from the quadrature sum of all uncertainties.

Source	$v_2(N_{\mathrm{ch}}^{\mathrm{rec}})$	$v_2(p_{\mathrm{T}})$	$v_3(N_{\mathrm{ch}}^{\mathrm{rec}})$	$v_3(p_{\mathrm{T}})$
$\Delta\eta$ pair cut	0–0.002	0.01–0.02	0–0.015	0–0.03
LM reference	0.001	0–0.02	0–0.005	0.03–0.06
ϕ binning	0.001	0–0.01	0.001	0–0.01
Mixed-event correction	0.001	0–0.01	0–0.005	0–0.01
Track $\Sigma_\gamma\Delta\eta$ exclusion	0.001	0–0.02	0.002	0–0.01
Purity	0–0.002	0–0.02	0.005	0–0.02
Total	0.001–0.002	0.005–0.04	0.005–0.015	0.03–0.07

Low-multiplicity reference. Photonuclear events with $15 \leq N_{\mathrm{ch}}^{\mathrm{rec}} \leq 20$ are used as the LM reference in the template fit to the other $N_{\mathrm{ch}}^{\mathrm{rec}}$ selections. In the template method, the shape of the non-flow contribution is assumed to be the same in the LM and HM selections. To test the possible variation of the non-flow contribution with multiplicity, the analysis may be repeated using an alternative reference for LM events. Additionally, a different multiplicity range may select a different sample of photonuclear events (i.e. distribution of photon energies, or mix of resolved and direct processes [18]), to which the results may be sensitive. An alternative selection, $10 \leq N_{\mathrm{ch}}^{\mathrm{rec}} < 15$, composed from the MB trigger data, is considered for the LM reference. The analysis is repeated and the difference in the results is included in the uncertainties.

$\Delta\phi$ binning. The sensitivity to the particular choice of $\Delta\phi$ binning was evaluated by repeating the fitting procedure after halving the number of bins. The resulting difference is included in the total uncertainty.

Acceptance effects in correlation function. For the nominal analysis, the $\Delta\phi$-dependent correlation functions are formed by projecting the 2-D correlation functions in the region $2 < |\Delta\eta| < 5$. To test the possible impact of acceptance effects that may result in a distortion of the $\Delta\phi$ distribution, the correlation functions are corrected by the projection of the mixed-event 2-D correlation function onto $\Delta\phi$, as described in Section 5. The differences in the results are assigned as a systematic uncertainty.

Exclusion of tracks from $\Sigma_\gamma\Delta\eta$. The default analysis excludes reconstructed tracks that are within the sum-of-gaps range from the two-particle correlations, i.e. those with $\eta > 4.9 - \Sigma_\gamma\Delta\eta$. As a systematic variation, these tracks are included in constructing the correlation functions. The resulting differences are included as a systematic uncertainty.

Photonuclear event purity. The estimate of the purity of photonuclear events in data relies on the description of γ+Pb event properties in simulation. To test the sensitivity to this description, the fit described in Section 5.3 was repeated using Pythia γ+p events as the model for photonuclear events and, alternatively, by fitting to the $N_{\mathrm{ch}}^{\mathrm{rec}}$ distribution, separately in different slices of $\Sigma_\gamma\Delta\eta$. In the latter case, the purity decreases to approximately 90% in events with $N_{\mathrm{ch}}^{\mathrm{rec}} = 15$–20 and to 80% in those with $N_{\mathrm{ch}}^{\mathrm{rec}} = 10$–15, which are the ranges used to define the nominal and alternative LM selections for the two-particle correlation analysis.

In the default analysis, no correction is made for a possible presence of backgrounds, primarily peripheral Pb+Pb events, in the selected sample of high-multiplicity γ+Pb events. As a systematic variation, the $\Delta\phi$ distributions in data are corrected by subtracting the contribution from these background events, scaled to match the purity in each $N_{\mathrm{ch}}^{\mathrm{rec}}$ range. Since the potential impact of the purity is much larger for events with

low $N_{\mathrm{ch}}^{\mathrm{rec}}$ than those with high $N_{\mathrm{ch}}^{\mathrm{rec}}$, the effect on the analysis is evaluated by accounting for the possible presence of backgrounds only in the LM reference. Additionally, since the purity was observed to be lower in the alternative LM reference events, $N_{\mathrm{ch}}^{\mathrm{rec}} = 10$–$15$, than in the nominal LM selection, the difference in the results using the alternative LM reference, with and without the purity correction, was taken as the uncertainty for this source. The model $\Delta\phi$ distributions for the background events are taken from pp collision data at $\sqrt{s} = 5$ TeV [57], with the same reconstruction, definition of $N_{\mathrm{ch}}^{\mathrm{rec}}$, and gap-based event selection, as this analysis. The resulting differences are included as a systematic uncertainty.

Other uncertainty sources and checks. Several other potential sources were investigated, and were found to have a negligible effect on the results and thus are not included in the total uncertainty. These include: comparing the results using only events where the photon is headed towards the A side of the detector with those where it is headed towards the C side; the number of Fourier terms used in parameterizing the LM reference distribution; the number of additional Fourier terms beyond $n = 4$ used in the template fit; the impact of a possible misalignment of the tracker on the charged-particle measurement; the impact of the correction for the finite tracking efficiency; and the impact of correcting for the trigger efficiency and different luminosities of the triggered event samples as a function of $N_{\mathrm{ch}}^{\mathrm{rec}}$ on a per-event basis.

While the $\Sigma_\gamma\Delta\eta > 2.5$ requirement is treated as an operational event definition which is not a source of uncertainty, the results using alternative definitions $\Sigma_\gamma\Delta\eta > 2.0$ and $\Sigma_\gamma\Delta\eta > 3.0$ were not significantly different from the nominal results. This demonstrates that the sample of photonuclear events in data is robust against small changes in their selection criteria and against detector effects in the measurement of $\Sigma_\gamma\Delta\eta$.

Finally, the template method carries an implicit assumption that the modulation in the HM selection is the same as that in the LM selection. If this is not the case, the extracted v_n values in the HM selection will be biased to be systematically closer to those in the LM selection. In recent measurements of azimuthal anisotropies in small systems [58], a 'one-step' correction was employed using two adjacent LM reference bins to account for the possibly changing v_n magnitudes with multiplicity. Since the measured v_n values were observed to have no $N_{\mathrm{ch}}^{\mathrm{rec}}$ dependence within uncertainties, this alternative method was not utilized here.

As can be seen in Table 1, the systematic uncertainty is not dominated by any single source, and typically those from the pair-pseudorapidity difference, the choice of LM reference, and the event purity are co-dominant. The systematic uncertainties tend to be larger for the p_{T}-dependent results than for the $N_{\mathrm{ch}}^{\mathrm{rec}}$-dependent results, and are typically larger for the v_3 results than for the v_2 results. For the v_2 and v_3 results as a function of $N_{\mathrm{ch}}^{\mathrm{rec}}$, the statistical uncertainties are typically larger than the systematic uncertainties. However, for the results as a function of $p_{\mathrm{T}}^{\mathrm{ch}}$, the systematic uncertainties are generally larger. This reflects, for example, the greater sensitivity to the choice of LM reference, which must be divided into different $p_{\mathrm{T}}^{\mathrm{ch}}$ selections.

7 Results and discussion

This section presents the measurement of the second- and third-order flow coefficients in photonuclear collisions, in both cases as a function of $N_{\mathrm{ch}}^{\mathrm{rec}}$ and charged-particle p_{T}. These results are compared with previous measurements of v_2 and v_3 for inclusive charged hadrons by ATLAS in inelastic, minimum-bias 13 TeV pp collisions and in 5.02 TeV p+Pb collisions [5].

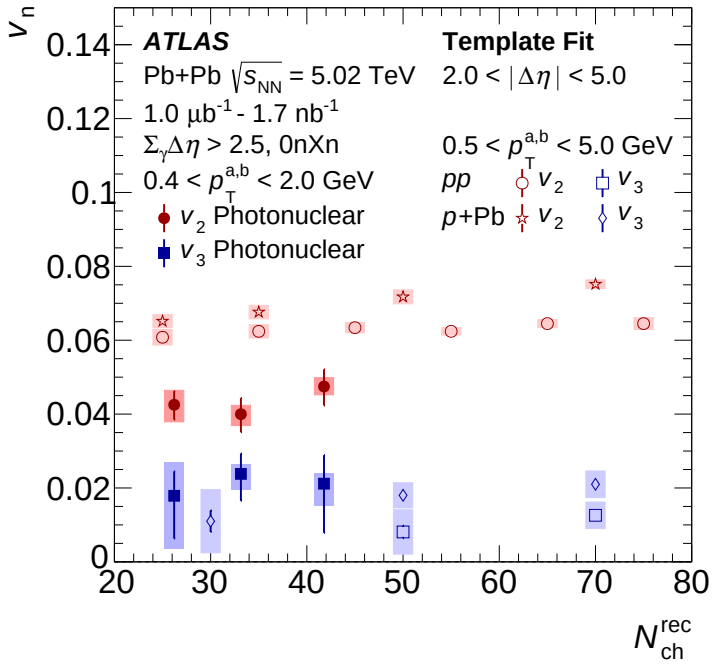

Figure 15: Flow coefficients v_2 and v_3 for charged particles with $0.5 < p_T < 2.0$ GeV in photonuclear events, reported as a function of charged-particle multiplicity N_{ch}^{rec}. The vertical error bars and colored boxes represent the statistical and total systematic uncertainties, respectively. The photonuclear data points are positioned at the average N_{ch}^{rec} value in each interval. The measurements in photonuclear events (solid symbols) are compared with those in pp collisions at 13 TeV and p+Pb collisions at 5.02 TeV [5] (open symbols), integrated over $0.5 < p_T < 5.0$ GeV.

Figure 15 presents the v_2 and v_3 values as a function of the event charged-particle multiplicity N_{ch}^{rec}. Significant, nonzero values for v_2 and v_3 are observed and they are compatible with no N_{ch}^{rec} dependence within uncertainties. The results are compared with previous measurements in pp and p+Pb collisions, presented here as a function of N_{ch}^{rec} for a slightly different p_T selection, $0.5 < p_T < 5$ GeV. Given the shape of the p_T distribution in high-multiplicity pp collisions [59] and the p_T-dependence of the v_2 values, the v_2 in pp collisions for $0.4 < p_T < 2$ GeV particles (the selection used in this measurement) may be at most 10% lower than the values presented for $0.5 < p_T < 5$ GeV. In photonuclear events, the v_2 values as a function of N_{ch}^{rec} are systematically below those in pp and p+Pb events, even after accounting for the different p_T ranges in the datasets. The v_3 values are compatible with those in pp and p+Pb events within significantly larger statistical and systematic uncertainties.

The v_2 and v_3 results as a function of charged-particle p_T are presented in Figure 16 for events with $20 < N_{ch}^{rec} \leq 60$. The v_2 results have central values similar to those plotted as a function of N_{ch}^{rec} in Figure 15 but have larger systematic and statistical uncertainties, due to the more limited size of the available data sample for the p_T-dependent LM references for these measurements. For v_2, the results trend towards negative values for $p_T \geq 2.0$ GeV, although with very large systematic uncertainties. It is notable that there is a statistically significant confirmation of factorization, as detailed in Section 5.2, only for v_2 with the selection $0.4 \leq p_T \leq 2.0$ GeV. Hence the values of v_2 and v_3 for $p_T \geq 2$ GeV have an additional caveat, arising from the fact that the magnitude of the flow signal relative to that of the non-flow contribution is significantly larger than at lower p_T. In particular, the trend towards negative v_2 values and rising v_3 values

suggests that the factorization assumption could be violated.

Figure 17 shows the same data as Figure 16, but zoomed in on the vertical axis to allow a better comparison with the analogous p_{T}-dependent values in the pp and p+Pb measurements described above, with the selection $N_{\mathrm{ch}}^{\mathrm{rec}} \geq 60$. In the region $0.4 < p_{\mathrm{T}} < 2$ GeV the central values of the v_2 are smaller than those in pp and p+Pb collisions, similar to that observed in the $N_{\mathrm{ch}}^{\mathrm{rec}}$-dependent results in Figure 15. However, due to the larger uncertainties in the p_{T}-dependent case, the v_2 values for photonuclear and pp collisions are compatible within the uncertainties of the former in the range $p_{\mathrm{T}} < 2$ GeV. The v_3 values are compatible between systems within large uncertainties.

There are currently no published theoretical predictions for flow coefficients in photonuclear collisions within a hydrodynamic or parton transport framework. In such frameworks, the elliptic and triangular flow coefficients scale with the initial geometry eccentricities, ε_2 and ε_3 respectively, and the charged-particle multiplicity $dN_{\mathrm{ch}}/d\eta$. In the vector-meson dominance picture, photon–hadron interactions arise through fluctuations of the photon into hadronic states with the same quantum numbers as vector mesons, which have a nontrivial initial transverse geometry. This geometry is determined by the spectrum of these fluctuations, and while models of this spectrum exist [60], they have not yet been adapted to provide quantitative models. In the absence of a complete model, the magnitude of the eccentricities can be estimated by noting that fluctuations of the photon into light vector-meson states such as the ρ give the largest contribution to the cross section. The initial geometries for ρ+Pb collisions can be computed with a Monte Carlo Glauber calculation [61] which treats the ρ meson as having two constituent quarks. The resulting mean values of the second- and third-order spatial eccentricities, ε_2 and ε_3, are nearly identical to those in the p+Pb case. Also, when comparing p+Pb and photonuclear events with the same $N_{\mathrm{ch}}^{\mathrm{rec}}$, in fact the relevant $dN_{\mathrm{ch}}/d\eta$ is larger in the photonuclear events since the particles are distributed over a smaller pseudorapidity region. Thus, one might naïvely expect the flow coefficients to be similar in photonuclear events and p+Pb collisions. However, in order to compare any such calculation with data, a full modeling of the photon fluctuations in the selected γ+Pb events needs to be carried out. In addition, correctly accounting for the boosted kinematics and limited acceptance using a fully three-dimensional simulation may be important.

An alternative interpretation of two-particle correlations in small collision systems involves interactions at the earliest time between gluon fields in the Color Glass Condensate (CGC) framework [62]. Recently such calculations have described heavy-flavor hadron and quarkonia azimuthal anisotropies in p+Pb collisions [63, 64], although calculations in the CGC framework fail to describe other aspects of the data, such as the charged-hadron flow coefficients in p+Pb at the LHC and small-systems collisions at RHIC [65, 66]. The authors have extended these calculations to consider a color dipole interacting with a Pb nucleus either at a future Electron Ion Collider or in photonuclear collisions at the LHC [31]. The CGC calculation for photonuclear collisions is shown in Figure 17 and is in reasonable agreement with the v_2 data within uncertainties. In these calculations, the Pb nucleus is described with a saturation scale $Q_s^2 = 5$ GeV^2 and typical parton transverse momentum $\Delta = 0.5$ GeV, as used in calculations of v_2 for heavy-flavor mesons and quarkonia [63, 64]. However, in the calculation for the photonuclear case, the parameter $B_p = 25$ GeV^{-2}, which controls the transverse area of the interaction and thus the number of color domains from the Pb nucleus taking part in the interaction, is significantly larger than in the previous calculations [63, 64]. A larger transverse area generally contains more color domains and results in a smaller value of v_2.

Finally, it is interesting to compare the data with results from DPMJET-III, which has neither CGC-related correlations nor hydrodynamic or parton scattering effects. This comparison sets a baseline and provides a check of the possible impact of issues such as the LM template choice (which accounts for non-flow) selecting events with photon energies that differ from the HM sample. The photon energy is expected to be

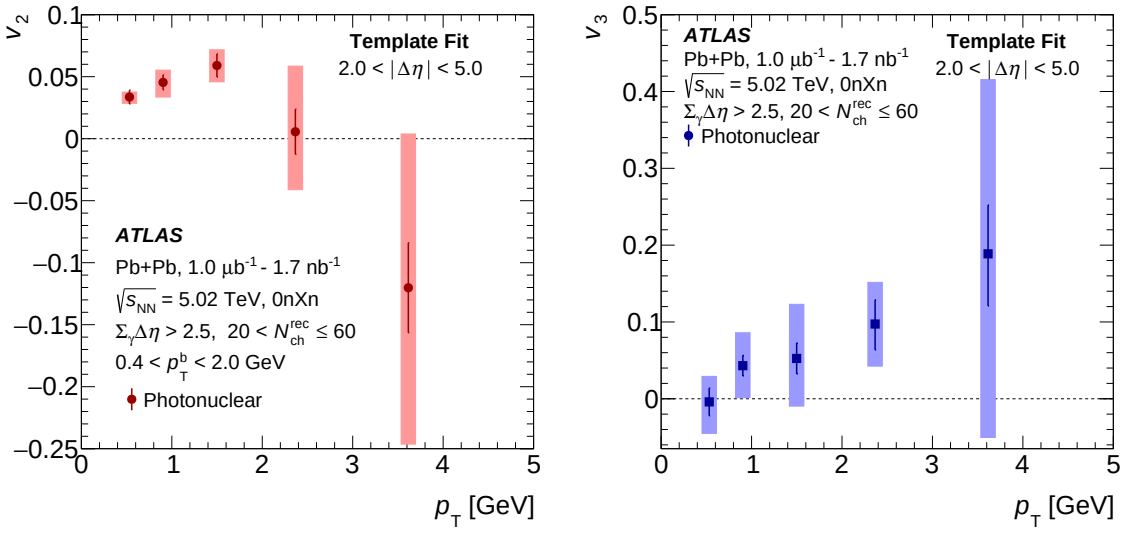

Figure 16: Charged-particle flow coefficients v_2 (left) and v_3 (right) in photonuclear events with $20 < N_{ch}^{rec} \leq 60$, reported as a function of particle p_T. The vertical error bars and colored boxes represent the statistical and total systematic uncertainties, respectively. The photonuclear data points are positioned at the average p_T value in each interval.

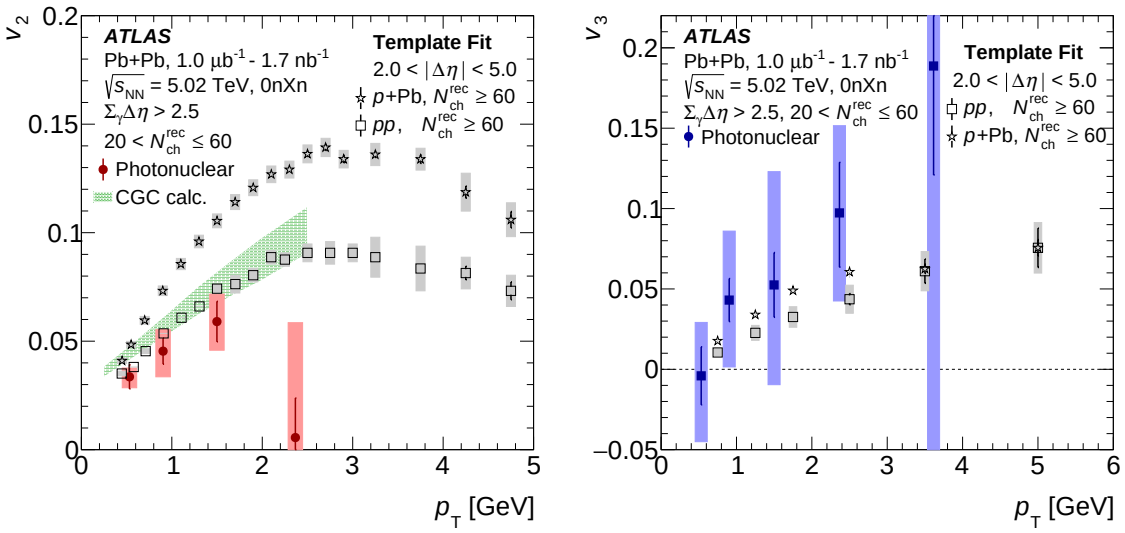

Figure 17: Charged-particle flow coefficients v_2 (left) and v_3 (right) in photonuclear events with $20 < N_{ch}^{rec} \leq 60$, reported as a function of particle p_T. The vertical error bars and colored boxes represent the statistical and total systematic uncertainties, respectively. The photonuclear data points are positioned at the average p_T value in each interval. The data are compared with the analogous measurements in pp collisions at 13 TeV and p+Pb collisions at 5.02 TeV for $N_{ch}^{rec} \geq 60$ [5]. The v_2 data are also compared with a CGC-based theory calculation from Ref. [31]. These photonuclear data are the same as in Figure 16 but with different y-axes ranges to allow comparison with additional data and theoretical predictions.

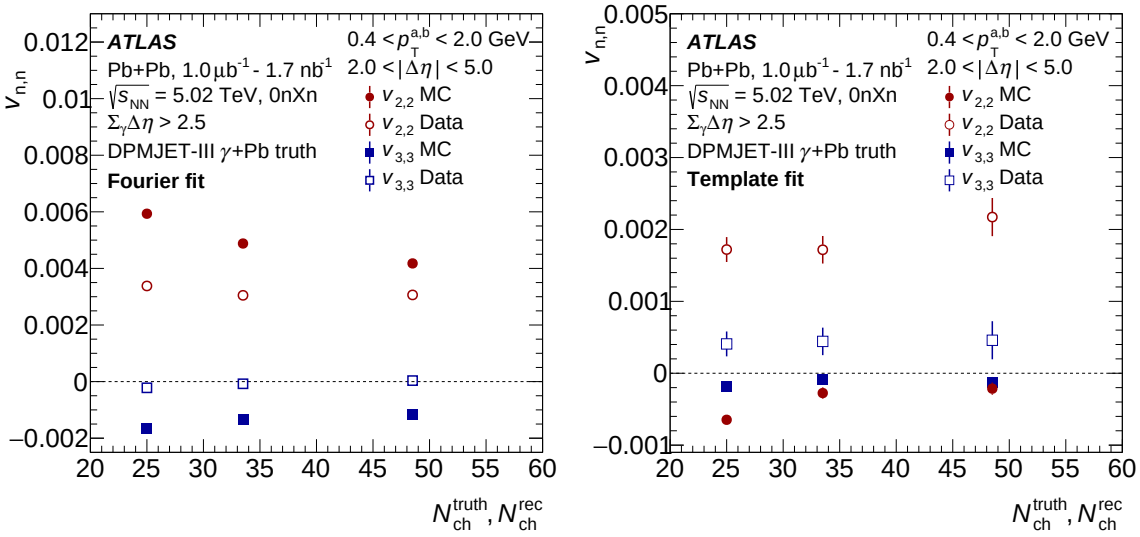

Figure 18: Comparison of results for raw Fourier coefficients $v_{2,2}$ and $v_{3,3}$ (left, without non-flow subtraction) and for non-flow subtracted coefficients $v_{2,2}$ and $v_{3,3}$ (right, with non-flow subtraction using the template method), shown in data (open points) and in DPMJET-III (filled points). The results in data and DPMJET-III are presented as a function of N_{ch}^{rec} and N_{ch}^{truth}, respectively.

a function of N_{ch}^{rec}, which is true within DPMJET-III as shown in Figure 6. If the non-flow contribution changes with photon energy, it may be that the non-flow correlation shape would not be the same in the LM and HM selections, which is an assumption of the non-flow subtraction procedure. In order to test if this effect might mimic the v_2 and v_3 signals observed, the DPMJET-III output has been run through the full analysis procedure, including the LM and HM selection and non-flow template fit. The resulting $v_{n,n}$ values are shown in Figure 18 for both data and DPMJET-III. The left panel shows the values that would result from a Fourier fit to the HM correlation function, without accounting for non-flow, while the right panel shows the template-subtracted results. In DPMJET-III, the template-subtracted $v_{n,n}$ values are both negative, in contradistinction to the opposite sign for these values observed in data. Since they give negative values, which are impossible in a flow factorization interpretation, one cannot extract v_2 and v_3 values to compare with the data. Nevertheless, this demonstrates that, at least within DPMJET-III, there is no trivial effect in the non-flow subtraction issue which could result in a false signal.

8 Conclusion

This paper reports a measurement of long-range two-particle correlations in high-energy photonuclear collisions. Events are selected from 1.7 nb^{-1} of Pb+Pb collision data at 5.02 TeV recorded by the ATLAS detector at the LHC in 2018 using a combination of criteria for the energy deposited exclusively in one side of the zero-degree calorimeter, and requirements on the sum-of-gaps in the photon-going direction ($\Sigma_\gamma\Delta\eta > 2.5$). Azimuthal correlation functions are reported for pairs of charged particles separated by $2 < |\Delta\eta| < 5$ units of pseudorapidity. A template-fitting method is used to subtract the non-flow contribution. The single-particle flow coefficients v_2 and v_3 are reported as a function of charged-particle multiplicity and single-particle p_T. Significant, nonzero v_2 and v_3 values are observed in photonuclear events, indicating that particles produced in these events participate in azimuthally dependent, collective

motion. The v_2 values are smaller than those reported in pp and p+Pb collisions at similar particle multiplicities. The results presented here provide new information about long-range collective behavior in an exotic collision system with different initial conditions than those in ordinary hadronic collisions. As such, they provide a new testing ground for different pictures of the physical origin of these correlations, and a starting point for understanding the systems which will be studied at the future Electron Ion Collider.

Acknowledgments

We thank CERN for the very successful operation of the LHC, as well as the support staff from our institutions without whom ATLAS could not be operated efficiently.

We acknowledge the support of ANPCyT, Argentina; YerPhI, Armenia; ARC, Australia; BMWFW and FWF, Austria; ANAS, Azerbaijan; SSTC, Belarus; CNPq and FAPESP, Brazil; NSERC, NRC and CFI, Canada; CERN; ANID, Chile; CAS, MOST and NSFC, China; COLCIENCIAS, Colombia; MSMT CR, MPO CR and VSC CR, Czech Republic; DNRF and DNSRC, Denmark; IN2P3-CNRS and CEA-DRF/IRFU, France; SRNSFG, Georgia; BMBF, HGF and MPG, Germany; GSRT, Greece; RGC and Hong Kong SAR, China; ISF and Benoziyo Center, Israel; INFN, Italy; MEXT and JSPS, Japan; CNRST, Morocco; NWO, Netherlands; RCN, Norway; MNiSW and NCN, Poland; FCT, Portugal; MNE/IFA, Romania; JINR; MES of Russia and NRC KI, Russian Federation; MESTD, Serbia; MSSR, Slovakia; ARRS and MIZŠ, Slovenia; DST/NRF, South Africa; MICINN, Spain; SRC and Wallenberg Foundation, Sweden; SERI, SNSF and Cantons of Bern and Geneva, Switzerland; MOST, Taiwan; TAEK, Turkey; STFC, United Kingdom; DOE and NSF, United States of America. In addition, individual groups and members have received support from BCKDF, CANARIE, Compute Canada, CRC and IVADO, Canada; Beijing Municipal Science & Technology Commission, China; COST, ERC, ERDF, Horizon 2020 and Marie Skłodowska-Curie Actions, European Union; Investissements d'Avenir Labex, Investissements d'Avenir Idex and ANR, France; DFG and AvH Foundation, Germany; Herakleitos, Thales and Aristeia programmes co-financed by EU-ESF and the Greek NSRF, Greece; BSF-NSF and GIF, Israel; La Caixa Banking Foundation, CERCA Programme Generalitat de Catalunya and PROMETEO and GenT Programmes Generalitat Valenciana, Spain; Göran Gustafssons Stiftelse, Sweden; The Royal Society and Leverhulme Trust, United Kingdom.

The crucial computing support from all WLCG partners is acknowledged gratefully, in particular from CERN, the ATLAS Tier-1 facilities at TRIUMF (Canada), NDGF (Denmark, Norway, Sweden), CC-IN2P3 (France), KIT/GridKA (Germany), INFN-CNAF (Italy), NL-T1 (Netherlands), PIC (Spain), ASGC (Taiwan), RAL (UK) and BNL (USA), the Tier-2 facilities worldwide and large non-WLCG resource providers. Major contributors of computing resources are listed in Ref. [67].

References

[1] W. Busza, K. Rajagopal and W. van der Schee, *Heavy Ion Collisions: The Big Picture, and the Big Questions*, Ann. Rev. Nucl. Part. Sci. **68** (2018) 339, arXiv: 1802.04801 [hep-ph].

[2] P. Romatschke and U. Romatschke, *Relativistic Fluid Dynamics In and Out of Equilibrium*, Cambridge Monographs on Mathematical Physics, Cambridge University Press, 2019, arXiv: 1712.05815 [nucl-th].

[3] U. Heinz and R. Snellings, *Collective Flow and Viscosity in Relativistic Heavy-Ion Collisions*, Ann. Rev. Nucl. Part. Sci. **63** (2013) 123, arXiv: 1301.2826 [nucl-th].

[4] ATLAS Collaboration, *Observation of Long-Range Elliptic Azimuthal Anisotropies in* $\sqrt{s} = 13$ *and* 2.76 *TeV pp Collisions with the ATLAS Detector*, Phys. Rev. Lett. **116** (2016) 172301, arXiv: 1509.04776 [hep-ex].

[5] ATLAS Collaboration, *Measurements of long-range azimuthal anisotropies and associated Fourier coefficients for pp collisions at* $\sqrt{s} = 5.02$ *and* 13 *TeV and p+Pb collisions at* $\sqrt{s_{NN}} = 5.02$ *TeV with the ATLAS detector*, Phys. Rev. C **96** (2017) 024908, arXiv: 1609.06213 [hep-ex].

[6] CMS Collaboration, *Evidence for Collective Multiparticle Correlations in pPb Collisions*, Phys. Rev. Lett. **115** (2015) 012301, arXiv: 1502.05382 [hep-ex].

[7] ATLAS Collaboration, *Measurement of long-range two-particle azimuthal correlations in Z-boson tagged pp collisions at* $\sqrt{s} = 8$ *and* 13 *TeV*, Eur. Phys. J. C **80** (2020) 64, arXiv: 1906.08290 [hep-ex].

[8] PHENIX Collaboration, *Measurements of Multiparticle Correlations in d* + Au *Collisions at 200, 62.4, 39, and 19.6 GeV and p* + Au *Collisions at 200 GeV and Implications for Collective Behavior*, Phys. Rev. Lett. **120** (2018) 062302, arXiv: 1707.06108 [nucl-ex].

[9] J. L. Nagle et al., *Minimal conditions for collectivity in* e^+e^- *and p + p collisions*, Phys. Rev. C **97** (2018) 024909, arXiv: 1707.02307 [nucl-th].

[10] J. L. Nagle and W. A. Zajc, *Small System Collectivity in Relativistic Hadronic and Nuclear Collisions*, Ann. Rev. Nucl. Part. Sci. **68** (2018) 211, arXiv: 1801.03477 [nucl-ex].

[11] PHENIX Collaboration, *Creation of quark-gluon plasma droplets with three distinct geometries*, Nature Phys. **15** (2019) 214, arXiv: 1805.02973 [nucl-ex].

[12] M. Greif, C. Greiner, B. Schenke, S. Schlichting and Z. Xu, *Importance of initial and final state effects for azimuthal correlations in p+Pb collisions*, Phys. Rev. D **96** (2017) 091504, arXiv: 1708.02076 [hep-ph].

[13] A. Badea et al., *Measurements of Two-Particle Correlations in* e^+e^- *Collisions at 91 GeV with ALEPH Archived Data*, Phys. Rev. Lett. **123** (2019) 212002, arXiv: 1906.00489 [hep-ex].

[14] ZEUS Collaboration, *Two-particle azimuthal correlations as a probe of collective behaviour in deep inelastic ep scattering at HERA*, JHEP **04** (2020) 070, arXiv: 1912.07431 [hep-ex].

[15] E. Fermi, *Über die Theorie des Stoßes zwischen Atomen und elektrisch geladenen Teilchen*, Z. Phys. **29** (1924) 315.

[16] C. F. von Weizsäcker, *Ausstrahlung bei Stößen sehr schneller Elektronen*, Z. Phys. **88** (1934) 612.

[17] E. J. Williams, *Nature of the High Energy Particles of Penetrating Radiation and Status of Ionization and Radiation Formulae*, Phys. Rev. **45** (1934) 729.

[18] C. A. Bertulani, S. R. Klein and J. Nystrand, *Physics of Ultra-Peripheral Nuclear Collisions*, Ann. Rev. Nucl. Part. Sci. **55** (2005) 271, arXiv: nucl-ex/0502005 [nucl-ex].

[19] S. Klein and P. Steinberg,
Photonuclear and Two-photon Interactions at High-Energy Nuclear Colliders, (2020),
arXiv: 2005.01872 [nucl-ex].

[20] ATLAS Collaboration,
Evidence for light-by-light scattering in heavy-ion collisions with the ATLAS detector at the LHC,
Nature Phys. **13** (2017) 852, arXiv: 1702.01625 [hep-ex].

[21] ATLAS Collaboration, *Observation of Light-by-Light Scattering in Ultraperipheral Pb+Pb Collisions with the ATLAS Detector*, Phys. Rev. Lett. **123** (2019) 052001,
arXiv: 1904.03536 [hep-ex].

[22] ATLAS Collaboration, *Measurement of light-by-light scattering and search for axion-like particles with 2.2 nb^{-1} of Pb+Pb data with the ATLAS detector*, (2020), arXiv: 2008.05355 [hep-ex].

[23] CMS Collaboration, *Evidence for light-by-light scattering and searches for axion-like particles in ultraperipheral PbPb collisions at* $\sqrt{s_{NN}} = 5.02$ *TeV*, Phys. Lett. B **797** (2019) 134826,
arXiv: 1810.04602 [hep-ex].

[24] ATLAS Collaboration,
Exclusive dimuon production in ultraperipheral Pb+Pb collisions at $\sqrt{s_{\mathrm{NN}}} = 5.02$ *TeV with ATLAS*,
(2020), arXiv: 2011.12211 [nucl-ex].

[25] CMS Collaboration, *Observation of forward neutron multiplicity dependence of dimuon acoplanarity in ultraperipheral PbPb collisions at* $\sqrt{s_{\mathrm{NN}}} = 5.02$ *TeV*, (2020),
arXiv: 2011.05239 [hep-ex].

[26] ALICE Collaboration, *Charmonium and* e^+e^- *pair photoproduction at mid-rapidity in ultra-peripheral Pb-Pb collisions at* $\sqrt{s_{\mathrm{NN}}}$=2.76 *TeV*, Eur. Phys. J. C **73** (2013) 2617,
arXiv: 1305.1467 [nucl-ex].

[27] CMS Collaboration, *Coherent* J/ψ *photoproduction in ultra-peripheral PbPb collisions at* $\sqrt{s_{NN}} = 2.76$ *TeV with the CMS experiment*, Phys. Lett. B **772** (2017) 489,
arXiv: 1605.06966 [hep-ex].

[28] ALICE Collaboration, *Coherent J/ψ photoproduction at forward rapidity in ultra-peripheral Pb-Pb collisions at* $\sqrt{s_{\mathrm{NN}}} = 5.02$ *TeV*, Phys. Lett. B **798** (2019) 134926, arXiv: 1904.06272 [nucl-ex].

[29] J. Sakurai, *Theory of strong interactions*, Annals Phys. **11** (1960) 1.

[30] A. Accardi et al.,
Electron Ion Collider: The Next QCD Frontier: Understanding the glue that binds us all,
Eur. Phys. J. A **52** (2016) 268, ed. by A. Deshpande, Z. Meziani and J. Qiu,
arXiv: 1212.1701 [nucl-ex].

[31] Y. Shi, L. Wang, S.-Y. Wei, B.-W. Xiao and L. Zheng,
Exploring the Collective Phenomenon at the Electron-Ion Collider, (2020),
arXiv: 2008.03569 [hep-ph].

[32] ATLAS Collaboration,
Rapidity gap cross sections measured with the ATLAS detector in pp *collisions at* $\sqrt{s} = 7$ *TeV*,
Eur. Phys. J. C **72** (2012) 1926, arXiv: 1201.2808 [hep-ex].

[33] CMS Collaboration,
Measurement of diffractive dissociation cross sections in pp collisions at $\sqrt{s} = 7$ TeV,
Phys. Rev. D **92** (2015) 012003, arXiv: 1503.08689 [hep-ex].

[34] ATLAS Collaboration, *Measurement of azimuthal anisotropy of muons from charm and bottom hadrons in pp collisions at $\sqrt{s} = 13$ TeV with the ATLAS detector*,
Phys. Rev. Lett. **124** (2020) 082301, arXiv: 1909.01650 [hep-ex].

[35] ATLAS Collaboration, *The ATLAS Experiment at the CERN Large Hadron Collider*,
JINST **3** (2008) S08003.

[36] ATLAS Collaboration, *ATLAS Insertable B-Layer: Technical Design Report*,
ATLAS-TDR-19; CERN-LHCC-2010-013, 2010,
URL: https://cds.cern.ch/record/1291633.

[37] ATLAS Collaboration, ATLAS-TDR-19-ADD-1; CERN-LHCC-2012-009, 2012,
URL: https://cds.cern.ch/record/1451888.

[38] B. Abbott et al., *Production and integration of the ATLAS Insertable B-Layer*,
JINST **13** (2018) T05008, arXiv: 1803.00844 [physics.ins-det].

[39] ATLAS Collaboration, *Performance of the ATLAS trigger system in 2015*,
Eur. Phys. J. C **77** (2017) 317, arXiv: 1611.09661 [hep-ex].

[40] S. Agostinelli et al., *GEANT4 – a simulation toolkit*, Nucl. Instrum. Meth. A **506** (2003) 250.

[41] ATLAS Collaboration, *The ATLAS Simulation Infrastructure*, Eur. Phys. J. C **70** (2010) 823,
arXiv: 1005.4568 [physics.ins-det].

[42] X.-N. Wang and M. Gyulassy,
HIJING: A Monte Carlo model for multiple jet production in pp, pA and AA collisions,
Phys. Rev. D **44** (1991) 3501.

[43] S. R. Klein, J. Nystrand, J. Seger, Y. Gorbunov and J. Butterworth,
STARlight: A Monte Carlo simulation program for ultra-peripheral collisions of relativistic ions,
Comput. Phys. Commun. **212** (2017) 258, arXiv: 1607.03838 [hep-ph].

[44] R. Engel,
Photoproduction within the two component Dual Parton Model: Amplitudes and cross sections,
Z. Phys. C **66** (1995) 203.

[45] S. Roesler, R. Engel and J. Ranft, 'The Monte Carlo Event Generator DPMJET-III',
International Conference on Advanced Monte Carlo for Radiation Physics, Particle Transport Simulation and Applications (MC 2000), 2000 1033, arXiv: hep-ph/0012252.

[46] T. Sjöstrand et al., *An introduction to PYTHIA 8.2*, Comput. Phys. Commun. **191** (2015) 159,
arXiv: 1410.3012 [hep-ph].

[47] R. D. Ball et al., *Parton distributions with LHC data*, Nucl. Phys. B **867** (2013) 244,
arXiv: 1207.1303 [hep-ph].

[48] ATLAS Collaboration, *ATLAS Pythia 8 tunes to 7 TeV data*, ATL-PHYS-PUB-2014-021, 2014,
URL: https://cds.cern.ch/record/1966419.

[49] ATLAS Collaboration,
Charged-particle multiplicities in pp interactions measured with the ATLAS detector at the LHC,
New J. Phys. **13** (2011) 053033, arXiv: 1012.5104 [hep-ex].

[50] A. Salzburger, *Optimisation of the ATLAS Track Reconstruction Software for Run-2*, ATL-SOFT-PROC-2015-056 (2015), URL: https://cds.cern.ch/record/2018442.

[51] ATLAS Collaboration, *Charged-particle distributions in $\sqrt{s}$ = 13 TeV pp interactions measured with the ATLAS detector at the LHC*, Phys. Lett. B **758** (2016) 67, arXiv: 1602.01633 [hep-ex].

[52] ATLAS Collaboration, *Topological cell clustering in the ATLAS calorimeters and its performance in LHC Run 1*, Eur. Phys. J. C **77** (2017) 490, arXiv: 1603.02934 [hep-ex].

[53] ATLAS Collaboration, *Measurement of the centrality dependence of the charged-particle pseudorapidity distribution in proton–lead collisions at $\sqrt{s_{NN}}$ = 5.02 TeV with the ATLAS detector*, Eur. Phys. J. C **76** (2016) 199, arXiv: 1508.00848 [hep-ex].

[54] ATLAS Collaboration, *Observation of Associated Near-Side and Away-Side Long-Range Correlations in $\sqrt{s_{NN}}$ = 5.02 TeV Proton–Lead Collisions with the ATLAS Detector*, Phys. Rev. Lett. **110** (2013) 182302, arXiv: 1212.5198 [hep-ex].

[55] ATLAS Collaboration, *Measurement of long-range pseudorapidity correlations and azimuthal harmonics in $\sqrt{s_{NN}}$ = 5.02 TeV proton–lead collisions with the ATLAS detector*, Phys. Rev. C **90** (2014) 044906, arXiv: 1409.1792 [hep-ex].

[56] ATLAS Collaboration, *Measurement of the azimuthal anisotropy for charged particle production in $\sqrt{s_{NN}}$ = 2.76 TeV lead–lead collisions with the ATLAS detector*, Phys. Rev. C **86** (2012) 014907, arXiv: 1203.3087 [hep-ex].

[57] ATLAS Collaboration, *Measurement of multi-particle azimuthal correlations in pp, p+Pb and low-multiplicity Pb+Pb collisions with the ATLAS detector*, Eur. Phys. J. C **77** (2017) 428, arXiv: 1705.04176 [hep-ex].

[58] ATLAS Collaboration, *Correlated long-range mixed-harmonic fluctuations measured in pp, p+Pb and low-multiplicity Pb+Pb collisions with the ATLAS detector*, Phys. Lett. B **789** (2019) 444, arXiv: 1807.02012 [hep-ex].

[59] ALICE Collaboration, *Charged-particle production as a function of multiplicity and transverse spherocity in pp collisions at $\sqrt{s}$ = 5.02 and 13 TeV*, Eur. Phys. J. C **79** (2019) 857, arXiv: 1905.07208 [nucl-ex].

[60] M. Alvioli, L. Frankfurt, V. Guzey, M. Strikman and M. Zhalov, *Mapping color fluctuations in the photon in ultraperipheral heavy ion collisions at the Large Hadron Collider*, Phys. Lett. B **767** (2017) 450, arXiv: 1605.06606 [hep-ph].

[61] C. Loizides, *Glauber modeling of high-energy nuclear collisions at the subnucleon level*, Phys. Rev. C **94** (2016) 024914, arXiv: 1603.07375 [nucl-ex].

[62] T. Lappi, B. Schenke, S. Schlichting and R. Venugopalan, *Tracing the origin of azimuthal gluon correlations in the color glass condensate*, JHEP **01** (2016) 061, arXiv: 1509.03499 [hep-ph].

[63] C. Zhang et al., *Collectivity of heavy mesons in proton-nucleus collisions*, Phys. Rev. D **102** (2020) 034010, arXiv: 2002.09878 [hep-ph].

[64] C. Zhang, C. Marquet, G.-Y. Qin, S.-Y. Wei and B.-W. Xiao, *Elliptic Flow of Heavy Quarkonia in pA Collisions*, Phys. Rev. Lett. **122** (2019) 172302, arXiv: 1901.10320 [hep-ph].

[65] M. Mace, V. V. Skokov, P. Tribedy and R. Venugopalan, *Hierarchy of Azimuthal Anisotropy Harmonics in Collisions of Small Systems from the Color Glass Condensate*, Phys. Rev. Lett. **121** (2018) 052301, [Erratum: Phys. Rev. Lett. **123** (2019) 039901], arXiv: 1805.09342 [hep-ph].

[66] M. Mace, V. V. Skokov, P. Tribedy and R. Venugopalan, *Systematics of azimuthal anisotropy harmonics in proton–nucleus collisions at the LHC from the Color Glass Condensate*, Phys. Lett. B **788** (2019) 161, [Erratum: Phys. Lett. B **799** (2019) 135006], arXiv: 1807.00825 [hep-ph].

[67] ATLAS Collaboration, *ATLAS Computing Acknowledgements*, ATL-SOFT-PUB-2020-001, URL: https://cds.cern.ch/record/2717821.

The ATLAS Collaboration

G. Aad[101], B. Abbott[127], D.C. Abbott[102], A. Abed Abud[36], K. Abeling[53], D.K. Abhayasinghe[93], S.H. Abidi[29], O.S. AbouZeid[40], N.L. Abraham[155], H. Abramowicz[160], H. Abreu[159], Y. Abulaiti[6], A.C. Abusleme Hoffman[145a], B.S. Acharya[66a,66b,o], B. Achkar[53], L. Adam[99], C. Adam Bourdarios[5], L. Adamczyk[83a], L. Adamek[165], J. Adelman[120], A. Adiguzel[12c,ad], S. Adorni[54], T. Adye[142], A.A. Affolder[144], Y. Afik[159], C. Agapopoulou[64], M.N. Agaras[38], A. Aggarwal[118], C. Agheorghiesei[27c], J.A. Aguilar-Saavedra[138f,138a,ac], A. Ahmad[36], F. Ahmadov[79], W.S. Ahmed[103], X. Ai[18], G. Aielli[73a,73b], S. Akatsuka[85], M. Akbiyik[99], T.P.A. Åkesson[96], E. Akilli[54], A.V. Akimov[110], K. Al Khoury[39], G.L. Alberghi[23b,23a], J. Albert[174], M.J. Alconada Verzini[160], S. Alderweireldt[36], M. Aleksa[36], I.N. Aleksandrov[79], C. Alexa[27b], T. Alexopoulos[10], A. Alfonsi[119], F. Alfonsi[23b,23a], M. Alhroob[127], B. Ali[140], S. Ali[157], M. Aliev[164], G. Alimonti[68a], C. Allaire[36], B.M.M. Allbrooke[155], P.P. Allport[21], A. Aloisio[69a,69b], F. Alonso[88], C. Alpigiani[147], E. Alunno Camelia[73a,73b], M. Alvarez Estevez[98], M.G. Alviggi[69a,69b], Y. Amaral Coutinho[80b], A. Ambler[103], L. Ambroz[133], C. Amelung[36], D. Amidei[105], S.P. Amor Dos Santos[138a], S. Amoroso[46], C.S. Amrouche[54], C. Anastopoulos[148], N. Andari[143], T. Andeen[11], J.K. Anders[20], S.Y. Andrean[45a,45b], A. Andreazza[68a,68b], V. Andrei[61a], C.R. Anelli[174], S. Angelidakis[9], A. Angerami[39], A.V. Anisenkov[121b,121a], A. Annovi[71a], C. Antel[54], M.T. Anthony[148], E. Antipov[128], M. Antonelli[51], D.J.A. Antrim[18], F. Anulli[72a], M. Aoki[81], J.A. Aparisi Pozo[172], M.A. Aparo[155], L. Aperio Bella[46], N. Aranzabal[36], V. Araujo Ferraz[80a], C. Arcangeletti[51], A.T.H. Arce[49], J-F. Arguin[109], S. Argyropoulos[52], J.-H. Arling[46], A.J. Armbruster[36], A. Armstrong[169], O. Arnaez[165], H. Arnold[36], Z.P. Arrubarrena Tame[113], G. Artoni[133], H. Asada[116], K. Asai[125], S. Asai[162], N. Asbah[59], E.M. Asimakopoulou[170], L. Asquith[155], J. Assahsah[35e], K. Assamagan[29], R. Astalos[28a], R.J. Atkin[33a], M. Atkinson[171], N.B. Atlay[19], H. Atmani[64], P.A. Atmasiddha[105], K. Augsten[140], V.A. Austrup[180], G. Avolio[36], M.K. Ayoub[15c], G. Azuelos[109,ak], D. Babal[28a], H. Bachacou[143], K. Bachas[161], F. Backman[45a,45b], P. Bagnaia[72a,72b], M. Bahmani[84], H. Bahrasemani[151], A.J. Bailey[172], V.R. Bailey[171], J.T. Baines[142], C. Bakalis[10], O.K. Baker[181], P.J. Bakker[119], E. Bakos[16], D. Bakshi Gupta[8], S. Balaji[156], R. Balasubramanian[119], E.M. Baldin[121b,121a], P. Balek[178], F. Balli[143], W.K. Balunas[133], J. Balz[99], E. Banas[84], M. Bandieramonte[137], A. Bandyopadhyay[19], L. Barak[160], W.M. Barbe[38], E.L. Barberio[104], D. Barberis[55b,55a], M. Barbero[101], G. Barbour[94], K.N. Barends[33a], T. Barillari[114], M-S. Barisits[36], J. Barkeloo[130], T. Barklow[152], B.M. Barnett[142], R.M. Barnett[18], Z. Barnovska-Blenessy[60a], A. Baroncelli[60a], G. Barone[29], A.J. Barr[133], L. Barranco Navarro[45a,45b], F. Barreiro[98], J. Barreiro Guimarães da Costa[15a], U. Barron[160], S. Barsov[136], F. Bartels[61a], R. Bartoldus[152], G. Bartolini[101], A.E. Barton[89], P. Bartos[28a], A. Basalaev[46], A. Basan[99], A. Bassalat[64,ah], M.J. Basso[165], C.R. Basson[100], R.L. Bates[57], S. Batlamous[35f], J.R. Batley[32], B. Batool[150], M. Battaglia[144], M. Bauce[72a,72b], F. Bauer[143,*], P. Bauer[24], H.S. Bawa[31], A. Bayirli[12c], J.B. Beacham[49], T. Beau[134], P.H. Beauchemin[168], F. Becherer[52], P. Bechtle[24], H.P. Beck[20,q], K. Becker[176], C. Becot[46], A.J. Beddall[12a], V.A. Bednyakov[79], C.P. Bee[154], T.A. Beermann[180], M. Begalli[80b], M. Begel[29], A. Behera[154], J.K. Behr[46], J.F. Beirer[53,36], F. Beisiegel[24], M. Belfkir[5], G. Bella[160], L. Bellagamba[23b], A. Bellerive[34], P. Bellos[21], K. Beloborodov[121b,121a], K. Belotskiy[111], N.L. Belyaev[111], D. Benchekroun[35a], N. Benekos[10], Y. Benhammou[160], D.P. Benjamin[6], M. Benoit[29], J.R. Bensinger[26], S. Bentvelsen[119], L. Beresford[133], M. Beretta[51], D. Berge[19], E. Bergeaas Kuutmann[170], N. Berger[5], B. Bergmann[140], L.J. Bergsten[26], J. Beringer[18], S. Berlendis[7], G. Bernardi[134], C. Bernius[152], F.U. Bernlochner[24], T. Berry[93], P. Berta[46], A. Berthold[48], I.A. Bertram[89], O. Bessidskaia Bylund[180], S. Bethke[114], A. Betti[42], A.J. Bevan[92], S. Bhatta[154], D.S. Bhattacharya[175], P. Bhattarai[26], V.S. Bhopatkar[6], R. Bi[137], R.M. Bianchi[137], O. Biebel[113], R. Bielski[36], K. Bierwagen[99], N.V. Biesuz[71a,71b], M. Biglietti[74a], T.R.V. Billoud[140], M. Bindi[53], A. Bingul[12d], C. Bini[72a,72b], S. Biondi[23b,23a], C.J. Birch-sykes[100], M. Birman[178], T. Bisanz[36],

J.P. Biswal[3], D. Biswas[179,j], A. Bitadze[100], C. Bittrich[48], K. Bjørke[132], T. Blazek[28a], I. Bloch[46], C. Blocker[26], A. Blue[57], U. Blumenschein[92], G.J. Bobbink[119], V.S. Bobrovnikov[121b,121a], D. Bogavac[14], A.G. Bogdanchikov[121b,121a], C. Bohm[45a], V. Boisvert[93], P. Bokan[170,53], T. Bold[83a], M. Bomben[134], M. Bona[92], J.S. Bonilla[130], M. Boonekamp[143], C.D. Booth[93], A.G. Borbély[57], H.M. Borecka-Bielska[90], L.S. Borgna[94], G. Borissov[89], D. Bortoletto[133], D. Boscherini[23b], M. Bosman[14], J.D. Bossio Sola[103], K. Bouaouda[35a], J. Boudreau[137], E.V. Bouhova-Thacker[89], D. Boumediene[38], R. Bouquet[134], A. Boveia[126], J. Boyd[36], D. Boye[29], I.R. Boyko[79], A.J. Bozson[93], J. Bracinik[21], N. Brahimi[60d,60c], G. Brandt[180], O. Brandt[32], F. Braren[46], B. Brau[102], J.E. Brau[130], W.D. Breaden Madden[57], K. Brendlinger[46], R. Brener[159], L. Brenner[36], R. Brenner[170], S. Bressler[178], B. Brickwedde[99], D.L. Briglin[21], D. Britton[57], D. Britzger[114], I. Brock[24], R. Brock[106], G. Brooijmans[39], W.K. Brooks[145d], E. Brost[29], P.A. Bruckman de Renstrom[84], B. Brüers[46], D. Bruncko[28b], A. Bruni[23b], G. Bruni[23b], M. Bruschi[23b], N. Bruscino[72a,72b], L. Bryngemark[152], T. Buanes[17], Q. Buat[154], P. Buchholz[150], A.G. Buckley[57], I.A. Budagov[79], M.K. Bugge[132], O. Bulekov[111], B.A. Bullard[59], T.J. Burch[120], S. Burdin[90], C.D. Burgard[46], A.M. Burger[128], B. Burghgrave[8], J.T.P. Burr[46], C.D. Burton[11], J.C. Burzynski[102], V. Büscher[99], E. Buschmann[53], P.J. Bussey[57], J.M. Butler[25], C.M. Buttar[57], J.M. Butterworth[94], W. Buttinger[142], C.J. Buxo Vazquez[106], A.R. Buzykaev[121b,121a], G. Cabras[23b,23a], S. Cabrera Urbán[172], D. Caforio[56], H. Cai[137], V.M.M. Cairo[152], O. Cakir[4a], N. Calace[36], P. Calafiura[18], G. Calderini[134], P. Calfayan[65], G. Callea[57], L.P. Caloba[80b], A. Caltabiano[73a,73b], S. Calvente Lopez[98], D. Calvet[38], S. Calvet[38], T.P. Calvet[101], M. Calvetti[71a,71b], R. Camacho Toro[134], S. Camarda[36], D. Camarero Munoz[98], P. Camarri[73a,73b], M.T. Camerlingo[74a,74b], D. Cameron[132], C. Camincher[36], M. Campanelli[94], A. Camplani[40], V. Canale[69a,69b], A. Canesse[103], M. Cano Bret[77], J. Cantero[128], Y. Cao[171], M. Capua[41b,41a], R. Cardarelli[73a], F. Cardillo[172], G. Carducci[41b,41a], T. Carli[36], G. Carlino[69a], B.T. Carlson[137], E.M. Carlson[174,166a], L. Carminati[68a,68b], M. Carnesale[72a,72b], R.M.D. Carney[152], S. Caron[118], E. Carquin[145d], S. Carrá[46], G. Carratta[23b,23a], J.W.S. Carter[165], T.M. Carter[50], M.P. Casado[14,g], A.F. Casha[165], E.G. Castiglia[181], F.L. Castillo[172], L. Castillo Garcia[14], V. Castillo Gimenez[172], N.F. Castro[138a,138e], A. Catinaccio[36], J.R. Catmore[132], A. Cattai[36], V. Cavaliere[29], V. Cavasinni[71a,71b], E. Celebi[12b], F. Celli[133], K. Cerny[129], A.S. Cerqueira[80a], A. Cerri[155], L. Cerrito[73a,73b], F. Cerutti[18], A. Cervelli[23b,23a], S.A. Cetin[12b], Z. Chadi[35a], D. Chakraborty[120], M. Chala[138f], J. Chan[179], W.S. Chan[119], W.Y. Chan[90], J.D. Chapman[32], B. Chargeishvili[158b], D.G. Charlton[21], T.P. Charman[92], M. Chatterjee[20], C.C. Chau[34], S. Chekanov[6], S.V. Chekulaev[166a], G.A. Chelkov[79,af], B. Chen[78], C. Chen[60a], C.H. Chen[78], H. Chen[15c], H. Chen[29], J. Chen[60a], J. Chen[39], J. Chen[26], S. Chen[135], S.J. Chen[15c], X. Chen[15b], Y. Chen[60a], Y-H. Chen[46], C.L. Cheng[179], H.C. Cheng[62a], H.J. Cheng[15a], A. Cheplakov[79], E. Cheremushkina[122], R. Cherkaoui El Moursli[35f], E. Cheu[7], K. Cheung[63], L. Chevalier[143], V. Chiarella[51], G. Chiarelli[71a], G. Chiodini[67a], A.S. Chisholm[21], A. Chitan[27b], I. Chiu[162], Y.H. Chiu[174], M.V. Chizhov[79,s], K. Choi[11], A.R. Chomont[72a,72b], Y. Chou[102], Y.S. Chow[119], L.D. Christopher[33e], M.C. Chu[62a], X. Chu[15a,15d], J. Chudoba[139], J.J. Chwastowski[84], D. Cieri[114], K.M. Ciesla[84], V. Cindro[91], I.A. Cioară[27b], A. Ciocio[18], F. Cirotto[69a,69b], Z.H. Citron[178,k], M. Citterio[68a], D.A. Ciubotaru[27b], B.M. Ciungu[165], A. Clark[54], P.J. Clark[50], S.E. Clawson[100], C. Clement[45a,45b], L. Clissa[23b,23a], Y. Coadou[101], M. Cobal[66a,66c], A. Coccaro[55b], J. Cochran[78], R. Coelho Lopes De Sa[102], S. Coelli[68a], H. Cohen[160], A.E.C. Coimbra[36], B. Cole[39], J. Collot[58], P. Conde Muiño[138a,138h], S.H. Connell[33c], I.A. Connelly[57], F. Conventi[69a,al], A.M. Cooper-Sarkar[133], F. Cormier[173], L.D. Corpe[94], M. Corradi[72a,72b], E.E. Corrigan[96], F. Corriveau[103,aa], M.J. Costa[172], F. Costanza[5], D. Costanzo[148], G. Cowan[93], J.W. Cowley[32], J. Crane[100], K. Cranmer[124], R.A. Creager[135], S. Crépé-Renaudin[58], F. Crescioli[134], M. Cristinziani[150], M. Cristoforetti[75a,75b], V. Croft[168], G. Crosetti[41b,41a], A. Cueto[5], T. Cuhadar Donszelmann[169], H. Cui[15a,15d], A.R. Cukierman[152], W.R. Cunningham[57], S. Czekierda[84], P. Czodrowski[36], M.M. Czurylo[61b], M.J. Da Cunha Sargedas De Sousa[60b], J.V. Da Fonseca Pinto[80b], C. Da Via[100], W. Dabrowski[83a], T. Dado[47], S. Dahbi[33e], T. Dai[105], C. Dallapiccola[102], M. Dam[40], G. D'amen[29],

V. D'Amico[74a,74b], J. Damp[99], J.R. Dandoy[135], M.F. Daneri[30], M. Danninger[151], V. Dao[36], G. Darbo[55b], A. Dattagupta[130], S. D'Auria[68a,68b], C. David[166b], T. Davidek[141], D.R. Davis[49], I. Dawson[148], K. De[8], R. De Asmundis[69a], M. De Beurs[119], S. De Castro[23b,23a], N. De Groot[118], P. de Jong[119], H. De la Torre[106], A. De Maria[15c], D. De Pedis[72a], A. De Salvo[72a], U. De Sanctis[73a,73b], M. De Santis[73a,73b], A. De Santo[155], J.B. De Vivie De Regie[58], D.V. Dedovich[79], J. Degens[119], A.M. Deiana[42], J. Del Peso[98], Y. Delabat Diaz[46], F. Deliot[143], C.M. Delitzsch[7], M. Della Pietra[69a,69b], D. Della Volpe[54], A. Dell'Acqua[36], L. Dell'Asta[73a,73b], M. Delmastro[5], C. Delporte[64], P.A. Delsart[58], S. Demers[181], M. Demichev[79], G. Demontigny[109], S.P. Denisov[122], L. D'Eramo[120], D. Derendarz[84], J.E. Derkaoui[35e], F. Derue[134], P. Dervan[90], K. Desch[24], K. Dette[165], C. Deutsch[24], P.O. Deviveiros[36], F.A. Di Bello[72a,72b], A. Di Ciaccio[73a,73b], L. Di Ciaccio[5], C. Di Donato[69a,69b], A. Di Girolamo[36], G. Di Gregorio[71a,71b], A. Di Luca[75a,75b], B. Di Micco[74a,74b], R. Di Nardo[74a,74b], C. Diaconu[101], F.A. Dias[119], T. Dias Do Vale[138a], M.A. Diaz[145a], F.G. Diaz Capriles[24], J. Dickinson[18], M. Didenko[164], E.B. Diehl[105], J. Dietrich[19], S. Díez Cornell[46], C. Diez Pardos[150], A. Dimitrievska[18], W. Ding[15b], J. Dingfelder[24], S.J. Dittmeier[61b], F. Dittus[36], F. Djama[101], T. Djobava[158b], J.I. Djuvsland[17], M.A.B. Do Vale[146], M. Dobre[27b], D. Dodsworth[26], C. Doglioni[96], J. Dolejsi[141], Z. Dolezal[141], M. Donadelli[80c], B. Dong[60c], J. Donini[38], A. D'onofrio[15c], M. D'Onofrio[90], J. Dopke[142], A. Doria[69a], M.T. Dova[88], A.T. Doyle[57], E. Drechsler[151], E. Dreyer[151], T. Dreyer[53], A.S. Drobac[168], D. Du[60b], T.A. du Pree[119], Y. Duan[60d], F. Dubinin[110], M. Dubovsky[28a], A. Dubreuil[54], E. Duchovni[178], G. Duckeck[113], O.A. Ducu[36,27b], D. Duda[114], A. Dudarev[36], A.C. Dudder[99], M. D'uffizi[100], L. Duflot[64], M. Dührssen[36], C. Dülsen[180], M. Dumancic[178], A.E. Dumitriu[27b], M. Dunford[61a], S. Dungs[47], A. Duperrin[101], H. Duran Yildiz[4a], M. Düren[56], A. Durglishvili[158b], B. Dutta[46], D. Duvnjak[1], G.I. Dyckes[135], M. Dyndal[36], S. Dysch[100], B.S. Dziedzic[84], B. Eckerova[28a], M.G. Eggleston[49], E. Egidio Purcino De Souza[80b], L.F. Ehrke[54], T. Eifert[8], G. Eigen[17], K. Einsweiler[18], T. Ekelof[170], H. El Jarrari[35f], A. El Moussaouy[35a], V. Ellajosyula[170], M. Ellert[170], F. Ellinghaus[180], A.A. Elliot[92], N. Ellis[36], J. Elmsheuser[29], M. Elsing[36], D. Emeliyanov[142], A. Emerman[39], Y. Enari[162], J. Erdmann[47], A. Ereditato[20], P.A. Erland[84], M. Errenst[180], M. Escalier[64], C. Escobar[172], O. Estrada Pastor[172], E. Etzion[160], G. Evans[138a], H. Evans[65], M.O. Evans[155], A. Ezhilov[136], F. Fabbri[57], L. Fabbri[23b,23a], V. Fabiani[118], G. Facini[176], R.M. Fakhrutdinov[122], S. Falciano[72a], P.J. Falke[24], S. Falke[36], J. Faltova[141], Y. Fang[15a], Y. Fang[15a], G. Fanourakis[44], M. Fanti[68a,68b], M. Faraj[60c], A. Farbin[8], A. Farilla[74a], E.M. Farina[70a,70b], T. Farooque[106], S.M. Farrington[50], P. Farthouat[36], F. Fassi[35f], D. Fassouliotis[9], M. Faucci Giannelli[73a,73b], W.J. Fawcett[32], L. Fayard[64], O.L. Fedin[136,p], A. Fehr[20], M. Feickert[171], L. Feligioni[101], A. Fell[148], C. Feng[60b], M. Feng[49], M.J. Fenton[169], A.B. Fenyuk[122], S.W. Ferguson[43], J. Ferrando[46], A. Ferrari[170], P. Ferrari[119], R. Ferrari[70a], D. Ferrere[54], C. Ferretti[105], F. Fiedler[99], A. Filipčič[91], F. Filthaut[118], K.D. Finelli[25], M.C.N. Fiolhais[138a,138c,a], L. Fiorini[172], F. Fischer[113], J. Fischer[99], W.C. Fisher[106], T. Fitschen[21], I. Fleck[150], P. Fleischmann[105], T. Flick[180], B.M. Flierl[113], L. Flores[135], L.R. Flores Castillo[62a], F.M. Follega[75a,75b], N. Fomin[17], J.H. Foo[165], G.T. Forcolin[75a,75b], B.C. Forland[65], A. Formica[143], F.A. Förster[14], A.C. Forti[100], E. Fortin[101], M.G. Foti[133], D. Fournier[64], H. Fox[89], P. Francavilla[71a,71b], S. Francescato[72a,72b], M. Franchini[23b,23a], S. Franchino[61a], D. Francis[36], L. Franco[5], L. Franconi[20], M. Franklin[59], G. Frattari[72a,72b], P.M. Freeman[21], B. Freund[109], W.S. Freund[80b], E.M. Freundlich[47], D.C. Frizzell[127], D. Froidevaux[36], J.A. Frost[133], Y. Fu[60a], M. Fujimoto[125], E. Fullana Torregrosa[172], T. Fusayasu[115], J. Fuster[172], A. Gabrielli[23b,23a], A. Gabrielli[36], P. Gadow[114], G. Gagliardi[55b,55a], L.G. Gagnon[109], G.E. Gallardo[133], E.J. Gallas[133], B.J. Gallop[142], R. Gamboa Goni[92], K.K. Gan[126], S. Ganguly[178], J. Gao[60a], Y. Gao[50], Y.S. Gao[31,m], F.M. Garay Walls[145a], C. García[172], J.E. García Navarro[172], J.A. García Pascual[15a], M. Garcia-Sciveres[18], R.W. Gardner[37], S. Gargiulo[52], C.A. Garner[165], V. Garonne[132], S.J. Gasiorowski[147], P. Gaspar[80b], G. Gaudio[70a], P. Gauzzi[72a,72b], I.L. Gavrilenko[110], A. Gavrilyuk[123], C. Gay[173], G. Gaycken[46], E.N. Gazis[10], A.A. Geanta[27b], C.M. Gee[144], C.N.P. Gee[142], J. Geisen[96], M. Geisen[99], C. Gemme[55b], M.H. Genest[58], C. Geng[105], S. Gentile[72a,72b], S. George[93], T. Geralis[44], L.O. Gerlach[53],

P. Gessinger-Befurt[99], G. Gessner[47], M. Ghasemi Bostanabad[174], M. Ghneimat[150], A. Ghosh[169], A. Ghosh[77], B. Giacobbe[23b], S. Giagu[72a,72b], N. Giangiacomi[165], P. Giannetti[71a], A. Giannini[69a,69b], S.M. Gibson[93], M. Gignac[144], D.T. Gil[83b], B.J. Gilbert[39], D. Gillberg[34], G. Gilles[180], N.E.K. Gillwald[46], D.M. Gingrich[3,ak], M.P. Giordani[66a,66c], P.F. Giraud[143], G. Giugliarelli[66a,66c], D. Giugni[68a], F. Giuli[73a,73b], S. Gkaitatzis[161], I. Gkialas[9,h], E.L. Gkougkousis[14], P. Gkountoumis[10], L.K. Gladilin[112], C. Glasman[98], G.R. Gledhill[130], I. Gnesi[41b,c], M. Goblirsch-Kolb[26], D. Godin[109], S. Goldfarb[104], T. Golling[54], D. Golubkov[122], A. Gomes[138a,138b], R. Goncalves Gama[53], R. Gonçalo[138a,138c], G. Gonella[130], L. Gonella[21], A. Gongadze[79], F. Gonnella[21], J.L. Gonski[39], S. González de la Hoz[172], S. Gonzalez Fernandez[14], R. Gonzalez Lopez[90], C. Gonzalez Renteria[18], R. Gonzalez Suarez[170], S. Gonzalez-Sevilla[54], G.R. Gonzalvo Rodriguez[172], L. Goossens[36], N.A. Gorasia[21], P.A. Gorbounov[123], H.A. Gordon[29], B. Gorini[36], E. Gorini[67a,67b], A. Gorišek[91], A.T. Goshaw[49], M.I. Gostkin[79], C.A. Gottardo[118], M. Gouighri[35b], A.G. Goussiou[147], N. Govender[33c], C. Goy[5], I. Grabowska-Bold[83a], E. Gramstad[132], S. Grancagnolo[19], M. Grandi[155], V. Gratchev[136], P.M. Gravila[27f], F.G. Gravili[67a,67b], C. Gray[57], H.M. Gray[18], C. Grefe[24], I.M. Gregor[46], P. Grenier[152], K. Grevtsov[46], C. Grieco[14], N.A. Grieser[127], A.A. Grillo[144], K. Grimm[31,l], S. Grinstein[14,w], J.-F. Grivaz[64], S. Groh[99], E. Gross[178], J. Grosse-Knetter[53], Z.J. Grout[94], C. Grud[105], A. Grummer[117], J.C. Grundy[133], L. Guan[105], W. Guan[179], C. Gubbels[173], J. Guenther[36], J.G.R. Guerrero Rojas[172], F. Guescini[114], D. Guest[19], R. Gugel[99], A. Guida[46], T. Guillemin[5], S. Guindon[36], J. Guo[60c], L. Guo[64], Y. Guo[105], Z. Guo[101], R. Gupta[46], S. Gurbuz[24], G. Gustavino[127], M. Guth[52], P. Gutierrez[127], L.F. Gutierrez Zagazeta[135], C. Gutschow[94], C. Guyot[143], C. Gwenlan[133], C.B. Gwilliam[90], E.S. Haaland[132], A. Haas[124], M.H. Habedank[19], C. Haber[18], H.K. Hadavand[8], A. Hadef[99], M. Haleem[175], J. Haley[128], J.J. Hall[148], G. Halladjian[106], G.D. Hallewell[101], K. Hamano[174], H. Hamdaoui[35f], M. Hamer[24], G.N. Hamity[50], K. Han[60a], L. Han[15c], L. Han[60a], S. Han[18], Y.F. Han[165], K. Hanagaki[81,u], M. Hance[144], M.D. Hank[37], R. Hankache[100], E. Hansen[96], J.B. Hansen[40], J.D. Hansen[40], M.C. Hansen[24], P.H. Hansen[40], E.C. Hanson[100], K. Hara[167], T. Harenberg[180], S. Harkusha[107], P.F. Harrison[176], N.M. Hartman[152], N.M. Hartmann[113], Y. Hasegawa[149], A. Hasib[50], S. Hassani[143], S. Haug[20], R. Hauser[106], M. Havranek[140], C.M. Hawkes[21], R.J. Hawkings[36], S. Hayashida[116], D. Hayden[106], C. Hayes[105], R.L. Hayes[173], C.P. Hays[133], J.M. Hays[92], H.S. Hayward[90], S.J. Haywood[142], F. He[60a], Y. He[163], Y. He[134], M.P. Heath[50], V. Hedberg[96], A.L. Heggelund[132], N.D. Hehir[92], C. Heidegger[52], K.K. Heidegger[52], W.D. Heidorn[78], J. Heilman[34], S. Heim[46], T. Heim[18], B. Heinemann[46,ai], J.G. Heinlein[135], J.J. Heinrich[130], L. Heinrich[36], J. Hejbal[139], L. Helary[46], A. Held[124], S. Hellesund[132], C.M. Helling[144], S. Hellman[45a,45b], C. Helsens[36], R.C.W. Henderson[89], L. Henkelmann[32], A.M. Henriques Correia[36], H. Herde[152], Y. Hernández Jiménez[33e], H. Herr[99], M.G. Herrmann[113], T. Herrmann[48], G. Herten[52], R. Hertenberger[113], L. Hervas[36], N.P. Hessey[166a], H. Hibi[82], S. Higashino[81], E. Higón-Rodriguez[172], K. Hildebrand[37], K.K. Hill[29], K.H. Hiller[46], S.J. Hillier[21], M. Hils[48], I. Hinchliffe[18], F. Hinterkeuser[24], M. Hirose[131], S. Hirose[167], D. Hirschbuehl[180], B. Hiti[91], O. Hladik[139], J. Hobbs[154], R. Hobincu[27e], N. Hod[178], M.C. Hodgkinson[148], A. Hoecker[36], D. Hohn[52], T. Holm[24], T.R. Holmes[37], M. Holzbock[114], L.B.A.H. Hommels[32], T.M. Hong[137], J.C. Honig[52], A. Hönle[114], B.H. Hooberman[171], W.H. Hopkins[6], Y. Horii[116], P. Horn[48], L.A. Horyn[37], S. Hou[157], J. Howarth[57], J. Hoya[88], M. Hrabovsky[129], A. Hrynevich[108], T. Hryn'ova[5], P.J. Hsu[63], S.-C. Hsu[147], Q. Hu[39], S. Hu[60c], Y.F. Hu[15a,15d,am], D.P. Huang[94], X. Huang[15c], Y. Huang[60a], Y. Huang[15a], Z. Hubacek[140], F. Hubaut[101], M. Huebner[24], F. Huegging[24], T.B. Huffman[133], M. Huhtinen[36], R. Hulsken[58], R.F.H. Hunter[34], N. Huseynov[79,ab], J. Huston[106], J. Huth[59], R. Hyneman[152], S. Hyrych[28a], G. Iacobucci[54], G. Iakovidis[29], I. Ibragimov[150], L. Iconomidou-Fayard[64], P. Iengo[36], R. Ignazzi[40], R. Iguchi[162], T. Iizawa[54], Y. Ikegami[81], N. Ilic[165,165], H. Imam[35a], G. Introzzi[70a,70b], M. Iodice[74a], K. Iordanidou[166a], V. Ippolito[72a,72b], M. Ishino[162], W. Islam[128], C. Issever[19,46], S. Istin[12c], J.M. Iturbe Ponce[62a], R. Iuppa[75a,75b], A. Ivina[178], J.M. Izen[43], V. Izzo[69a], P. Jacka[139], P. Jackson[1], R.M. Jacobs[46], B.P. Jaeger[151], C.S. Jagfeld[113], G. Jäkel[180], K.B. Jakobi[99], K. Jakobs[52], T. Jakoubek[178], J. Jamieson[57], K.W. Janas[83a], P.A. Janus[83a], G. Jarlskog[96],

A.E. Jaspan[90], N. Javadov[79,ab], T. Javůrek[36], M. Javurkova[102], F. Jeanneau[143], L. Jeanty[130], J. Jejelava[158a], P. Jenni[52,d], S. Jézéquel[5], J. Jia[154], Z. Jia[15c], Y. Jiang[60a], S. Jiggins[52], F.A. Jimenez Morales[38], J. Jimenez Pena[114], S. Jin[15c], A. Jinaru[27b], O. Jinnouchi[163], H. Jivan[33e], P. Johansson[148], K.A. Johns[7], C.A. Johnson[65], E. Jones[176], R.W.L. Jones[89], T.J. Jones[90], J. Jovicevic[36], X. Ju[18], J.J. Junggeburth[114], A. Juste Rozas[14,w], A. Kaczmarska[84], M. Kado[72a,72b], H. Kagan[126], M. Kagan[152], A. Kahn[39], C. Kahra[99], T. Kaji[177], E. Kajomovitz[159], C.W. Kalderon[29], A. Kaluza[99], A. Kamenshchikov[122], M. Kaneda[162], N.J. Kang[144], S. Kang[78], Y. Kano[116], J. Kanzaki[81], D. Kar[33e], K. Karava[133], M.J. Kareem[166b], I. Karkanias[161], S.N. Karpov[79], Z.M. Karpova[79], V. Kartvelishvili[89], A.N. Karyukhin[122], E. Kasimi[161], C. Kato[60d], J. Katzy[46], K. Kawade[149], K. Kawagoe[87], T. Kawaguchi[116], T. Kawamoto[143], G. Kawamura[53], E.F. Kay[174], F.I. Kaya[168], S. Kazakos[14], V.F. Kazanin[121b,121a], Y. Ke[154], J.M. Keaveney[33a], R. Keeler[174], J.S. Keller[34], D. Kelsey[155], J.J. Kempster[21], J. Kendrick[21], K.E. Kennedy[39], O. Kepka[139], S. Kersten[180], B.P. Kerševan[91], S. Ketabchi Haghighat[165], F. Khalil-Zada[13], M. Khandoga[143], A. Khanov[128], A.G. Kharlamov[121b,121a], T. Kharlamova[121b,121a], E.E. Khoda[173], T.J. Khoo[19], G. Khoriauli[175], E. Khramov[79], J. Khubua[158b], S. Kido[82], M. Kiehn[36], A. Kilgallon[130], E. Kim[163], Y.K. Kim[37], N. Kimura[94], A. Kirchhoff[53], D. Kirchmeier[48], J. Kirk[142], A.E. Kiryunin[114], T. Kishimoto[162], D.P. Kisliuk[165], V. Kitali[46], C. Kitsaki[10], O. Kivernyk[24], T. Klapdor-Kleingrothaus[52], M. Klassen[61a], C. Klein[34], L. Klein[175], M.H. Klein[105], M. Klein[90], U. Klein[90], P. Klimek[36], A. Klimentov[29], F. Klimpel[36], T. Klingl[24], T. Klioutchnikova[36], F.F. Klitzner[113], P. Kluit[119], S. Kluth[114], E. Kneringer[76], A. Knue[52], D. Kobayashi[87], M. Kobel[48], M. Kocian[152], T. Kodama[162], P. Kodys[141], D.M. Koeck[155], P.T. Koenig[24], T. Koffas[34], N.M. Köhler[36], M. Kolb[143], I. Koletsou[5], T. Komarek[129], K. Köneke[52], A.X.Y. Kong[1], T. Kono[125], V. Konstantinides[94], N. Konstantinidis[94], B. Konya[96], R. Kopeliansky[65], S. Koperny[83a], K. Korcyl[84], K. Kordas[161], G. Koren[160], A. Korn[94], S. Korn[53], I. Korolkov[14], E.V. Korolkova[148], N. Korotkova[112], O. Kortner[114], S. Kortner[114], V.V. Kostyukhin[148,164], A. Kotsokechagia[64], A. Kotwal[49], A. Koulouris[10], A. Kourkoumeli-Charalampidi[70a,70b], C. Kourkoumelis[9], E. Kourlitis[6], R. Kowalewski[174], W. Kozanecki[143], A.S. Kozhin[122], V.A. Kramarenko[112], G. Kramberger[91], D. Krasnopevtsev[60a], M.W. Krasny[134], A. Krasznahorkay[36], J.A. Kremer[99], J. Kretzschmar[90], K. Kreul[19], P. Krieger[165], F. Krieter[113], S. Krishnamurthy[102], A. Krishnan[61b], M. Krivos[141], K. Krizka[18], K. Kroeninger[47], H. Kroha[114], J. Kroll[139], J. Kroll[135], K.S. Krowpman[106], U. Kruchonak[79], H. Krüger[24], N. Krumnack[78], M.C. Kruse[49], J.A. Krzysiak[84], A. Kubota[163], O. Kuchinskaia[164], S. Kuday[4b], D. Kuechler[46], J.T. Kuechler[46], S. Kuehn[36], T. Kuhl[46], V. Kukhtin[79], Y. Kulchitsky[107,ae], S. Kuleshov[145b], M. Kumar[33e], M. Kuna[58], A. Kupco[139], T. Kupfer[47], O. Kuprash[52], H. Kurashige[82], L.L. Kurchaninov[166a], Y.A. Kurochkin[107], A. Kurova[111], M.G. Kurth[15a,15d], E.S. Kuwertz[36], M. Kuze[163], A.K. Kvam[147], J. Kvita[129], T. Kwan[103], C. Lacasta[172], F. Lacava[72a,72b], D.P.J. Lack[100], H. Lacker[19], D. Lacour[134], E. Ladygin[79], R. Lafaye[5], B. Laforge[134], T. Lagouri[145c], S. Lai[53], I.K. Lakomiec[83a], J.E. Lambert[127], S. Lammers[65], W. Lampl[7], C. Lampoudis[161], E. Lançon[29], U. Landgraf[52], M.P.J. Landon[92], V.S. Lang[52], J.C. Lange[53], R.J. Langenberg[102], A.J. Lankford[169], F. Lanni[29], K. Lantzsch[24], A. Lanza[70a], A. Lapertosa[55b,55a], J.F. Laporte[143], T. Lari[68a], F. Lasagni Manghi[23b,23a], M. Lassnig[36], V. Latonova[139], T.S. Lau[62a], A. Laudrain[99], A. Laurier[34], M. Lavorgna[69a,69b], S.D. Lawlor[93], M. Lazzaroni[68a,68b], B. Le[100], A. Lebedev[78], M. LeBlanc[7], T. LeCompte[6], F. Ledroit-Guillon[58], A.C.A. Lee[94], C.A. Lee[29], G.R. Lee[17], L. Lee[59], S.C. Lee[157], S. Lee[78], L.L. Leeuw[33c], B. Lefebvre[166a], H.P. Lefebvre[93], M. Lefebvre[174], C. Leggett[18], K. Lehmann[151], N. Lehmann[20], G. Lehmann Miotto[36], W.A. Leight[46], A. Leisos[161,v], M.A.L. Leite[80c], C.E. Leitgeb[113], R. Leitner[141], K.J.C. Leney[42], T. Lenz[24], S. Leone[71a], C. Leonidopoulos[50], A. Leopold[134], C. Leroy[109], R. Les[106], C.G. Lester[32], M. Levchenko[136], J. Levêque[5], D. Levin[105], L.J. Levinson[178], D.J. Lewis[21], B. Li[15b], B. Li[105], C-Q. Li[60c,60d], F. Li[60c], H. Li[60a], H. Li[60b], J. Li[60c], K. Li[147], L. Li[60c], M. Li[15a,15d], Q.Y. Li[60a], S. Li[60d,60c,b], X. Li[46], Y. Li[46], Z. Li[60b], Z. Li[133], Z. Li[103], Z. Li[90], Z. Liang[15a], M. Liberatore[46], B. Liberti[73a], K. Lie[62c], C.Y. Lin[32], K. Lin[106], R.A. Linck[65], R.E. Lindley[7], J.H. Lindon[21], A. Linss[46], A.L. Lionti[54], E. Lipeles[135], A. Lipniacka[17],

T.M. Liss[171,aj], A. Lister[173], J.D. Little[8], B. Liu[15a], B.X. Liu[151], J.B. Liu[60a], J.K.K. Liu[37], K. Liu[60d,60c], M. Liu[60a], M.Y. Liu[60a], P. Liu[15a], X. Liu[60a], Y. Liu[46], Y. Liu[15a,15d], Y.L. Liu[105], Y.W. Liu[60a], M. Livan[70a,70b], A. Lleres[58], J. Llorente Merino[151], S.L. Lloyd[92], E.M. Lobodzinska[46], P. Loch[7], S. Loffredo[73a,73b], T. Lohse[19], K. Lohwasser[148], M. Lokajicek[139], J.D. Long[171], R.E. Long[89], I. Longarini[72a,72b], L. Longo[36], R. Longo[171], I. Lopez Paz[100], A. Lopez Solis[46], J. Lorenz[113], N. Lorenzo Martinez[5], A.M. Lory[113], A. Lösle[52], X. Lou[45a,45b], X. Lou[15a], A. Lounis[64], J. Love[6], P.A. Love[89], J.J. Lozano Bahilo[172], G. Lu[15a], M. Lu[60a], S. Lu[135], Y.J. Lu[63], H.J. Lubatti[147], C. Luci[72a,72b], F.L. Lucio Alves[15c], A. Lucotte[58], F. Luehring[65], I. Luise[154], L. Luminari[72a], B. Lund-Jensen[153], N.A. Luongo[130], M.S. Lutz[160], D. Lynn[29], H. Lyons[90], R. Lysak[139], E. Lytken[96], F. Lyu[15a], V. Lyubushkin[79], T. Lyubushkina[79], H. Ma[29], L.L. Ma[60b], Y. Ma[94], D.M. Mac Donell[174], G. Maccarrone[51], C.M. Macdonald[148], J.C. MacDonald[148], J. Machado Miguens[135], R. Madar[38], W.F. Mader[48], M. Madugoda Ralalage Don[128], N. Madysa[48], J. Maeda[82], T. Maeno[29], M. Maerker[48], V. Magerl[52], J. Magro[66a,66c], D.J. Mahon[39], C. Maidantchik[80b], A. Maio[138a,138b,138d], K. Maj[83a], O. Majersky[28a], S. Majewski[130], N. Makovec[64], B. Malaescu[134], Pa. Malecki[84], V.P. Maleev[136], F. Malek[58], D. Malito[41b,41a], U. Mallik[77], C. Malone[32], S. Maltezos[10], S. Malyukov[79], J. Mamuzic[172], G. Mancini[51], J.P. Mandalia[92], I. Mandić[91], L. Manhaes de Andrade Filho[80a], I.M. Maniatis[161], M. Manisha[143], J. Manjarres Ramos[48], K.H. Mankinen[96], A. Mann[113], A. Manousos[76], B. Mansoulie[143], I. Manthos[161], S. Manzoni[119], A. Marantis[161], L. Marchese[133], G. Marchiori[134], M. Marcisovsky[139], L. Marcoccia[73a,73b], C. Marcon[96], M. Marjanovic[127], Z. Marshall[18], M.U.F. Martensson[170], S. Marti-Garcia[172], T.A. Martin[176], V.J. Martin[50], B. Martin dit Latour[17], L. Martinelli[74a,74b], M. Martinez[14,w], P. Martinez Agullo[172], V.I. Martinez Outschoorn[102], S. Martin-Haugh[142], V.S. Martoiu[27b], A.C. Martyniuk[94], A. Marzin[36], S.R. Maschek[114], L. Masetti[99], T. Mashimo[162], R. Mashinistov[110], J. Masik[100], A.L. Maslennikov[121b,121a], L. Massa[23b,23a], P. Massarotti[69a,69b], P. Mastrandrea[71a,71b], A. Mastroberardino[41b,41a], T. Masubuchi[162], D. Matakias[29], T. Mathisen[170], A. Matic[113], N. Matsuzawa[162], J. Maurer[27b], B. Maček[91], D.A. Maximov[121b,121a], R. Mazini[157], I. Maznas[161], S.M. Mazza[144], C. Mc Ginn[29], J.P. Mc Gowan[103], S.P. Mc Kee[105], T.G. McCarthy[114], W.P. McCormack[18], E.F. McDonald[104], A.E. McDougall[119], J.A. Mcfayden[155], G. Mchedlidze[158b], M.A. McKay[42], K.D. McLean[174], S.J. McMahon[142], P.C. McNamara[104], R.A. McPherson[174,aa], J.E. Mdhluli[33e], Z.A. Meadows[102], S. Meehan[36], T. Megy[38], S. Mehlhase[113], A. Mehta[90], B. Meirose[43], D. Melini[159], B.R. Mellado Garcia[33e], F. Meloni[46], A. Melzer[24], E.D. Mendes Gouveia[138a,138e], A.M. Mendes Jacques Da Costa[21], H.Y. Meng[165], L. Meng[36], S. Menke[114], E. Meoni[41b,41a], S.A.M. Merkt[137], C. Merlassino[133], P. Mermod[54], L. Merola[69a,69b], C. Meroni[68a], G. Merz[105], O. Meshkov[112,110], J.K.R. Meshreki[150], J. Metcalfe[6], A.S. Mete[6], C. Meyer[65], J-P. Meyer[143], M. Michetti[19], R.P. Middleton[142], L. Mijović[50], G. Mikenberg[178], M. Mikestikova[139], M. Mikuž[91], H. Mildner[148], A. Milic[165], C.D. Milke[42], D.W. Miller[37], L.S. Miller[34], A. Milov[178], D.A. Milstead[45a,45b], A.A. Minaenko[122], I.A. Minashvili[158b], L. Mince[57], A.I. Mincer[124], B. Mindur[83a], M. Mineev[79], Y. Minegishi[162], Y. Mino[85], L.M. Mir[14], M. Miralles Lopez[172], M. Mironova[133], T. Mitani[177], V.A. Mitsou[172], M. Mittal[60c], O. Miu[165], A. Miucci[20], P.S. Miyagawa[92], A. Mizukami[81], J.U. Mjörnmark[96], T. Mkrtchyan[61a], M. Mlynarikova[120], T. Moa[45a,45b], S. Mobius[53], K. Mochizuki[109], P. Moder[46], P. Mogg[113], S. Mohapatra[39], G. Mokgatitswane[33e], B. Mondal[150], S. Mondal[140], K. Mönig[46], E. Monnier[101], A. Montalbano[151], J. Montejo Berlingen[36], M. Montella[94], F. Monticelli[88], N. Morange[64], A.L. Moreira De Carvalho[138a], M. Moreno Llácer[172], C. Moreno Martinez[14], P. Morettini[55b], M. Morgenstern[159], S. Morgenstern[176], D. Mori[151], M. Morii[59], M. Morinaga[177], V. Morisbak[132], A.K. Morley[36], A.P. Morris[94], L. Morvaj[36], P. Moschovakos[36], B. Moser[119], M. Mosidze[158b], T. Moskalets[143], P. Moskvitina[118], J. Moss[31,n], E.J.W. Moyse[102], S. Muanza[101], J. Mueller[137], D. Muenstermann[89], G.A. Mullier[96], J.J. Mullin[135], D.P. Mungo[68a,68b], J.L. Munoz Martinez[14], F.J. Munoz Sanchez[100], P. Murin[28b], W.J. Murray[176,142], A. Murrone[68a,68b], J.M. Muse[127], M. Muškinja[18], C. Mwewa[29], A.G. Myagkov[122,af], A.A. Myers[137], G. Myers[65], J. Myers[130], M. Myska[140], B.P. Nachman[18],

O. Nackenhorst[47], A.Nag Nag[48], K. Nagai[133], K. Nagano[81], J.L. Nagle[29], E. Nagy[101], A.M. Nairz[36], Y. Nakahama[116], K. Nakamura[81], H. Nanjo[131], F. Napolitano[61a], R.F. Naranjo Garcia[46], R. Narayan[42], I. Naryshkin[136], M. Naseri[34], T. Naumann[46], G. Navarro[22a], J. Navarro-Gonzalez[172], P.Y. Nechaeva[110], F. Nechansky[46], T.J. Neep[21], A. Negri[70a,70b], M. Negrini[23b], C. Nellist[118], C. Nelson[103], K. Nelson[105], M.E. Nelson[45a,45b], S. Nemecek[139], M. Nessi[36,f], M.S. Neubauer[171], F. Neuhaus[99], M. Neumann[180], R. Newhouse[173], P.R. Newman[21], C.W. Ng[137], Y.S. Ng[19], Y.W.Y. Ng[169], B. Ngair[35f], H.D.N. Nguyen[101], T. Nguyen Manh[109], E. Nibigira[38], R.B. Nickerson[133], R. Nicolaidou[143], D.S. Nielsen[40], J. Nielsen[144], M. Niemeyer[53], N. Nikiforou[11], V. Nikolaenko[122,af], I. Nikolic-Audit[134], K. Nikolopoulos[21], P. Nilsson[29], H.R. Nindhito[54], A. Nisati[72a], N. Nishu[60c], R. Nisius[114], T. Nitta[177], T. Nobe[162], D.L. Noel[32], Y. Noguchi[85], I. Nomidis[134], M.A. Nomura[29], R.R.B. Norisam[94], J. Novak[91], T. Novak[46], O. Novgorodova[48], R. Novotny[117], L. Nozka[129], K. Ntekas[169], E. Nurse[94], F.G. Oakham[34,ak], J. Ocariz[134], A. Ochi[82], I. Ochoa[138a], J.P. Ochoa-Ricoux[145a], K. O'Connor[26], S. Oda[87], S. Odaka[81], S. Oerdek[53], A. Ogrodnik[83a], A. Oh[100], C.C. Ohm[153], H. Oide[163], R. Oishi[162], M.L. Ojeda[165], Y. Okazaki[85], M.W. O'Keefe[90], Y. Okumura[162], A. Olariu[27b], L.F. Oleiro Seabra[138a], S.A. Olivares Pino[145c], D. Oliveira Damazio[29], D. Oliveira Goncalves[80a], J.L. Oliver[1], M.J.R. Olsson[169], A. Olszewski[84], J. Olszowska[84], Ö.O. Öncel[24], D.C. O'Neil[151], A.P. O'neill[133], A. Onofre[138a,138e], P.U.E. Onyisi[11], H. Oppen[132], R.G. Oreamuno Madriz[120], M.J. Oreglia[37], G.E. Orellana[88], D. Orestano[74a,74b], N. Orlando[14], R.S. Orr[165], V. O'Shea[57], R. Ospanov[60a], G. Otero y Garzon[30], H. Otono[87], P.S. Ott[61a], G.J. Ottino[18], M. Ouchrif[35e], J. Ouellette[29], F. Ould-Saada[132], A. Ouraou[143,*], Q. Ouyang[15a], M. Owen[57], R.E. Owen[142], V.E. Ozcan[12c], N. Ozturk[8], J. Pacalt[129], H.A. Pacey[32], K. Pachal[49], A. Pacheco Pages[14], C. Padilla Aranda[14], S. Pagan Griso[18], G. Palacino[65], S. Palazzo[50], S. Palestini[36], M. Palka[83b], P. Palni[83a], D.K. Panchal[11], C.E. Pandini[54], J.G. Panduro Vazquez[93], P. Pani[46], G. Panizzo[66a,66c], L. Paolozzi[54], C. Papadatos[109], S. Parajuli[42], A. Paramonov[6], C. Paraskevopoulos[10], D. Paredes Hernandez[62b], S.R. Paredes Saenz[133], B. Parida[178], T.H. Park[165], A.J. Parker[31], M.A. Parker[32], F. Parodi[55b,55a], E.W. Parrish[120], J.A. Parsons[39], U. Parzefall[52], L. Pascual Dominguez[134], V.R. Pascuzzi[18], J.M.P. Pasner[144], F. Pasquali[119], E. Pasqualucci[72a], S. Passaggio[55b], F. Pastore[93], P. Pasuwan[45a,45b], J.R. Pater[100], A. Pathak[179,j], J. Patton[90], T. Pauly[36], J. Pearkes[152], M. Pedersen[132], L. Pedraza Diaz[118], R. Pedro[138a], T. Peiffer[53], S.V. Peleganchuk[121b,121a], O. Penc[139], C. Peng[62b], H. Peng[60a], M. Penzin[164], B.S. Peralva[80a], M.M. Perego[64], A.P. Pereira Peixoto[138a], L. Pereira Sanchez[45a,45b], D.V. Perepelitsa[29], E. Perez Codina[166a], M. Perganti[10], L. Perini[68a,68b], H. Pernegger[36], S. Perrella[36], A. Perrevoort[119], K. Peters[46], R.F.Y. Peters[100], B.A. Petersen[36], T.C. Petersen[40], E. Petit[101], V. Petousis[140], C. Petridou[161], P. Petroff[64], F. Petrucci[74a,74b], M. Pettee[181], N.E. Pettersson[102], K. Petukhova[141], A. Peyaud[143], R. Pezoa[145d], L. Pezzotti[70a,70b], G. Pezzullo[181], T. Pham[104], P.W. Phillips[142], M.W. Phipps[171], G. Piacquadio[154], E. Pianori[18], A. Picazio[102], R. Piegaia[30], D. Pietreanu[27b], J.E. Pilcher[37], A.D. Pilkington[100], M. Pinamonti[66a,66c], J.L. Pinfold[3], C. Pitman Donaldson[94], D.A. Pizzi[34], L. Pizzimento[73a,73b], A. Pizzini[119], M.-A. Pleier[29], V. Plesanovs[52], V. Pleskot[141], E. Plotnikova[79], P. Podberezko[121b,121a], R. Poettgen[96], R. Poggi[54], L. Poggioli[134], I. Pogrebnyak[106], D. Pohl[24], I. Pokharel[53], G. Polesello[70a], A. Poley[151,166a], A. Policicchio[72a,72b], R. Polifka[141], A. Polini[23b], C.S. Pollard[46], V. Polychronakos[29], D. Ponomarenko[111], L. Pontecorvo[36], S. Popa[27a], G.A. Popeneciu[27d], L. Portales[5], D.M. Portillo Quintero[58], S. Pospisil[140], P. Postolache[27c], K. Potamianos[133], I.N. Potrap[79], C.J. Potter[32], H. Potti[11], T. Poulsen[46], J. Poveda[172], T.D. Powell[148], G. Pownall[46], M.E. Pozo Astigarraga[36], A. Prades Ibanez[172], P. Pralavorio[101], M.M. Prapa[44], S. Prell[78], D. Price[100], M. Primavera[67a], M.L. Proffitt[147], N. Proklova[111], K. Prokofiev[62c], F. Prokoshin[79], S. Protopopescu[29], J. Proudfoot[6], M. Przybycien[83a], D. Pudzha[136], P. Puzo[64], D. Pyatiizbyantseva[111], J. Qian[105], Y. Qin[100], A. Quadt[53], M. Queitsch-Maitland[36], G. Rabanal Bolanos[59], F. Ragusa[68a,68b], G. Rahal[97], J.A. Raine[54], S. Rajagopalan[29], K. Ran[15a,15d], D.F. Rassloff[61a], D.M. Rauch[46], S. Rave[99], B. Ravina[57], I. Ravinovich[178], M. Raymond[36], A.L. Read[132], N.P. Readioff[148], M. Reale[67a,67b], D.M. Rebuzzi[70a,70b], G. Redlinger[29],

K. Reeves[43], D. Reikher[160], A. Reiss[99], A. Rej[150], C. Rembser[36], A. Renardi[46], M. Renda[27b], M.B. Rendel[114], A.G. Rennie[57], S. Resconi[68a], E.D. Resseguie[18], S. Rettie[94], B. Reynolds[126], E. Reynolds[21], M. Rezaei Estabragh[180], O.L. Rezanova[121b,121a], P. Reznicek[141], E. Ricci[75a,75b], R. Richter[114], S. Richter[46], E. Richter-Was[83b], M. Ridel[134], P. Rieck[114], O. Rifki[46], M. Rijssenbeek[154], A. Rimoldi[70a,70b], M. Rimoldi[46], L. Rinaldi[23b], T.T. Rinn[171], M.P. Rinnagel[113], G. Ripellino[153], I. Riu[14], P. Rivadeneira[46], J.C. Rivera Vergara[174], F. Rizatdinova[128], E. Rizvi[92], C. Rizzi[54], S.H. Robertson[103,aa], M. Robin[46], D. Robinson[32], C.M. Robles Gajardo[145d], M. Robles Manzano[99], A. Robson[57], A. Rocchi[73a,73b], C. Roda[71a,71b], S. Rodriguez Bosca[172], A. Rodriguez Rodriguez[52], A.M. Rodríguez Vera[166b], S. Roe[36], J. Roggel[180], O. Røhne[132], R.A. Rojas[145d], B. Roland[52], C.P.A. Roland[65], J. Roloff[29], A. Romaniouk[111], M. Romano[23b,23a], N. Rompotis[90], M. Ronzani[124], L. Roos[134], S. Rosati[72a], G. Rosin[102], B.J. Rosser[135], E. Rossi[46], E. Rossi[5], E. Rossi[69a,69b], L.P. Rossi[55b], L. Rossini[46], R. Rosten[126], M. Rotaru[27b], B. Rottler[52], D. Rousseau[64], G. Rovelli[70a,70b], A. Roy[11], A. Rozanov[101], Y. Rozen[159], X. Ruan[33e], A.J. Ruby[90], T.A. Ruggeri[1], F. Rühr[52], A. Ruiz-Martinez[172], A. Rummler[36], Z. Rurikova[52], N.A. Rusakovich[79], H.L. Russell[36], L. Rustige[38], J.P. Rutherfoord[7], E.M. Rüttinger[148], M. Rybar[141], E.B. Rye[132], A. Ryzhov[122], J.A. Sabater Iglesias[46], P. Sabatini[172], L. Sabetta[72a,72b], H.F-W. Sadrozinski[144], R. Sadykov[79], F. Safai Tehrani[72a], B. Safarzadeh Samani[155], M. Safdari[152], P. Saha[120], S. Saha[103], M. Sahinsoy[114], A. Sahu[180], M. Saimpert[36], M. Saito[162], T. Saito[162], D. Salamani[54], G. Salamanna[74a,74b], A. Salnikov[152], J. Salt[172], A. Salvador Salas[14], D. Salvatore[41b,41a], F. Salvatore[155], A. Salzburger[36], D. Sammel[52], D. Sampsonidis[161], D. Sampsonidou[60d,60c], J. Sánchez[172], A. Sanchez Pineda[66a,36,66c], H. Sandaker[132], C.O. Sander[46], I.G. Sanderswood[89], M. Sandhoff[180], C. Sandoval[22b], D.P.C. Sankey[142], M. Sannino[55b,55a], Y. Sano[116], A. Sansoni[51], C. Santoni[38], H. Santos[138a,138b], S.N. Santpur[18], A. Santra[178], K.A. Saoucha[148], A. Sapronov[79], J.G. Saraiva[138a,138d], O. Sasaki[81], K. Sato[167], F. Sauerburger[52], E. Sauvan[5], P. Savard[165,ak], R. Sawada[162], C. Sawyer[142], L. Sawyer[95], I. Sayago Galvan[172], C. Sbarra[23b], A. Sbrizzi[66a,66c], T. Scanlon[94], J. Schaarschmidt[147], P. Schacht[114], D. Schaefer[37], L. Schaefer[135], U. Schäfer[99], A.C. Schaffer[64], D. Schaile[113], R.D. Schamberger[154], E. Schanet[113], C. Scharf[19], N. Scharmberg[100], V.A. Schegelsky[136], D. Scheirich[141], F. Schenck[19], M. Schernau[169], C. Schiavi[55b,55a], L.K. Schildgen[24], Z.M. Schillaci[26], E.J. Schioppa[67a,67b], M. Schioppa[41b,41a], K.E. Schleicher[52], S. Schlenker[36], K. Schmieden[99], C. Schmitt[99], S. Schmitt[46], L. Schoeffel[143], A. Schoening[61b], P.G. Scholer[52], E. Schopf[133], M. Schott[99], J. Schovancova[36], S. Schramm[54], F. Schroeder[180], A. Schulte[99], H-C. Schultz-Coulon[61a], M. Schumacher[52], B.A. Schumm[144], Ph. Schune[143], A. Schwartzman[152], T.A. Schwarz[105], Ph. Schwemling[143], R. Schwienhorst[106], A. Sciandra[144], G. Sciolla[26], F. Scuri[71a], F. Scutti[104], C.D. Sebastiani[90], K. Sedlaczek[47], P. Seema[19], S.C. Seidel[117], A. Seiden[144], B.D. Seidlitz[29], T. Seiss[37], C. Seitz[46], J.M. Seixas[80b], G. Sekhniaidze[69a], S.J. Sekula[42], L.P. Selem[5], N. Semprini-Cesari[23b,23a], S. Sen[49], C. Serfon[29], L. Serin[64], L. Serkin[66a,66b], M. Sessa[60a], H. Severini[127], S. Sevova[152], F. Sforza[55b,55a], A. Sfyrla[54], E. Shabalina[53], J.D. Shahinian[135], N.W. Shaikh[45a,45b], D. Shaked Renous[178], L.Y. Shan[15a], M. Shapiro[18], A. Sharma[36], A.S. Sharma[1], P.B. Shatalov[123], K. Shaw[155], S.M. Shaw[100], M. Shehade[178], Y. Shen[127], P. Sherwood[94], L. Shi[94], C.O. Shimmin[181], Y. Shimogama[177], M. Shimojima[115], J.D. Shinner[93], I.P.J. Shipsey[133], S. Shirabe[163], M. Shiyakova[79,y], J. Shlomi[178], M.J. Shochet[37], J. Shojaii[104], D.R. Shope[153], S. Shrestha[126], E.M. Shrif[33e], M.J. Shroff[174], E. Shulga[178], P. Sicho[139], A.M. Sickles[171], E. Sideras Haddad[33e], O. Sidiropoulou[36], A. Sidoti[23b,23a], F. Siegert[48], Dj. Sijacki[16], M.V. Silva Oliveira[36], S.B. Silverstein[45a], S. Simion[64], R. Simoniello[36], S. Simsek[12b], P. Sinervo[165], V. Sinetckii[112], S. Singh[151], S. Sinha[33e], M. Sioli[23b,23a], I. Siral[130], S.Yu. Sivoklokov[112], J. Sjölin[45a,45b], A. Skaf[53], E. Skorda[96], P. Skubic[127], M. Slawinska[84], K. Sliwa[168], V. Smakhtin[178], B.H. Smart[142], J. Smiesko[141], S.Yu. Smirnov[111], Y. Smirnov[111], L.N. Smirnova[112,r], O. Smirnova[96], E.A. Smith[37], H.A. Smith[133], M. Smizanska[89], K. Smolek[140], A. Smykiewicz[84], A.A. Snesarev[110], H.L. Snoek[119], I.M. Snyder[130], S. Snyder[29], R. Sobie[174,aa], A. Soffer[160], A. Søgaard[50], F. Sohns[53], C.A. Solans Sanchez[36],

E.Yu. Soldatov[111], U. Soldevila[172], A.A. Solodkov[122], S. Solomon[52], A. Soloshenko[79], O.V. Solovyanov[122], V. Solovyev[136], P. Sommer[148], H. Son[168], A. Sonay[14], W.Y. Song[166b], A. Sopczak[140], A.L. Sopio[94], F. Sopkova[28b], S. Sottocornola[70a,70b], R. Soualah[66a,66c], A.M. Soukharev[121b,121a], Z. Soumaimi[35f], D. South[46], S. Spagnolo[67a,67b], M. Spalla[114], M. Spangenberg[176], F. Spanò[93], D. Sperlich[52], T.M. Spieker[61a], G. Spigo[36], M. Spina[155], D.P. Spiteri[57], M. Spousta[141], A. Stabile[68a,68b], B.L. Stamas[120], R. Stamen[61a], M. Stamenkovic[119], A. Stampekis[21], E. Stanecka[84], B. Stanislaus[133], M.M. Stanitzki[46], M. Stankaityte[133], B. Stapf[119], E.A. Starchenko[122], G.H. Stark[144], J. Stark[101], P. Staroba[139], P. Starovoitov[61a], S. Stärz[103], R. Staszewski[84], G. Stavropoulos[44], P. Steinberg[29], A.L. Steinhebel[130], B. Stelzer[151,166a], H.J. Stelzer[137], O. Stelzer-Chilton[166a], H. Stenzel[56], T.J. Stevenson[155], G.A. Stewart[36], M.C. Stockton[36], G. Stoicea[27b], M. Stolarski[138a], S. Stonjek[114], A. Straessner[48], J. Strandberg[153], S. Strandberg[45a,45b], M. Strauss[127], T. Strebler[101], P. Strizenec[28b], R. Ströhmer[175], D.M. Strom[130], L.R. Strom[46], R. Stroynowski[42], A. Strubig[45a,45b], S.A. Stucci[29], B. Stugu[17], J. Stupak[127], N.A. Styles[46], D. Su[152], W. Su[60d,147,60c], X. Su[60a], N.B. Suarez[137], V.V. Sulin[110], M.J. Sullivan[90], D.M.S. Sultan[54], S. Sultansoy[4c], T. Sumida[85], S. Sun[105], S. Sun[179], X. Sun[100], C.J.E. Suster[156], M.R. Sutton[155], M. Svatos[139], M. Swiatlowski[166a], S.P. Swift[2], T. Swirski[175], A. Sydorenko[99], I. Sykora[28a], M. Sykora[141], T. Sykora[141], D. Ta[99], K. Tackmann[46,x], A. Taffard[169], R. Tafirout[166a], E. Tagiev[122], R.H.M. Taibah[134], R. Takashima[86], K. Takeda[82], T. Takeshita[149], E.P. Takeva[50], Y. Takubo[81], M. Talby[101], A.A. Talyshev[121b,121a], K.C. Tam[62b], N.M. Tamir[160], J. Tanaka[162], R. Tanaka[64], S. Tapia Araya[171], S. Tapprogge[99], A. Tarek Abouelfadl Mohamed[106], S. Tarem[159], K. Tariq[60b], G. Tarna[27b,e], G.F. Tartarelli[68a], P. Tas[141], M. Tasevsky[139], E. Tassi[41b,41a], G. Tateno[162], Y. Tayalati[35f], G.N. Taylor[104], W. Taylor[166b], H. Teagle[90], A.S. Tee[89], R. Teixeira De Lima[152], P. Teixeira-Dias[93], H. Ten Kate[36], J.J. Teoh[119], K. Terashi[162], J. Terron[98], S. Terzo[14], M. Testa[51], R.J. Teuscher[165,aa], N. Themistokleous[50], T. Theveneaux-Pelzer[19], D.W. Thomas[93], J.P. Thomas[21], E.A. Thompson[46], P.D. Thompson[21], E. Thomson[135], E.J. Thorpe[92], V.O. Tikhomirov[110,ag], Yu.A. Tikhonov[121b,121a], S. Timoshenko[111], P. Tipton[181], S. Tisserant[101], S.H. Tlou[33e], A. Tnourji[38], K. Todome[23b,23a], S. Todorova-Nova[141], S. Todt[48], J. Tojo[87], S. Tokár[28a], K. Tokushuku[81], E. Tolley[126], R. Tombs[32], M. Tomoto[81,116], L. Tompkins[152], P. Tornambe[102], E. Torrence[130], H. Torres[48], E. Torró Pastor[172], M. Toscani[30], C. Tosciri[37], J. Toth[101,z], D.R. Tovey[148], A. Traeet[17], C.J. Treado[124], T. Trefzger[175], A. Tricoli[29], I.M. Trigger[166a], S. Trincaz-Duvoid[134], D.A. Trischuk[173], W. Trischuk[165], B. Trocmé[58], A. Trofymov[64], C. Troncon[68a], F. Trovato[155], L. Truong[33c], M. Trzebinski[84], A. Trzupek[84], F. Tsai[46], P.V. Tsiareshka[107,ae], A. Tsirigotis[161,v], V. Tsiskaridze[154], E.G. Tskhadadze[158a], M. Tsopoulou[161], I.I. Tsukerman[123], V. Tsulaia[18], S. Tsuno[81], D. Tsybychev[154], Y. Tu[62b], A. Tudorache[27b], V. Tudorache[27b], A.N. Tuna[36], S. Turchikhin[79], D. Turgeman[178], I. Turk Cakir[4b,t], R.J. Turner[21], R. Turra[68a], P.M. Tuts[39], S. Tzamarias[161], P. Tzanis[10], E. Tzovara[99], K. Uchida[162], F. Ukegawa[167], G. Unal[36], M. Unal[11], A. Undrus[29], G. Unel[169], F.C. Ungaro[104], K. Uno[162], J. Urban[28b], P. Urquijo[104], G. Usai[8], Z. Uysal[12d], V. Vacek[140], B. Vachon[103], K.O.H. Vadla[132], T. Vafeiadis[36], C. Valderanis[113], E. Valdes Santurio[45a,45b], M. Valente[166a], S. Valentinetti[23b,23a], A. Valero[172], L. Valéry[46], R.A. Vallance[21], A. Vallier[36], J.A. Valls Ferrer[172], T.R. Van Daalen[14], P. Van Gemmeren[6], S. Van Stroud[94], I. Van Vulpen[119], M. Vanadia[73a,73b], W. Vandelli[36], M. Vandenbroucke[143], E.R. Vandewall[128], D. Vannicola[72a,72b], R. Vari[72a], E.W. Varnes[7], C. Varni[55b,55a], T. Varol[157], D. Varouchas[64], K.E. Varvell[156], M.E. Vasile[27b], L. Vaslin[38], G.A. Vasquez[174], F. Vazeille[38], D. Vazquez Furelos[14], T. Vazquez Schroeder[36], J. Veatch[53], V. Vecchio[100], M.J. Veen[119], L.M. Veloce[165], F. Veloso[138a,138c], S. Veneziano[72a], A. Ventura[67a,67b], A. Verbytskyi[114], M. Verducci[71a,71b], C. Vergis[24], M. Verissimo De Araujo[80b], W. Verkerke[119], A.T. Vermeulen[119], J.C. Vermeulen[119], C. Vernieri[152], P.J. Verschuuren[93], M.L. Vesterbacka[124], M.C. Vetterli[151,ak], N. Viaux Maira[145d], T. Vickey[148], O.E. Vickey Boeriu[148], G.H.A. Viehhauser[133], L. Vigani[61b], M. Villa[23b,23a], M. Villaplana Perez[172], E.M. Villhauer[50], E. Vilucchi[51], M.G. Vincter[34], G.S. Virdee[21], A. Vishwakarma[50], C. Vittori[23b,23a], I. Vivarelli[155], V. Vladimirov[176], M. Vogel[180], P. Vokac[140],

J. Von Ahnen[46], S.E. von Buddenbrock[33e], E. Von Toerne[24], V. Vorobel[141], K. Vorobev[111], M. Vos[172], J.H. Vossebeld[90], M. Vozak[100], N. Vranjes[16], M. Vranjes Milosavljevic[16], V. Vrba[140,*], M. Vreeswijk[119], N.K. Vu[101], R. Vuillermet[36], I. Vukotic[37], S. Wada[167], C. Wagner[102], P. Wagner[24], W. Wagner[180], S. Wahdan[180], H. Wahlberg[88], R. Wakasa[167], V.M. Walbrecht[114], J. Walder[142], R. Walker[113], S.D. Walker[93], W. Walkowiak[150], V. Wallangen[45a,45b], A.M. Wang[59], A.Z. Wang[179], C. Wang[60a], C. Wang[60c], H. Wang[18], J. Wang[62a], P. Wang[42], R.-J. Wang[99], R. Wang[60a], R. Wang[120], S.M. Wang[157], S. Wang[60b], T. Wang[60a], W.T. Wang[60a], W.X. Wang[60a], Y. Wang[60a], Z. Wang[105], C. Wanotayaroj[36], A. Warburton[103], C.P. Ward[32], R.J. Ward[21], N. Warrack[57], A.T. Watson[21], M.F. Watson[21], G. Watts[147], B.M. Waugh[94], A.F. Webb[11], C. Weber[29], M.S. Weber[20], S.A. Weber[34], S.M. Weber[61a], C. Wei[60a], Y. Wei[133], A.R. Weidberg[133], J. Weingarten[47], M. Weirich[99], C. Weiser[52], P.S. Wells[36], T. Wenaus[29], B. Wendland[47], T. Wengler[36], S. Wenig[36], N. Wermes[24], M. Wessels[61a], T.D. Weston[20], K. Whalen[130], A.M. Wharton[89], A.S. White[59], A. White[8], M.J. White[1], D. Whiteson[169], W. Wiedenmann[179], C. Wiel[48], M. Wielers[142], N. Wieseotte[99], C. Wiglesworth[40], L.A.M. Wiik-Fuchs[52], H.G. Wilkens[36], L.J. Wilkins[93], D.M. Williams[39], H.H. Williams[135], S. Williams[32], S. Willocq[102], P.J. Windischhofer[133], I. Wingerter-Seez[5], F. Winklmeier[130], B.T. Winter[52], M. Wittgen[152], M. Wobisch[95], A. Wolf[99], R. Wölker[133], J. Wollrath[52], M.W. Wolter[84], H. Wolters[138a,138c], V.W.S. Wong[173], A.F. Wongel[46], N.L. Woods[144], S.D. Worm[46], B.K. Wosiek[84], K.W. Woźniak[84], K. Wraight[57], J. Wu[15a,15d], S.L. Wu[179], X. Wu[54], Y. Wu[60a], Z. Wu[143], J. Wuerzinger[133], T.R. Wyatt[100], B.M. Wynne[50], S. Xella[40], J. Xiang[62c], X. Xiao[105], X. Xie[60a], I. Xiotidis[155], D. Xu[15a], H. Xu[60a], H. Xu[60a], L. Xu[60a], R. Xu[135], T. Xu[143], W. Xu[105], Y. Xu[15b], Z. Xu[60b], Z. Xu[152], B. Yabsley[156], S. Yacoob[33a], D.P. Yallup[94], N. Yamaguchi[87], Y. Yamaguchi[163], M. Yamatani[162], H. Yamauchi[167], T. Yamazaki[18], Y. Yamazaki[82], J. Yan[60c], Z. Yan[25], H.J. Yang[60c,60d], H.T. Yang[18], S. Yang[60a], T. Yang[62c], X. Yang[60a], X. Yang[15a], Y. Yang[162], Z. Yang[60a], W-M. Yao[18], Y.C. Yap[46], H. Ye[15c], J. Ye[42], S. Ye[29], I. Yeletskikh[79], M.R. Yexley[89], P. Yin[39], K. Yorita[177], K. Yoshihara[78], C.J.S. Young[36], C. Young[152], R. Yuan[60b,i], X. Yue[61a], M. Zaazoua[35f], B. Zabinski[84], G. Zacharis[10], E. Zaffaroni[54], J. Zahreddine[101], A.M. Zaitsev[122,af], T. Zakareishvili[158b], N. Zakharchuk[34], S. Zambito[36], D. Zanzi[52], S.V. Zeißner[47], C. Zeitnitz[180], G. Zemaityte[133], J.C. Zeng[171], O. Zenin[122], T. Ženiš[28a], S. Zenz[92], S. Zerradi[35a], D. Zerwas[64], M. Zgubič[133], B. Zhang[15c], D.F. Zhang[15b], G. Zhang[15b], J. Zhang[6], K. Zhang[15a], L. Zhang[15c], L. Zhang[60a], M. Zhang[171], R. Zhang[179], S. Zhang[105], X. Zhang[60c], X. Zhang[60b], Z. Zhang[64], P. Zhao[49], Y. Zhao[144], Z. Zhao[60a], A. Zhemchugov[79], Z. Zheng[105], D. Zhong[171], B. Zhou[105], C. Zhou[179], H. Zhou[7], M. Zhou[154], N. Zhou[60c], Y. Zhou[7], C.G. Zhu[60b], C. Zhu[15a,15d], H.L. Zhu[60a], H. Zhu[15a], J. Zhu[105], Y. Zhu[60a], X. Zhuang[15a], K. Zhukov[110], V. Zhulanov[121b,121a], D. Zieminska[65], N.I. Zimine[79], S. Zimmermann[52,*], Z. Zinonos[114], M. Ziolkowski[150], L. Živković[16], A. Zoccoli[23b,23a], K. Zoch[53], T.G. Zorbas[148], R. Zou[37], W. Zou[39], L. Zwalinski[36].

[1]Department of Physics, University of Adelaide, Adelaide; Australia.
[2]Physics Department, SUNY Albany, Albany NY; United States of America.
[3]Department of Physics, University of Alberta, Edmonton AB; Canada.
[4(a)]Department of Physics, Ankara University, Ankara;[(b)]Istanbul Aydin University, Application and Research Center for Advanced Studies, Istanbul;[(c)]Division of Physics, TOBB University of Economics and Technology, Ankara; Turkey.
[5]LAPP, Université Grenoble Alpes, Université Savoie Mont Blanc, CNRS/IN2P3, Annecy; France.
[6]High Energy Physics Division, Argonne National Laboratory, Argonne IL; United States of America.
[7]Department of Physics, University of Arizona, Tucson AZ; United States of America.
[8]Department of Physics, University of Texas at Arlington, Arlington TX; United States of America.
[9]Physics Department, National and Kapodistrian University of Athens, Athens; Greece.
[10]Physics Department, National Technical University of Athens, Zografou; Greece.
[11]Department of Physics, University of Texas at Austin, Austin TX; United States of America.

[12(a)]Bahcesehir University, Faculty of Engineering and Natural Sciences, Istanbul;[(b)]Istanbul Bilgi University, Faculty of Engineering and Natural Sciences, Istanbul;[(c)]Department of Physics, Bogazici University, Istanbul;[(d)]Department of Physics Engineering, Gaziantep University, Gaziantep; Turkey.
[13]Institute of Physics, Azerbaijan Academy of Sciences, Baku; Azerbaijan.
[14]Institut de Física d'Altes Energies (IFAE), Barcelona Institute of Science and Technology, Barcelona; Spain.
[15(a)]Institute of High Energy Physics, Chinese Academy of Sciences, Beijing;[(b)]Physics Department, Tsinghua University, Beijing;[(c)]Department of Physics, Nanjing University, Nanjing;[(d)]University of Chinese Academy of Science (UCAS), Beijing; China.
[16]Institute of Physics, University of Belgrade, Belgrade; Serbia.
[17]Department for Physics and Technology, University of Bergen, Bergen; Norway.
[18]Physics Division, Lawrence Berkeley National Laboratory and University of California, Berkeley CA; United States of America.
[19]Institut für Physik, Humboldt Universität zu Berlin, Berlin; Germany.
[20]Albert Einstein Center for Fundamental Physics and Laboratory for High Energy Physics, University of Bern, Bern; Switzerland.
[21]School of Physics and Astronomy, University of Birmingham, Birmingham; United Kingdom.
[22(a)]Facultad de Ciencias y Centro de Investigaciónes, Universidad Antonio Nariño, Bogotá;[(b)]Departamento de Física, Universidad Nacional de Colombia, Bogotá, Colombia; Colombia.
[23(a)]INFN Bologna and Universita' di Bologna, Dipartimento di Fisica;[(b)]INFN Sezione di Bologna; Italy.
[24]Physikalisches Institut, Universität Bonn, Bonn; Germany.
[25]Department of Physics, Boston University, Boston MA; United States of America.
[26]Department of Physics, Brandeis University, Waltham MA; United States of America.
[27(a)]Transilvania University of Brasov, Brasov;[(b)]Horia Hulubei National Institute of Physics and Nuclear Engineering, Bucharest;[(c)]Department of Physics, Alexandru Ioan Cuza University of Iasi, Iasi;[(d)]National Institute for Research and Development of Isotopic and Molecular Technologies, Physics Department, Cluj-Napoca;[(e)]University Politehnica Bucharest, Bucharest;[(f)]West University in Timisoara, Timisoara; Romania.
[28(a)]Faculty of Mathematics, Physics and Informatics, Comenius University, Bratislava;[(b)]Department of Subnuclear Physics, Institute of Experimental Physics of the Slovak Academy of Sciences, Kosice; Slovak Republic.
[29]Physics Department, Brookhaven National Laboratory, Upton NY; United States of America.
[30]Departamento de Física, Universidad de Buenos Aires, Buenos Aires; Argentina.
[31]California State University, CA; United States of America.
[32]Cavendish Laboratory, University of Cambridge, Cambridge; United Kingdom.
[33(a)]Department of Physics, University of Cape Town, Cape Town;[(b)]iThemba Labs, Western Cape;[(c)]Department of Mechanical Engineering Science, University of Johannesburg, Johannesburg;[(d)]University of South Africa, Department of Physics, Pretoria;[(e)]School of Physics, University of the Witwatersrand, Johannesburg; South Africa.
[34]Department of Physics, Carleton University, Ottawa ON; Canada.
[35(a)]Faculté des Sciences Ain Chock, Réseau Universitaire de Physique des Hautes Energies - Université Hassan II, Casablanca;[(b)]Faculté des Sciences, Université Ibn-Tofail, Kénitra;[(c)]Faculté des Sciences Semlalia, Université Cadi Ayyad, LPHEA-Marrakech;[(d)]Moroccan Foundation for Advanced Science Innovation and Research (MAScIR), Rabat;[(e)]LPMR, Faculté des Sciences, Université Mohamed Premier, Oujda;[(f)]Faculté des sciences, Université Mohammed V, Rabat; Morocco.
[36]CERN, Geneva; Switzerland.
[37]Enrico Fermi Institute, University of Chicago, Chicago IL; United States of America.

[38]LPC, Université Clermont Auvergne, CNRS/IN2P3, Clermont-Ferrand; France.
[39]Nevis Laboratory, Columbia University, Irvington NY; United States of America.
[40]Niels Bohr Institute, University of Copenhagen, Copenhagen; Denmark.
[41(a)]Dipartimento di Fisica, Università della Calabria, Rende;[(b)]INFN Gruppo Collegato di Cosenza, Laboratori Nazionali di Frascati; Italy.
[42]Physics Department, Southern Methodist University, Dallas TX; United States of America.
[43]Physics Department, University of Texas at Dallas, Richardson TX; United States of America.
[44]National Centre for Scientific Research "Demokritos", Agia Paraskevi; Greece.
[45(a)]Department of Physics, Stockholm University;[(b)]Oskar Klein Centre, Stockholm; Sweden.
[46]Deutsches Elektronen-Synchrotron DESY, Hamburg and Zeuthen; Germany.
[47]Lehrstuhl für Experimentelle Physik IV, Technische Universität Dortmund, Dortmund; Germany.
[48]Institut für Kern- und Teilchenphysik, Technische Universität Dresden, Dresden; Germany.
[49]Department of Physics, Duke University, Durham NC; United States of America.
[50]SUPA - School of Physics and Astronomy, University of Edinburgh, Edinburgh; United Kingdom.
[51]INFN e Laboratori Nazionali di Frascati, Frascati; Italy.
[52]Physikalisches Institut, Albert-Ludwigs-Universität Freiburg, Freiburg; Germany.
[53]II. Physikalisches Institut, Georg-August-Universität Göttingen, Göttingen; Germany.
[54]Département de Physique Nucléaire et Corpusculaire, Université de Genève, Genève; Switzerland.
[55(a)]Dipartimento di Fisica, Università di Genova, Genova;[(b)]INFN Sezione di Genova; Italy.
[56]II. Physikalisches Institut, Justus-Liebig-Universität Giessen, Giessen; Germany.
[57]SUPA - School of Physics and Astronomy, University of Glasgow, Glasgow; United Kingdom.
[58]LPSC, Université Grenoble Alpes, CNRS/IN2P3, Grenoble INP, Grenoble; France.
[59]Laboratory for Particle Physics and Cosmology, Harvard University, Cambridge MA; United States of America.
[60(a)]Department of Modern Physics and State Key Laboratory of Particle Detection and Electronics, University of Science and Technology of China, Hefei;[(b)]Institute of Frontier and Interdisciplinary Science and Key Laboratory of Particle Physics and Particle Irradiation (MOE), Shandong University, Qingdao;[(c)]School of Physics and Astronomy, Shanghai Jiao Tong University, Key Laboratory for Particle Astrophysics and Cosmology (MOE), SKLPPC, Shanghai;[(d)]Tsung-Dao Lee Institute, Shanghai; China.
[61(a)]Kirchhoff-Institut für Physik, Ruprecht-Karls-Universität Heidelberg, Heidelberg;[(b)]Physikalisches Institut, Ruprecht-Karls-Universität Heidelberg, Heidelberg; Germany.
[62(a)]Department of Physics, Chinese University of Hong Kong, Shatin, N.T., Hong Kong;[(b)]Department of Physics, University of Hong Kong, Hong Kong;[(c)]Department of Physics and Institute for Advanced Study, Hong Kong University of Science and Technology, Clear Water Bay, Kowloon, Hong Kong; China.
[63]Department of Physics, National Tsing Hua University, Hsinchu; Taiwan.
[64]IJCLab, Université Paris-Saclay, CNRS/IN2P3, 91405, Orsay; France.
[65]Department of Physics, Indiana University, Bloomington IN; United States of America.
[66(a)]INFN Gruppo Collegato di Udine, Sezione di Trieste, Udine;[(b)]ICTP, Trieste;[(c)]Dipartimento Politecnico di Ingegneria e Architettura, Università di Udine, Udine; Italy.
[67(a)]INFN Sezione di Lecce;[(b)]Dipartimento di Matematica e Fisica, Università del Salento, Lecce; Italy.
[68(a)]INFN Sezione di Milano;[(b)]Dipartimento di Fisica, Università di Milano, Milano; Italy.
[69(a)]INFN Sezione di Napoli;[(b)]Dipartimento di Fisica, Università di Napoli, Napoli; Italy.
[70(a)]INFN Sezione di Pavia;[(b)]Dipartimento di Fisica, Università di Pavia, Pavia; Italy.
[71(a)]INFN Sezione di Pisa;[(b)]Dipartimento di Fisica E. Fermi, Università di Pisa, Pisa; Italy.
[72(a)]INFN Sezione di Roma;[(b)]Dipartimento di Fisica, Sapienza Università di Roma, Roma; Italy.
[73(a)]INFN Sezione di Roma Tor Vergata;[(b)]Dipartimento di Fisica, Università di Roma Tor Vergata, Roma; Italy.

[74](a) INFN Sezione di Roma Tre;(b) Dipartimento di Matematica e Fisica, Università Roma Tre, Roma; Italy.
[75](a) INFN-TIFPA;(b) Università degli Studi di Trento, Trento; Italy.
[76] Institut für Astro- und Teilchenphysik, Leopold-Franzens-Universität, Innsbruck; Austria.
[77] University of Iowa, Iowa City IA; United States of America.
[78] Department of Physics and Astronomy, Iowa State University, Ames IA; United States of America.
[79] Joint Institute for Nuclear Research, Dubna; Russia.
[80](a) Departamento de Engenharia Elétrica, Universidade Federal de Juiz de Fora (UFJF), Juiz de Fora;(b) Universidade Federal do Rio De Janeiro COPPE/EE/IF, Rio de Janeiro;(c) Instituto de Física, Universidade de São Paulo, São Paulo; Brazil.
[81] KEK, High Energy Accelerator Research Organization, Tsukuba; Japan.
[82] Graduate School of Science, Kobe University, Kobe; Japan.
[83](a) AGH University of Science and Technology, Faculty of Physics and Applied Computer Science, Krakow;(b) Marian Smoluchowski Institute of Physics, Jagiellonian University, Krakow; Poland.
[84] Institute of Nuclear Physics Polish Academy of Sciences, Krakow; Poland.
[85] Faculty of Science, Kyoto University, Kyoto; Japan.
[86] Kyoto University of Education, Kyoto; Japan.
[87] Research Center for Advanced Particle Physics and Department of Physics, Kyushu University, Fukuoka ; Japan.
[88] Instituto de Física La Plata, Universidad Nacional de La Plata and CONICET, La Plata; Argentina.
[89] Physics Department, Lancaster University, Lancaster; United Kingdom.
[90] Oliver Lodge Laboratory, University of Liverpool, Liverpool; United Kingdom.
[91] Department of Experimental Particle Physics, Jožef Stefan Institute and Department of Physics, University of Ljubljana, Ljubljana; Slovenia.
[92] School of Physics and Astronomy, Queen Mary University of London, London; United Kingdom.
[93] Department of Physics, Royal Holloway University of London, Egham; United Kingdom.
[94] Department of Physics and Astronomy, University College London, London; United Kingdom.
[95] Louisiana Tech University, Ruston LA; United States of America.
[96] Fysiska institutionen, Lunds universitet, Lund; Sweden.
[97] Centre de Calcul de l'Institut National de Physique Nucléaire et de Physique des Particules (IN2P3), Villeurbanne; France.
[98] Departamento de Física Teorica C-15 and CIAFF, Universidad Autónoma de Madrid, Madrid; Spain.
[99] Institut für Physik, Universität Mainz, Mainz; Germany.
[100] School of Physics and Astronomy, University of Manchester, Manchester; United Kingdom.
[101] CPPM, Aix-Marseille Université, CNRS/IN2P3, Marseille; France.
[102] Department of Physics, University of Massachusetts, Amherst MA; United States of America.
[103] Department of Physics, McGill University, Montreal QC; Canada.
[104] School of Physics, University of Melbourne, Victoria; Australia.
[105] Department of Physics, University of Michigan, Ann Arbor MI; United States of America.
[106] Department of Physics and Astronomy, Michigan State University, East Lansing MI; United States of America.
[107] B.I. Stepanov Institute of Physics, National Academy of Sciences of Belarus, Minsk; Belarus.
[108] Research Institute for Nuclear Problems of Byelorussian State University, Minsk; Belarus.
[109] Group of Particle Physics, University of Montreal, Montreal QC; Canada.
[110] P.N. Lebedev Physical Institute of the Russian Academy of Sciences, Moscow; Russia.
[111] National Research Nuclear University MEPhI, Moscow; Russia.
[112] D.V. Skobeltsyn Institute of Nuclear Physics, M.V. Lomonosov Moscow State University, Moscow;

Russia.
[113]Fakultät für Physik, Ludwig-Maximilians-Universität München, München; Germany.
[114]Max-Planck-Institut für Physik (Werner-Heisenberg-Institut), München; Germany.
[115]Nagasaki Institute of Applied Science, Nagasaki; Japan.
[116]Graduate School of Science and Kobayashi-Maskawa Institute, Nagoya University, Nagoya; Japan.
[117]Department of Physics and Astronomy, University of New Mexico, Albuquerque NM; United States of America.
[118]Institute for Mathematics, Astrophysics and Particle Physics, Radboud University/Nikhef, Nijmegen; Netherlands.
[119]Nikhef National Institute for Subatomic Physics and University of Amsterdam, Amsterdam; Netherlands.
[120]Department of Physics, Northern Illinois University, DeKalb IL; United States of America.
[121 (a)]Budker Institute of Nuclear Physics and NSU, SB RAS, Novosibirsk;[(b)]Novosibirsk State University Novosibirsk; Russia.
[122]Institute for High Energy Physics of the National Research Centre Kurchatov Institute, Protvino; Russia.
[123]Institute for Theoretical and Experimental Physics named by A.I. Alikhanov of National Research Centre "Kurchatov Institute", Moscow; Russia.
[124]Department of Physics, New York University, New York NY; United States of America.
[125]Ochanomizu University, Otsuka, Bunkyo-ku, Tokyo; Japan.
[126]Ohio State University, Columbus OH; United States of America.
[127]Homer L. Dodge Department of Physics and Astronomy, University of Oklahoma, Norman OK; United States of America.
[128]Department of Physics, Oklahoma State University, Stillwater OK; United States of America.
[129]Palacký University, RCPTM, Joint Laboratory of Optics, Olomouc; Czech Republic.
[130]Institute for Fundamental Science, University of Oregon, Eugene, OR; United States of America.
[131]Graduate School of Science, Osaka University, Osaka; Japan.
[132]Department of Physics, University of Oslo, Oslo; Norway.
[133]Department of Physics, Oxford University, Oxford; United Kingdom.
[134]LPNHE, Sorbonne Université, Université de Paris, CNRS/IN2P3, Paris; France.
[135]Department of Physics, University of Pennsylvania, Philadelphia PA; United States of America.
[136]Konstantinov Nuclear Physics Institute of National Research Centre "Kurchatov Institute", PNPI, St. Petersburg; Russia.
[137]Department of Physics and Astronomy, University of Pittsburgh, Pittsburgh PA; United States of America.
[138 (a)]Laboratório de Instrumentação e Física Experimental de Partículas - LIP, Lisboa;[(b)]Departamento de Física, Faculdade de Ciências, Universidade de Lisboa, Lisboa;[(c)]Departamento de Física, Universidade de Coimbra, Coimbra;[(d)]Centro de Física Nuclear da Universidade de Lisboa, Lisboa;[(e)]Departamento de Física, Universidade do Minho, Braga;[(f)]Departamento de Física Teórica y del Cosmos, Universidad de Granada, Granada (Spain);[(g)]Dep Física and CEFITEC of Faculdade de Ciências e Tecnologia, Universidade Nova de Lisboa, Caparica;[(h)]Instituto Superior Técnico, Universidade de Lisboa, Lisboa; Portugal.
[139]Institute of Physics of the Czech Academy of Sciences, Prague; Czech Republic.
[140]Czech Technical University in Prague, Prague; Czech Republic.
[141]Charles University, Faculty of Mathematics and Physics, Prague; Czech Republic.
[142]Particle Physics Department, Rutherford Appleton Laboratory, Didcot; United Kingdom.
[143]IRFU, CEA, Université Paris-Saclay, Gif-sur-Yvette; France.
[144]Santa Cruz Institute for Particle Physics, University of California Santa Cruz, Santa Cruz CA; United

States of America.
[145](a)Departamento de Física, Pontificia Universidad Católica de Chile, Santiago;(b)Universidad Andres Bello, Department of Physics, Santiago;(c)Instituto de Alta Investigación, Universidad de Tarapacá;(d)Departamento de Física, Universidad Técnica Federico Santa María, Valparaíso; Chile.
[146]Universidade Federal de São João del Rei (UFSJ), São João del Rei; Brazil.
[147]Department of Physics, University of Washington, Seattle WA; United States of America.
[148]Department of Physics and Astronomy, University of Sheffield, Sheffield; United Kingdom.
[149]Department of Physics, Shinshu University, Nagano; Japan.
[150]Department Physik, Universität Siegen, Siegen; Germany.
[151]Department of Physics, Simon Fraser University, Burnaby BC; Canada.
[152]SLAC National Accelerator Laboratory, Stanford CA; United States of America.
[153]Physics Department, Royal Institute of Technology, Stockholm; Sweden.
[154]Departments of Physics and Astronomy, Stony Brook University, Stony Brook NY; United States of America.
[155]Department of Physics and Astronomy, University of Sussex, Brighton; United Kingdom.
[156]School of Physics, University of Sydney, Sydney; Australia.
[157]Institute of Physics, Academia Sinica, Taipei; Taiwan.
[158](a)E. Andronikashvili Institute of Physics, Iv. Javakhishvili Tbilisi State University, Tbilisi;(b)High Energy Physics Institute, Tbilisi State University, Tbilisi; Georgia.
[159]Department of Physics, Technion, Israel Institute of Technology, Haifa; Israel.
[160]Raymond and Beverly Sackler School of Physics and Astronomy, Tel Aviv University, Tel Aviv; Israel.
[161]Department of Physics, Aristotle University of Thessaloniki, Thessaloniki; Greece.
[162]International Center for Elementary Particle Physics and Department of Physics, University of Tokyo, Tokyo; Japan.
[163]Department of Physics, Tokyo Institute of Technology, Tokyo; Japan.
[164]Tomsk State University, Tomsk; Russia.
[165]Department of Physics, University of Toronto, Toronto ON; Canada.
[166](a)TRIUMF, Vancouver BC;(b)Department of Physics and Astronomy, York University, Toronto ON; Canada.
[167]Division of Physics and Tomonaga Center for the History of the Universe, Faculty of Pure and Applied Sciences, University of Tsukuba, Tsukuba; Japan.
[168]Department of Physics and Astronomy, Tufts University, Medford MA; United States of America.
[169]Department of Physics and Astronomy, University of California Irvine, Irvine CA; United States of America.
[170]Department of Physics and Astronomy, University of Uppsala, Uppsala; Sweden.
[171]Department of Physics, University of Illinois, Urbana IL; United States of America.
[172]Instituto de Física Corpuscular (IFIC), Centro Mixto Universidad de Valencia - CSIC, Valencia; Spain.
[173]Department of Physics, University of British Columbia, Vancouver BC; Canada.
[174]Department of Physics and Astronomy, University of Victoria, Victoria BC; Canada.
[175]Fakultät für Physik und Astronomie, Julius-Maximilians-Universität Würzburg, Würzburg; Germany.
[176]Department of Physics, University of Warwick, Coventry; United Kingdom.
[177]Waseda University, Tokyo; Japan.
[178]Department of Particle Physics and Astrophysics, Weizmann Institute of Science, Rehovot; Israel.
[179]Department of Physics, University of Wisconsin, Madison WI; United States of America.
[180]Fakultät für Mathematik und Naturwissenschaften, Fachgruppe Physik, Bergische Universität Wuppertal, Wuppertal; Germany.
[181]Department of Physics, Yale University, New Haven CT; United States of America.

[a] Also at Borough of Manhattan Community College, City University of New York, New York NY; United States of America.
[b] Also at Center for High Energy Physics, Peking University; China.
[c] Also at Centro Studi e Ricerche Enrico Fermi; Italy.
[d] Also at CERN, Geneva; Switzerland.
[e] Also at CPPM, Aix-Marseille Université, CNRS/IN2P3, Marseille; France.
[f] Also at Département de Physique Nucléaire et Corpusculaire, Université de Genève, Genève; Switzerland.
[g] Also at Departament de Fisica de la Universitat Autonoma de Barcelona, Barcelona; Spain.
[h] Also at Department of Financial and Management Engineering, University of the Aegean, Chios; Greece.
[i] Also at Department of Physics and Astronomy, Michigan State University, East Lansing MI; United States of America.
[j] Also at Department of Physics and Astronomy, University of Louisville, Louisville, KY; United States of America.
[k] Also at Department of Physics, Ben Gurion University of the Negev, Beer Sheva; Israel.
[l] Also at Department of Physics, California State University, East Bay; United States of America.
[m] Also at Department of Physics, California State University, Fresno; United States of America.
[n] Also at Department of Physics, California State University, Sacramento; United States of America.
[o] Also at Department of Physics, King's College London, London; United Kingdom.
[p] Also at Department of Physics, St. Petersburg State Polytechnical University, St. Petersburg; Russia.
[q] Also at Department of Physics, University of Fribourg, Fribourg; Switzerland.
[r] Also at Faculty of Physics, M.V. Lomonosov Moscow State University, Moscow; Russia.
[s] Also at Faculty of Physics, Sofia University, 'St. Kliment Ohridski', Sofia; Bulgaria.
[t] Also at Giresun University, Faculty of Engineering, Giresun; Turkey.
[u] Also at Graduate School of Science, Osaka University, Osaka; Japan.
[v] Also at Hellenic Open University, Patras; Greece.
[w] Also at Institucio Catalana de Recerca i Estudis Avancats, ICREA, Barcelona; Spain.
[x] Also at Institut für Experimentalphysik, Universität Hamburg, Hamburg; Germany.
[y] Also at Institute for Nuclear Research and Nuclear Energy (INRNE) of the Bulgarian Academy of Sciences, Sofia; Bulgaria.
[z] Also at Institute for Particle and Nuclear Physics, Wigner Research Centre for Physics, Budapest; Hungary.
[aa] Also at Institute of Particle Physics (IPP); Canada.
[ab] Also at Institute of Physics, Azerbaijan Academy of Sciences, Baku; Azerbaijan.
[ac] Also at Instituto de Fisica Teorica, IFT-UAM/CSIC, Madrid; Spain.
[ad] Also at Istanbul University, Dept. of Physics, Istanbul; Turkey.
[ae] Also at Joint Institute for Nuclear Research, Dubna; Russia.
[af] Also at Moscow Institute of Physics and Technology State University, Dolgoprudny; Russia.
[ag] Also at National Research Nuclear University MEPhI, Moscow; Russia.
[ah] Also at Physics Department, An-Najah National University, Nablus; Palestine.
[ai] Also at Physikalisches Institut, Albert-Ludwigs-Universität Freiburg, Freiburg; Germany.
[aj] Also at The City College of New York, New York NY; United States of America.
[ak] Also at TRIUMF, Vancouver BC; Canada.
[al] Also at Universita di Napoli Parthenope, Napoli; Italy.
[am] Also at University of Chinese Academy of Sciences (UCAS), Beijing; China.
[*] Deceased